STUDY OF A THERMONUCLEAR REACTOR BLANKET WITH FISSILE NUCLIDES

LASZLO N. LONTAI

TECHNICAL REPORT 436

JULY 6, 1965

MASSACHUSETTS INSTITUTE OF TECHNOLOGY
RESEARCH LABORATORY OF ELECTRONICS
CAMBRIDGE, MASSACHUSETTS

The Research Laboratory of Electronics is an interdepartmental laboratory in which faculty members and graduate students from numerous academic departments conduct research.

The research reported in this document was made possible in part by support extended the Massachusetts Institute of Technology, Research Laboratory of Electronics, by the JOINT SERVICES ELECTRONICS PROGRAMS (U.S. Army, U.S. Navy, and U.S. Air Force) under Contract No. DA36-039-AMC-03200(E); additional support was received from the National Science Foundation (Grant GK-57).

MASSACHUSETTS INSTITUTE OF TECHNOLOGY

RESEARCH LABORATORY OF ELECTRONICS

Technical Report No. 436 July 6, 1965

STUDY OF A THERMONUCLEAR REACTOR BLANKET WITH FISSILE NUCLIDES

Laszlo N. Lontai

Submitted to the Department of Nuclear Engineering, M. I. T., May 17, 1963, in partial fulfillment of the requirements for the degree of Master of Science in Nuclear Engineering.

(Manuscript received March 31, 1965)

Abstract

The use of fissile nuclides in a fusion power reactor heat-extraction blanket is investigated from the point of view of tritium regeneration and power production. The existence of a stable, steady-state D-T plasma in a cylindrical configuration is postulated.

Nuclear reaction rates are analyzed with the aid of theoretical methods and multigroup, multiregion computer codes developed by A. J. Impink, Jr. Codes developed by W. G. Homeyer have been used to calculate nuclear heating rates.

Optimization studies of several blanket configurations show that a blanket with a thin Mo first wall, a narrow, fused $(LiF)_2BeF_2$ first-wall coolant region, and ~50 cm 21% C and 79% fused (LiF-BeF_2-UF_4) primary attenuator region with 17 to 27 mole per cent $(U^{238})F_4$ and ~50% Li^6 enrichment is feasible and practical. The calculated tritium regeneration is adequate. The total heat recovery is approximately twice that in a nonfissile blanket; approximately 90% of the heat is liberated in the primary attenuator region. The heating rate in the first wall and in the coolant region is independent of the UF_4 salt composition. The thermonuclear power limit is ~5 Mw/m^2 of neutron energy incident on the first wall.

The performance of blankets with a UF_4 fused-salt coolant region has been found to be marginal; fissioning metallic first-wall configurations are not feasible.

PREFACE

This is the third in a series of five reports on Fusion Blanket research.
A list of the authors and titles of the other four reports in this series follows.

Technical Report 434	Albert J. Impink, Jr., "Neutron Economy in Fusion Reactor Blanket Assemblies"
Technical Report 435	William G. Homeyer, "Thermal and Chemical Properties of the Thermonuclear Blanket Problem"
Technical Report 437	Patrick S. Spangler, "Fusion Reactor Blanket Experiment"
Technical Report 438	Lester M. Petrie, Jr., "Gamma-Ray Spectra in Fusion Blanket Mock-ups"

TABLE OF CONTENTS

I. INTRODUCTION

A program to study the several aspects of a thermonuclear power reactor blanket assembly has been initiated. The blanket consists of the vacuum wall, heat-transfer medium, and tritium regeneration mechanism (the last for a D-T reactor), that must surround any controlled fusion plasma. Investigation of the blanket problem is motivated by two principal facts: (i) present understanding of plasma physics allows a fairly reliable estimate of the general characteristics of a steady-state fusion reactor (if plasma stability can be achieved); (ii) a controlled fusion system will consist of much more than the plasma.

The reactor postulated by Rose and Clark[1] has been assumed as the basis of this study. The primary source of energy will be the deuterium-tritium fusion reaction. Approximately 80% of the fusion energy appears as neutron kinetic energy, the remainder as α-particle energy. A considerable fraction of the α-particle energy will be transferred to plasma electrons and will appear as electromagnetic radiation (x-ray and millimeter radiation). Energy recovery, therefore, requires a blanket assembly that absorbs the plasma radiation and moderates the neutrons. The blanket must also regenerate tritium, using the 14.1 Mev D-T fusion neutrons to ensure continued reactor operation. The use of superconducting magnetic coils to generate the confining field requires that the blanket be a coil shield.

These considerations are the foundation of the blanket study. Theoretical analyses of blankets without fissile nuclides have been completed. A. J. Impink[2] has investigated the neutron transport and the nuclear reaction rates in the blanket. W. G. Homeyer[3] has analyzed the thermal and chemical aspects of the problem. Presently, experimental studies of blanket arrangements will be conducted by P. S. Spangler[4] and L. M. Petrie[5] with the aim of testing the validity of the theoretical results.

The present work explores the nuclear and thermal problems in fusion reactor blankets in which fissile nuclides constitute a significant part of the system. Thorium 232 and uranium 238 are the only reasonable choices of nuclides because both have large fast-fission cross sections, and both are relatively abundant. These fissionable materials, however, absorb neutrons as well as yield them by fission and other reactions; also, thermal stress and heat transfer problems may be made more difficult by the occurrence of fission. Hence, the two primary objectives of this study are:

1. To investigate the feasibility of a blanket with fissile nuclides, in view of the imposed requirements.

2. To estimate the practicality of such a system. The generally favorable results obtained for nonfissile blanket systems and the additional problems (corrosion, increased radiation damage, long-lived fission products) introduced by the use of fissile nuclides, imply that the advantages of a fissile blanket must be great for it to be considered practical.

This study makes use of the methods and computer codes developed by Impink and by

Homeyer in treating the corresponding problems of tritium regeneration and of nuclear heating of the blanket. Three distinct blanket configurations are investigated: (i) the fissile first wall; (ii) the fissile first-wall coolant; and (iii) the fissile primary attenuator configurations. In the first case the fissionable nuclide is in metallic form, in the second and third, it is a constituent of a fused salt. This report is organized as follows: Section II is devoted to a brief sketch of the history and the conceptual development of the fissile blanket. The tritium regeneration analysis is presented in Section III. The heating rate calculations and related topics are discussed in Section IV. Section V gives a summary of the conclusions derived from the investigation. The derivation of the resonance absorption model for a homogeneous mixture of nuclides is presented in Appendix A. The summary of the nuclear cross section data for Th^{232} and U^{238} is given in Appendix B. Appendix C gives an outline of the heat-transfer calculations.

Three important considerations pertaining to the problem are intentionally excluded from detailed analysis. The first two are the problem of corrosion associated with high temperature UF_4 fused salts, and the problem of fission product build-up in the system. The corrosion problem is similar to that encountered in a molten salt fission reactor, and research is under way to develop means of controlling it.[6] The build-up of long-lived isotopes constitutes a health hazard and a disposal problem, but imposes no serious physical limitation on the blanket. Third, and extensive study of the economic implications of the use of fissile nuclides in a blanket assembly is beyond the scope of this work.

There will be frequent mention of the work of A. J. Impink and of W. G. Homeyer and their names will be cited without further reference.

II. CONCEPTUAL DEVELOPMENT OF THE BLANKET

2.1 FUNCTIONS OF THE BLANKET

The requirements of the blanket assembly have been established in previous studies.[1-3] They fall under the general headings of tritium regeneration, heat extraction and superconducting coil shieldings. These topics will be discussed briefly here.

a. Tritium Regeneration

Tritium regeneration by the fusion D-T neutrons is essential. The yield should be as great as possible, and a lower limit is approximately 1.15 tritons per triton consumed in the fusion reaction.[7] (The excess regeneration is required to offset the losses incurred in recycling the tritium through the plasma, in recovering the tritium produced in the blanket, and by natural radioactive decay throughout the system.) The principal tritium-producing reactions are

$$Li^6 + n \longrightarrow T^3 + He^4 + 4.8 \text{ Mev}$$

and

$$Li^7 + n + 2.8 \text{ Mev} \longrightarrow T^3 + He^4 + n'$$

Calculations by Impink have shown that the "effective" multiplication of Li^7 (92.58% of natural Li) is not nearly enough to compensate for leakage and parasitic capture. Thus (n, 2n) reactions from Be^9 and from intermediate or heavy nuclides are required for additional neutron multiplication. The last also competes with inelastic down-scattering.

Substantial neutron multiplication may be gained from Th^{232} and U^{238} fast fission, which yields approximately 3 neutrons per reaction. The large (n, 2n) and (n, 3n) cross sections at high energies further increase the multiplication potential of these nuclides. The multiplication cross sections (the product of the reaction cross section and the neutron yield) of Th^{232} and U^{238} are compared with those of Mo and Be in Fig. 1.

b. Heat Extraction

The energy released in the D-T fusion reaction

$$D + T \rightarrow He^4 \text{ (3.5 Mev)} + n \text{ (14.1 Mev)}$$

induces two forms of blanket heating. A fraction of the α-particle energy (which is transferred to the plasma electrons) will be absorbed on the first surface of the vacuum wall as cyclotron radiation and Bremsstrahlung x-rays. The energy of the fast neutron is recovered within the blanket as the neutron is slowed down to thermal energy by elastic and inelastic scattering events. Neutron-induced exoergic reactions (for example, Li^6 (n, t), U^{238} (n, γ) and U^{238} (n, f)) provide additional volume heat generation. The energy of the neutron reactions appears as residual nucleus and charged-particle kinetic energy (local heat source), and secondary γ-radiation (diffuse heat source).

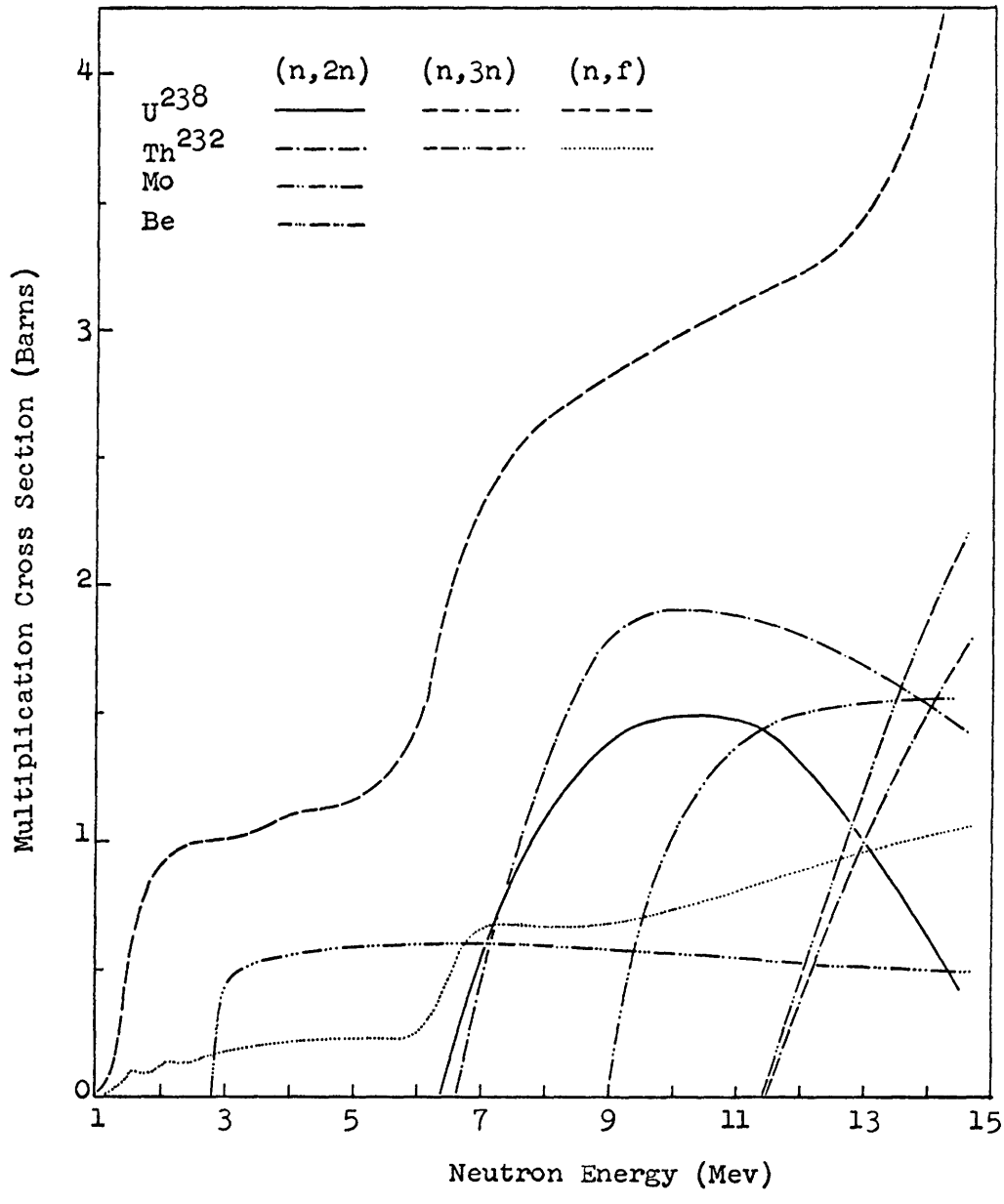

Fig. 1. Multiplication cross sections.

Impink and Homeyer have established that the use of a refractory metal vacuum wall is mandatory, and that the requirements of low pressure, high heat transfer, stability, nonconducting coolant, 500°C operating temperature, and tritium regeneration make $(LiF)_2BeF_2$ by far the best choice for a nonfissile coolant.

c. Superconducting Coil Shielding

The superconducting magnet, located outside the blanket assembly, will be maintained at a temperature below 4°K. The large temperature difference between the coils and the exterior environment necessitates high power expenditure for the removal of relatively small quantities of heat. Homeyer estimated that the maximum tolerable heat generation in the coil region is of the order of 10^{-5} of the neutron energy flux incident on the blanket first wall. Therefore, the coil-shielding region must provide for a high degree of neutron (leakage from the heat-extraction region) absorption and x-ray attenuation. No energy recovery is expected in the coil shield, and it will be separated from the inner blanket by a thermal shield.

2.2 BLANKET ASSEMBLY WITHOUT FISSILE NUCLIDES

The calculations of Impink and Homeyer indicate that the nonfissile blanket configuration shown in Fig. 2 is of satisfactory design. The blanket produces approximately 1.22 tritons per incident neutron. The heat generation in the blanket is approximately 123% of the incident neutron energy flux; the heating in the magnetic coils is 2×10^{-5} of the recoverable heat.

2.3 EARLIER PROPOSALS FOR FISSILE BLANKETS

a. Driven Thermonuclear Reactor with a Fissile Blanket

A new fusion reactor design in which most of the power output would be derived from the fast fission reaction in a depleted uranium blanket was proposed by Powell.[8] In this system, 14-Mev neutrons would be supplied by a driven D-T fusion reactor (a mirror device containing a 1-2 kev tritium plasma of 10^{14} to 10^{15} ions/cm^3 density which is bombarded by 200-250 kev deuterons). An estimated 1-2 fissions would be induced in the U^{238} blanket for each fusion reaction, resulting in nearly fivefold neutron multiplication, and approximately 200% increase in power production. Neutron capture in U^{238} would produce Pu^{239} (with a breeding ratio of 4) for fission reactor fuel; and the Li^6 (n, t) reaction would regenerate sufficient tritium to maintain continued reactor operation. The problem of heat extraction was ignored, and only rough calculations of neutron economy were made. No further development of this reactor concept was pursued.

b. Fusion-Fission Reactor

L. G. Barrett[9] proposed a scheme to improve the heat-extraction blanket of a stellarator-type fusion reactor. The blanket would consist of a series of fission reactors

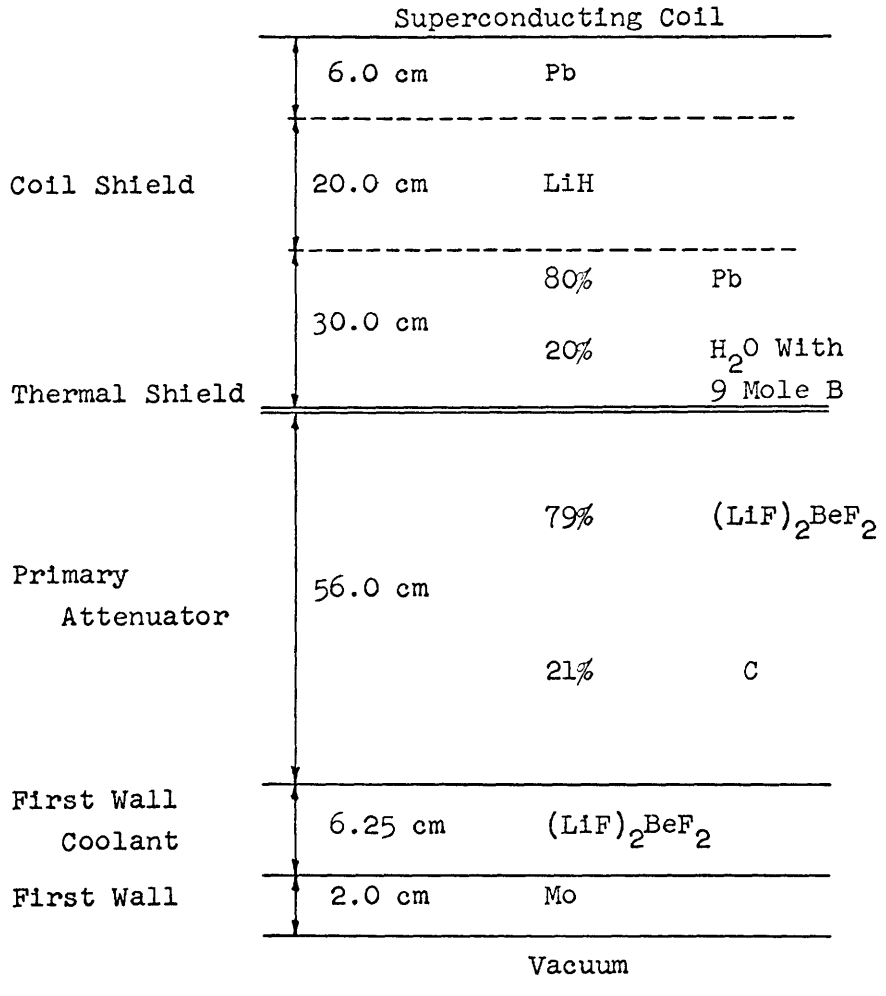

Fig. 2. Schematic diagram of the standard nonfissile blanket.

capable of critical operation independently of the fusion device. The heat recovery region would be composed of primary cooling channels containing a circulating aqueous solution of enriched UO_2SO_4, followed by secondary cooling channels containing a similar depleted uranium solution. The critical operation of the blanket fission reactor would be controlled by the uranium concentration in the primary coolant system. Pu^{239} would be produced in the depleted uranium system; and tritium regeneration would be accomplished by circulating metallic Li^6 outside the heat-recovery region. (An alternative tritium-breeding system would consist of placing Li^6 near the exterior loop of the cooling system, and the Li^6 (n, α)t reaction would be induced by delayed fission neutrons; in this scheme ohmic pumping losses would be eliminated.) The anticipated advantages cited for this fissile blanket configuration are

1. The blanket assembly could be preheated by the fission (thermal) reactors.

2. The fusion-fission reactor power could be maintained by the fission reaction alone in the event of temporary shutdown of the fusion device.

3. During steady-state operation, the fusion energy would be multiplied severalfold by the D-T fusion neutron-induced fast fissions.

4. The fission reaction would provide sufficient neutron multiplication to maintain Pu^{239} and tritium regeneration. Pu^{239} would be recycled in the primary coolant system (the thermal reactor), and thus a self-sustaining fuel cycle for both the fission and the fusion reaction might be achieved.

No neutronic calculations and engineering analyses were made for this blanket; and development of the concept was not carried out.

2.4 PRESENT PROPOSED BLANKET WITH FISSILE NUCLIDES

Several blankets with fissile nuclides were investigated in this study, and the following configuration was found to be feasible and practical: The blanket retains some of the characteristics of Impink's nonfissile blanket. The Mo vacuum wall is followed by a narrow nonfissile fused-salt cooling region. The primary attenuator contains a LiF-BeF-$(U^{238})F_4$ fused-salt (17 to 27 mole per cent UF_4) cooling medium channeled through a graphite matrix. (Figure 17 shows a schematic diagram of the inner blanket.) A coil-shielding region, similar to that designed for a nonfissile blanket, surrounds the heat-recovery region. The proposed blanket offers adequate tritium regeneration (~1.2 tritons per incident neutron), and substantial gains (approximately 100%) in power output. Economic benefits may be derived from the recovery of Pu^{239} produced by U^{238} neutron capture.

III. TRITIUM REGENERATION

3.1 METHODS OF ANALYSIS

Requirements for the analysis are: (i) appropriate formulation of multigroup neutron transport theory which is adaptable to machine calculation; (ii) approximation of the several neutron reactions with suitable mathematical models; and (iii) reliable experimental neutron cross-section data for the elements of interest. Fortunately, the computational techniques and scattering models had already been developed by Impink at the beginning of this study. Also, scattering data and reaction cross sections for all nonfissile nuclides used in the investigation were available.

Computer codes were devised to calculate neutron transport and reaction rate distributions in slab, cylindrical, and spherical blanket configurations. The codes for the treatment of an infinite slab blanket with three homogeneous regions were equipped to consider the fast fission reaction, although Impink calculated only fission-free systems. The calculations are made in 50 neutron energy groups by using integral transport theory in the energy range above ~5 Mev and differential transport theory at lower energies. The codes can be used directly, with insertion of suitable cross sections.

The neutron scattering models developed for heavy nuclides were entirely adequate for treating Th^{232} and U^{238}. The statistical-model calculations were modified slightly to account for the (n, 3n) reaction, which did not enter into the previous investigation. The validity of using these models for describing the nonelastic scattering spectra in heavy nuclides may be inferred from the favorable agreement between Impink's calculations and experimental measurements for lead. The calculated scattering spectra and measured scattering and multiplication cross sections (excluding fission) were used to determine the neutron group transfer probabilities for the fissile nuclides. (The neutron cross sections are given in Appendix B.)

Reliable experimental cross sections above a few kev are available for both Th^{232} and U^{238}. At lower energy, however, the effective cross sections for scattering and resonance capture must be determined empirically. The elastic scattering cross section below ~1 kev was simply assumed to be equal to the potential scattering cross section. Neutron capture is more important, and a more exact treatment is desired. The energy distribution of the neutron flux in the blanket precludes the use of the effective resonance integral method for calculating the neutron absorption. Impink derived a method for determining the effective capture cross section per energy group for an absorbing medium containing a single nuclide. The study of fused-salt regions containing fissile isotopes required the further development of the model to include homogeneous mixtures of nuclides. The derivation is presented in Appendix A.

3.2 BLANKETS WITH FISSILE FIRST WALLS

a. Material Choice and Configuration

To derive maximum benefit from the fast fission reaction in a blanket, it is desirable to locate a high concentration of fissile nuclides near the incident source of 14 Mev neutrons. Consequently, let us investigate the vacuum wall. Physical and mechanical properties of U^{238} (Table 1) preclude its use on the grounds of a low melting point. Th^{232}, however, has good refractory properties, and it may be useful at the first-wall temperature, $\leq$ 1000°C maximum. But the mechanical strength of thorium is at best marginal

Table 1. Physical and mechanical properties of Mo, Th, and U at 20°C. (Data from Tipton[10])

		Mo	Th	U
Density	$\frac{g}{cm^3}$	10.2	11.7	19.0
Melting Point	°C	2622	1750	1130
Thermal Conductivity	$\frac{cal}{sec\ cm\ ^oC}$	0.32	0.090	0.065
Thermal Expansion Coefficient	$(^oC)^{-1}$	5.1×10^{-6}	11.0×10^{-6}	43×10^{-6}
Young's Modulus	psi	46×10^6	10.6×10^6	29×10^6
Yield Strength	psi	84,000	25,000	35,000
Ult. Strength	psi	116,000	35,000	90,000
Poisson's Ratio		0.324	0.27	0.22

for the vacuum wall, and the use of the pure metal without additional structural support is unlikely. Modest alloying might improve the strength, probably at the cost of some nuclear benefits; but we have no reliable information on this matter, and assume pure Th^{232} for the subsequent calculations.

The general characteristics of the fissile first wall blanket are shown in Fig. 3. Except for the vacuum wall, the assembly is identical with the standard nonfissile blanket investigated by Impink. The nonfissile blanket was a reasonable design, and a comparison will be made with it.

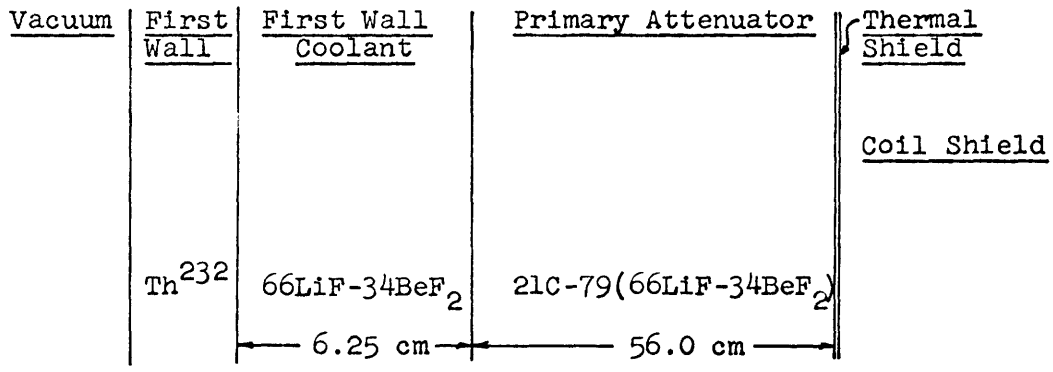

Fig. 3. Fissile first-wall blanket configuration.

b. Analysis and Tritium Regeneration

The Th^{232} wall thickness selected for initial calculation was 2.0 cm; the $(LiF)_2BeF_2$ salt in the blanket contained natural Li (7.42% Li^6, 92.58% Li^7). The calculated tritium

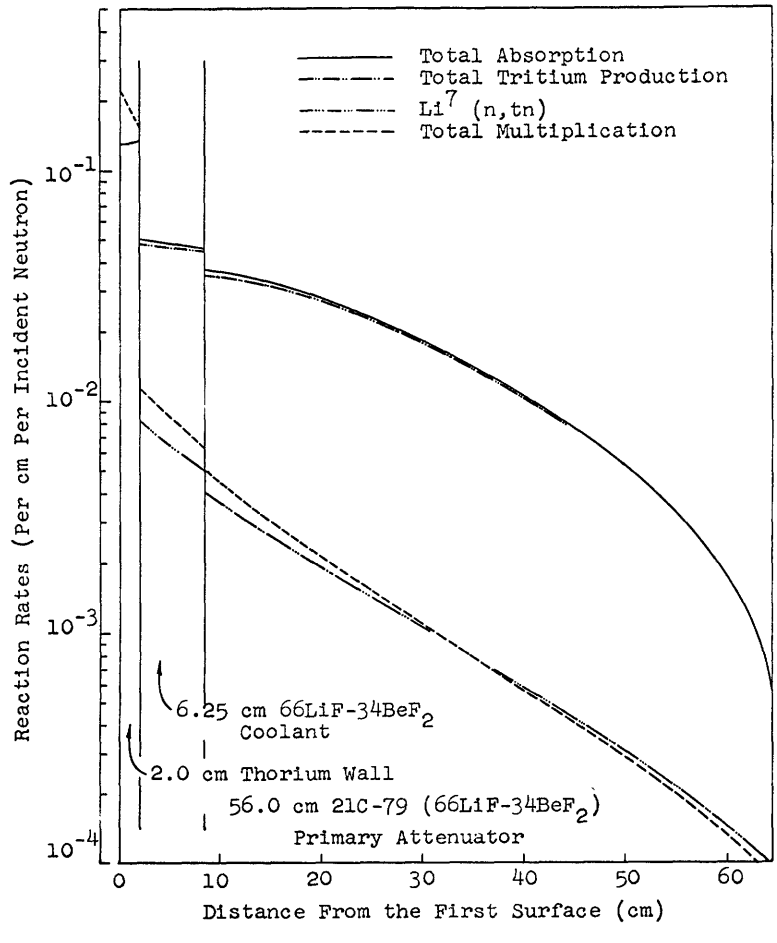

Fig. 4. Reaction distributions in a Th^{232} first-wall blanket with natural Li.

regeneration for this blanket is 1.135 tritons per incident neutron. The first wall yields 75% of the total neutron multiplication (~0.495 neutron per incident neutron) but the Th^{232} neutron capture reduces its net contribution to approximately 0.111 neutron per incident neutron. The reaction distributions in the blanket are shown in Fig. 4.

The maximum useful width of a Th^{232} wall may be approximated by extrapolating the total multiplication and absorption rate curves (Fig. 5) to their point of intersection.

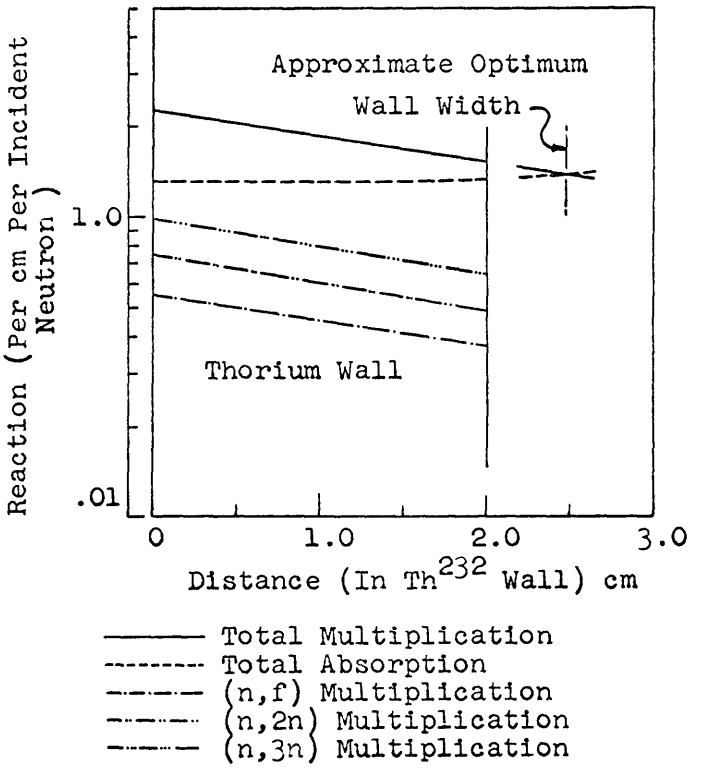

Fig. 5. Reaction-rate distributions in a Th^{232} wall.

It appears that increasing the first-wall width beyond 2.5 cm will result in a net loss of neutrons. The estimated tritium regeneration in a 2.5-cm Th^{232} first-wall blanket is ~1.14 tritons per incident neutron; and in our opinion, it is marginal.

The large Li^6 (n, t) cross section at low energies suggests that an increased Li^6 isotopic concentration in the fused salt may reduce both the Th^{232} neutron capture and the neutron leakage. Thus a blanket with 50% isotopic Li^6, but otherwise identical to the one described above, was analyzed. The regeneration ratio is 1.263 tritons per incident neutron. The increase in tritium production results entirely from the reduction of the Th^{232} absorption rate; the benefits from increased Li^6 (n, 2n) multiplication and reduced neutron leakage are cancelled by the loss of nearly half of the Li^7 (n, tn) reactions. The high Li^6 concentration in the blanket affects only the low-energy neutron reactions; therefore, the high-energy reactions in the other nuclides (except Li^7) are unchanged.

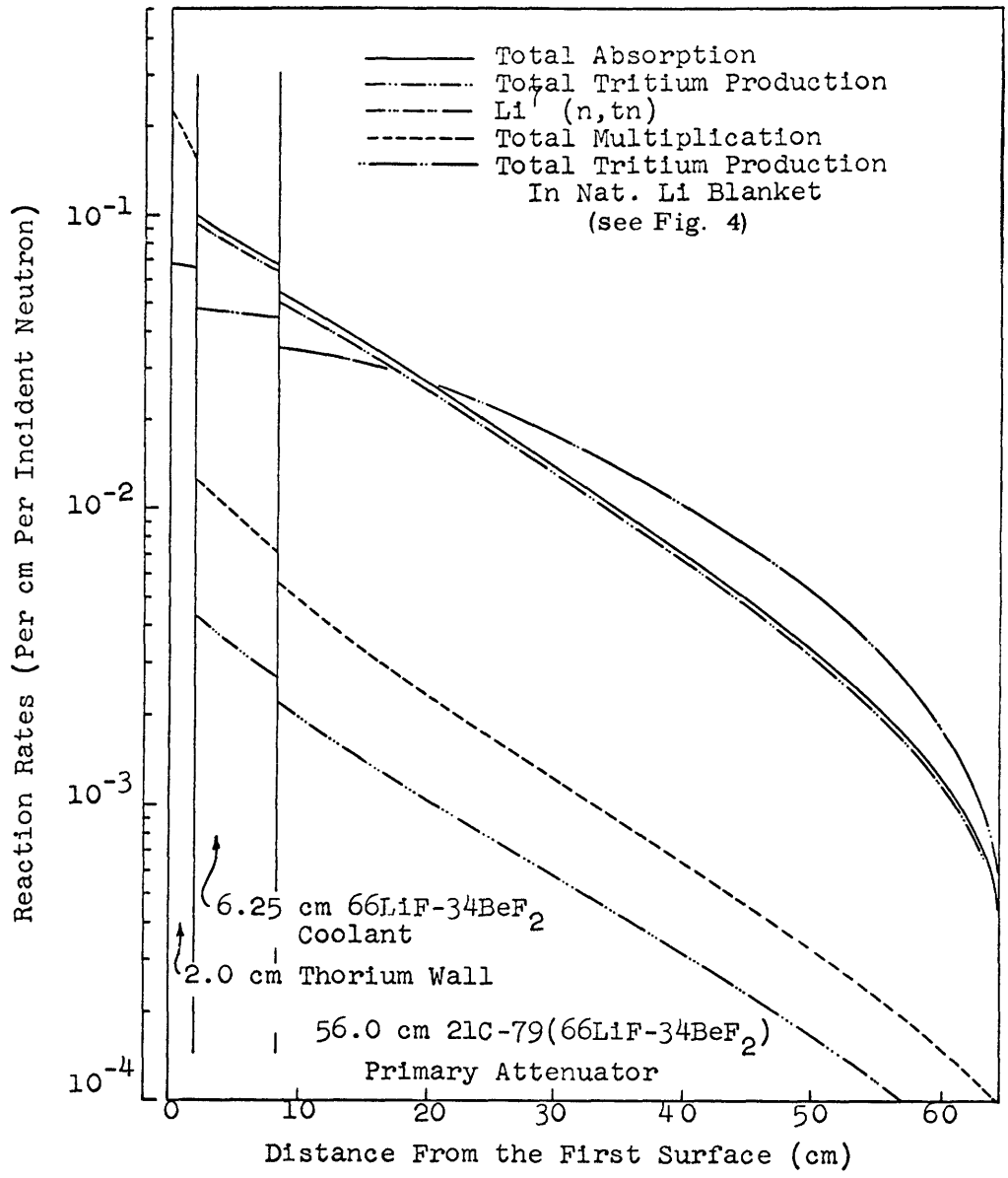

Fig. 6. Reaction distributions in a Th^{232} first-wall blanket with 50% Li^{6}.

The pronounced shift of the various absorption reactions in the fused-salt regions toward the first wall (shown in Fig. 6) indicates the rapid attenuation of the low-energy neutrons.

The increased tritium production resulting from the Li^6 enrichment in the fused salt permits some reduction in the neutron-producing Th^{232} wall thickness. Therefore, calculations were made for 1.0-cm and 1.5-cm thick first-wall configurations; the corresponding tritium regeneration ratios are 1.183 and 1.229. The net worth of the Th^{232} region in terms of total tritium production is shown in Fig. 7. The net-worth curve extrapolates to a minimum acceptable first-wall thickness of approximately 0.75 cm. Structural considerations, however, make such a reduction in the wall thickness undesirable.

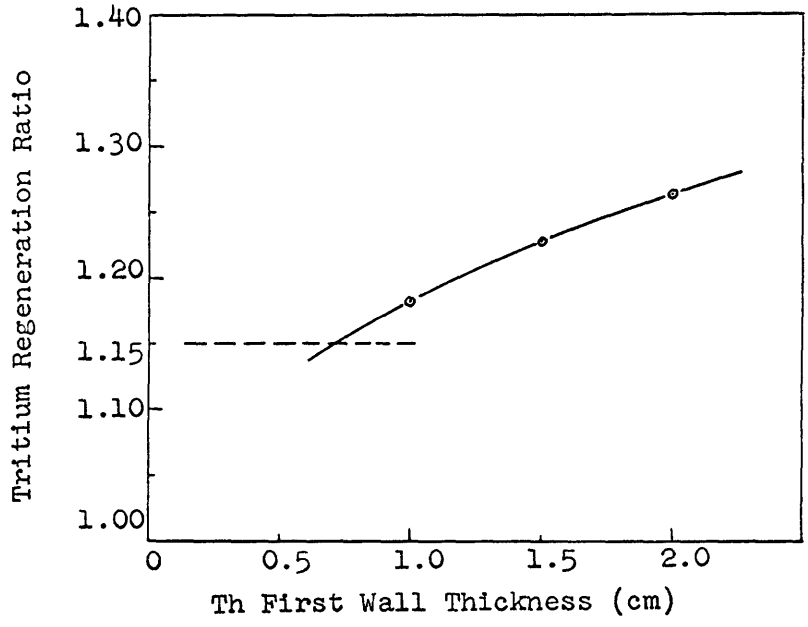

Fig. 7. Net worth of Th^{232} in a 50% Li^6 system.

The results of the Th^{232} first-wall calculations are compared with those for a U^{238} and a Mo first-wall blanket in Table 2. The 1.5-cm U^{238} wall contains roughly the same number of atoms as the 2.0-cm Th^{232} wall; consequently, these results are comparable on a per atom basis. The superiority of U^{238} from the point of neutron multiplication is evident. The major contributing factor is the greater fast fission cross section of U^{238}. The resonance capture in Th^{232} is approximately 20% higher than in U^{238} (the high total U^{238} (n, γ) reaction rate indicated in Table 2 is due to a larger neutron population in the first wall); this effect decreases the relative net multiplication in Th^{232} even more. The nonfissile blanket compares favorably with the corresponding Th^{232} configuration. The neutron multiplication in the Th^{232} wall is approximately 45% greater than in the Mo wall; but the high Th^{232} neutron absorption leaves the fissile blanket with

Table 2. Comparison of reaction rates.

Run Number	3-531	3.530	3-517	3-503	3-504	3-132[a]
First Wall	Th	Th	Th	Th	U	Mo
Thickness	1.0 cm	1.5 cm	2.0 cm	2.0 cm	1.5 cm	2.0 cm
Li^6 Enrichment	50%	50%	50%	Natural	Natural	50%
Total Multiplication	0.3657	0.4414	0.5098	0.4951	0.8493	0.3905
First Wall Mult.	0.2062	0.2936	0.3727	0.3721	0.7205	0.2579
Total Fission	0.0182	0.0260	0.0332	0.0331	0.1689	
Total Absorption	1.3377	1.4143	1.4840	1.4363	1.7917	1.3652
First Wall Absorption	0.0548	0.0925	0.1343	0.2614	0.3435	0.0655
Total Tritium	1.1831	1.2292	1.2634	1.1351	1.4055	1.2163
$Li^6(n,t)$	1.1173	1.1683	1.2069	1.0311	1.2985	1.1614
Leakage (<0.4 Mev)	0.0096	0.0091	0.0085	0.0349	0.0378	0.0083
Leakage (>0.4 Mev)	0.0215	0.0203	0.0192	0.0209	0.0211	0.0188

a) Calculations were made by A. J. Impink
All calculations were made for 6.25 cm 66LiF-34BeF_2 First Wall Coolant
and 56.0 cm 21 C-79(66 LiF-34BeF_2) Primary Attenuator
Results are per unit incident neutron.

only a 4% advantage in tritium regeneration.

c. Evaluation of Results

The calculations indicate that adequate tritium regeneration may be achieved in a Th^{232} first-wall blanket by increasing the Li^6 isotopic concentration in the fused salt. Nonfissile blankets offer, however, nearly the same tritium production with fewer penalties, such as lack of strength, corrosion, and fission damage, than are expected with Th^{232}. We conclude, therefore, that the use of a thorium first wall offers no neutronic advantage over a nonfissile configuration.

A second conclusion, which will affect the remainder of this study may be drawn: U^{238} demonstrated marked superiority to Th^{232} and, consequently, only U^{238} possesses potential usefulness in fusion reactor blanket application.

3.3 BLANKETS WITH URANIUM-FUSED SALTS

a. Choice of Salts

The fused-salt coolant in a blanket must meet the following requirements:

(a) Melting point less than 500°C;
(b) Viscosity less than 20 centipoises near 600°C;
(c) High heat capacity and thermal conductivity;
(d) Chemical stability at all operating temperatures;
(e) Chemical compatibility with other blanket materials;
(f) Provision for tritium regeneration;
(g) Low non tritium-producing neutron capture; and
(h) Provision for substantial neutron multiplication.

In view of these requirements, the use of thorium salts is rejected in favor of uranium systems. The preceding results show that U^{238} gives better neutron multiplication than Th^{232}; we also found that the melting point of thorium salts is generally higher than that of corresponding uranium salts.[11] The LiF-BeF_2 based UF_4 ternary system seems to be the best choice for a coolant. These salts have been investigated experimentally, and physical and chemical data are available.[6, 10, 11] Figure 8 shows a portion of the ternary phase equilibrium diagram for the LiF-BeF_2-UF_4 salts.[2] The region of interest is bounded by the 500°C melting curve and the arbitrary lower limit of 10 mole fraction per cent of UF_4. The salt compositions used in this study are indicated in the phase diagram, and some of their physical properties are listed in Table 3. The mixtures were chosen to give insight into the behavior of various ranges of composition. All of the fused salt in each blanket configuration did not contain uranium. The $(LiF)_2BeF_2$ eutectic mixture, g on the diagram, was used in all nonfissile regions.

Limited experimental results indicate that the corrosive properties of the salts increase rapidly with increase of UF_4 content.[12] In this problem we assume that it will be solved by chemical and metallurgical advances in the future and, owing to the lack of comprehensive data, the effect of corrosion is neglected here.

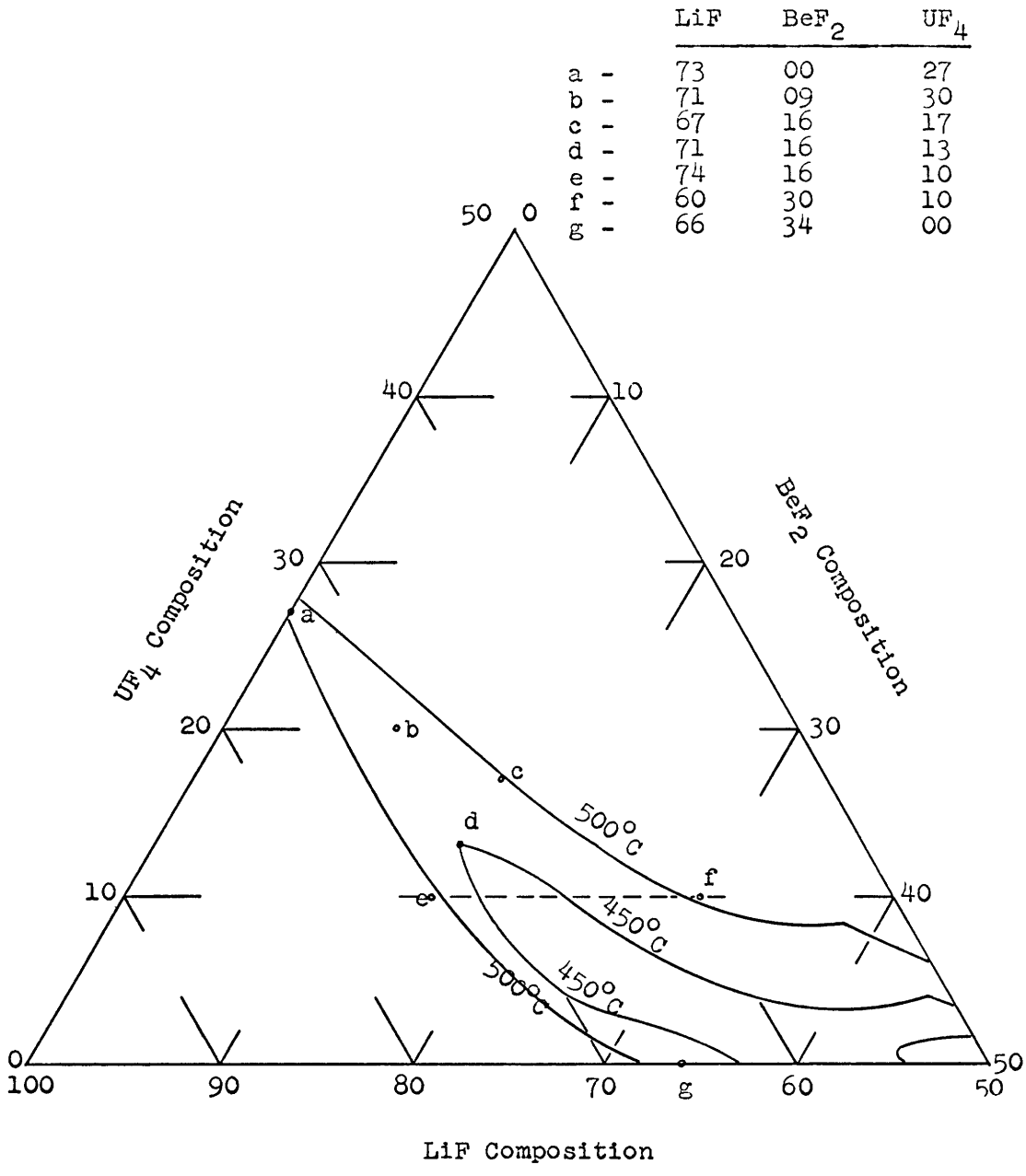

Fig. 8. Phase diagram for the LiF-BeF_2-UF_4 ternary salt system. (All compositions are given in mole fraction percentages.)

Table 3. Physical properties of the fused salts at 600°C.
(Data from Tipton,[10] unless otherwise noted.)

Composition (Mole %) $LiF-BeF_2-UF_4$	Melting[a] Point (°C)	ρ (gm/cm^3)	μ (cp)	C_p ($\frac{cal}{gm\,^oC}$)	k ($\frac{cal}{sec\ cm\,^oC}$)	Atomic Density[d] (atoms/cm^3 x 10^{-24}) Li	Be	U^{238}	F
73-00-27	490	4.52	18.1			0.01916		0.00709	0.04752
71-09-20	470	4.00	13.8	0.27[b]	(0.003)[c]	0.02022	0.00256	0.00570	0.04814
67-16-17	500	3.70	12.6			0.01946	0.00465	0.00494	0.04852
71-16-13	450	3.33	11.5	0.37	(0.005)[c]	0.02184	0.00492	0.00400	0.04768
74-16-10	500	2.87	10.8			0.02263	0.00490	0.00306	0.04467
60-30-10	500	2.96	13.1			0.01815	0.00907	0.00302	0.04837
66-34-00[e]	455	1.92	7.5	0.67	0.0145	0.02360	0.01215		0.04790

a) Melting points were determined from the $LiF-BeF_2-UF_4$ ternary phase diagrams presented by Thoma .[11]

b) ORNL Molten Salt Reactor Project .[12]

c) Estimated values based on data given by Tipton .[10]

d) Calculated values.

e) Data assembled by Homeyer.

In the discussions below, the various salt compositions are abbreviated by listing the mole percentages of the LiF, BeF_2 and UF_4 constituents (for example, the 60LiF-30BeF_2-10UF_4 salt is denoted 60-30-10).

b. Blankets with UF_4 in the First-Wall Coolant

The configuration for this study is shown in Fig. 9; it is similar to that of the standard nonfissile blanket. The major departure consists of replacing the nonfissile first-wall coolant salt with a ternary UF_4 salt. The primary attenuator is identical with Impink's standard system, but its total width is reduced approximately 15% to facilitate the computer calculations. Since the nuclear reaction rates are relatively low in the back region of the attenuator, this reduction will have only a minor effect on the results.

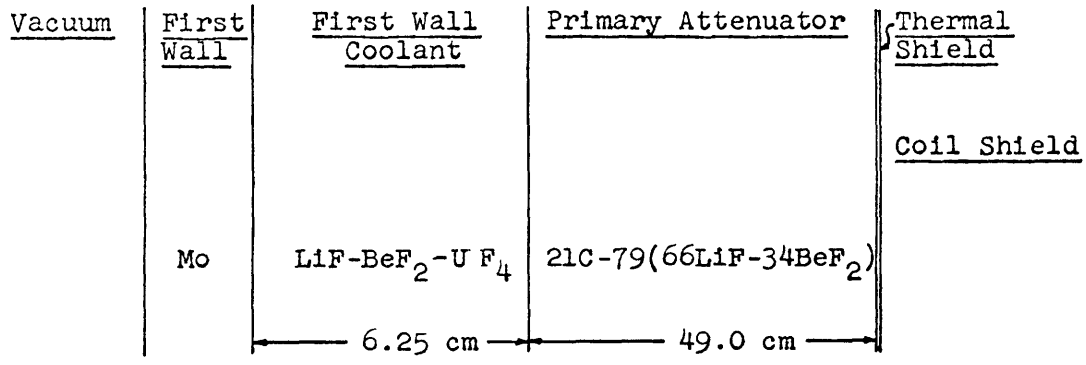

Fig. 9. Fissile-coolant blanket configuration.

Calculations were made for the 73-00-27 and the 60-30-10 coolant systems to determine the effects of varying the Mo first-wall thickness. The results are given in Table 4. Figure 10 shows the net worth of the Mo wall in terms of tritium regeneration for the two configurations. The optimum wall thickness varies inversely with the uranium content of the coolant, and is approximately 1.3 cm for the 27% UF_4 (natural Li) salt. The net neutron multiplication of U^{238} decreases rapidly with increased Mo thickness, as is seen in Fig. 11. Therefore, to optimize the U^{238} multiplication, the standard Mo first wall was chosen to be 1.0 cm wide.

Tables 5 and 6 show the results of the calculations for several fused-salt compositions. The tritium regeneration in a standard blanket configuration with natural Li salts is roughly independent of the U^{238} content, and is ~1.08 tritons per incident neutron (see Fig. 12). The identical blankets with 20% Li^6 isotopic concentration in both the uranium and the nonfissile salts yield adequate tritium regeneration; the increase in tritium production, for enriched Li, is proportional to the amount of U^{238} in the system. (The deviations of the calculated points from the curves indicated in Fig. 12 result from the variation of the BeF_2:LiF ratio of the salts.) Comparison with Impink's calculations

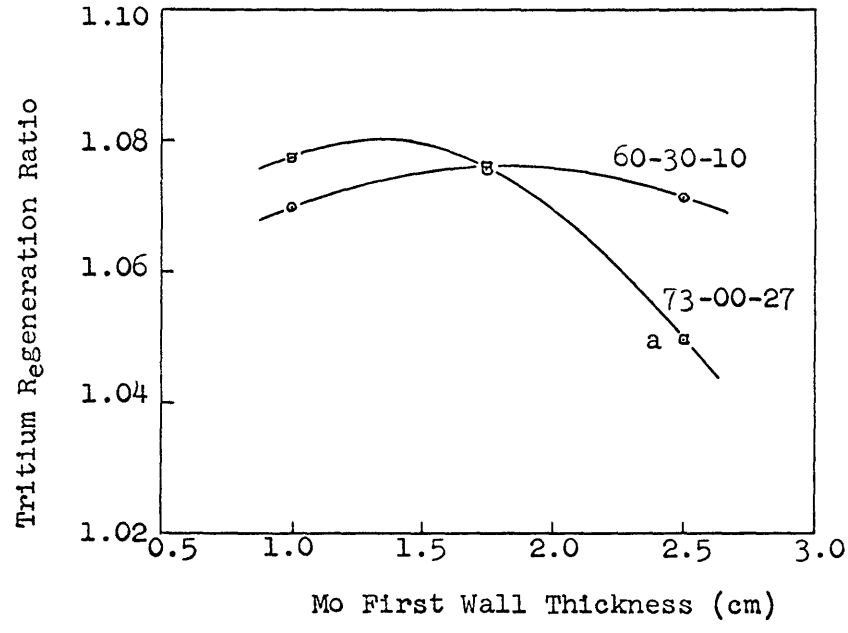

a) Calculations for 6.68 cm Coolant Region

Fig. 10. Net worth of the molybdenum wall.

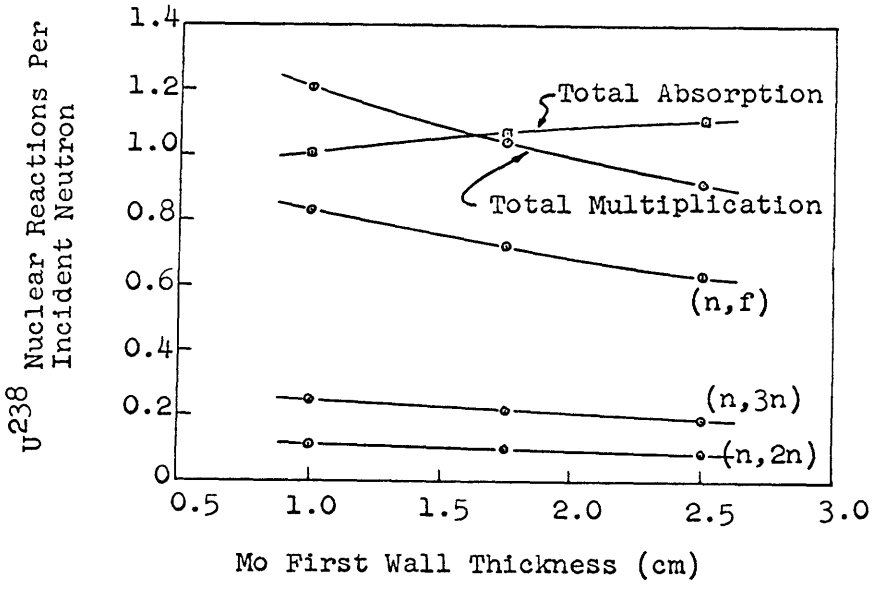

Fig. 11. Variation of the U^{238} reactions in the 60-30-10 salt with first-wall thickness.

Table 4. Results of calculations for standard blanket with varying Mo wall width.

Coolant Salt		73 LiF - 27 UF_4		60 LiF - 30 BeF_2 - 10 UF_4		
Run Number	3-505[a]	3-528	3-506[a]	3-507	3-529	3-508
Mo Thickness	2.50 cm	1.75 cm	1.00 cm	2.50 cm	1.75 cm	1.00 cm
Total Multiplication	0.5971	0.5512	0.5196	0.4963	0.4461	0.3882
Mo Multiplication	0.3067	0.2315	0.1436	0.3067	0.2315	0.1436
U^{238} Multiplication	0.2224	0.2419	0.2907	0.0920	0.1047	0.1204
Be Multiplication	0.0448	0.0517	0.0556	0.0738	0.0830	0.0938
Total Fission	0.506	0.0548	0.0660	0.0206	0.0235	0.0269
Total Absorption	1.5147	1.4562	1.4223	1.4074	1.3518	1.2887
Mo Absorption	0.1830	0.1226	0.0667	0.1830	0.1214	0.0643
U^{238} Absorption	0.2455	0.2253	0.2317	0.1111	0.1071	0.1010
Total Tritium	1.0497	1.0765	1.0773	1.0714	1.0761	1.0700
$Li^6(n,t)$	0.9725	0.9898	0.9800	0.9903	0.9851	0.9672
Leakage <0.4 Mev	0.0484	0.0535	0.0558	0.0498	0.0534	0.0572
Leakage >0.4 Mev	0.0271	0.0309	0.0327	0.0294	0.0323	0.0355

a) 6.68 cm Wide Coolant Region

Results are per unit incident neutron.

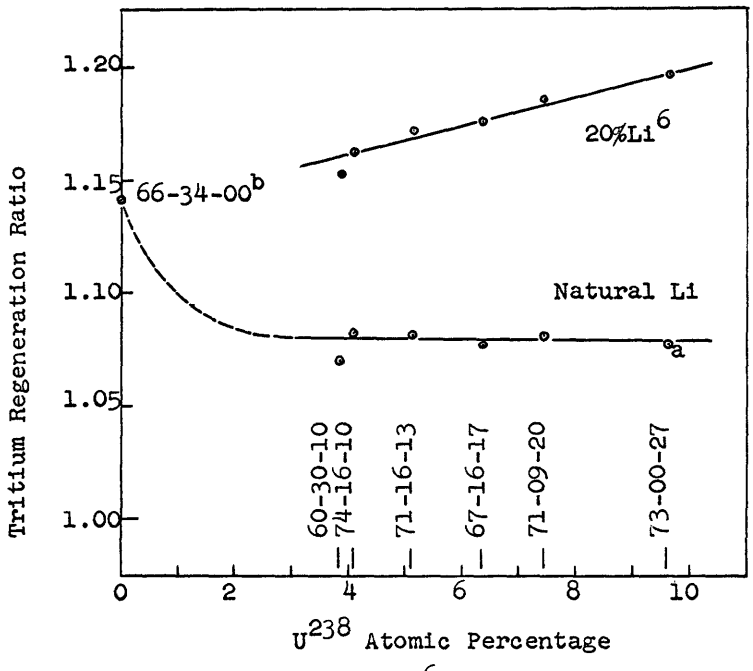

a) 73-00-27 (Nat. Li^6) with 6.68 cm Coolant Region

b) Run 3-111, A. J. Impink

Fig. 12.

Net worth of U^{238} for natural and 20% Li^6 enrichment in the standard blanket.

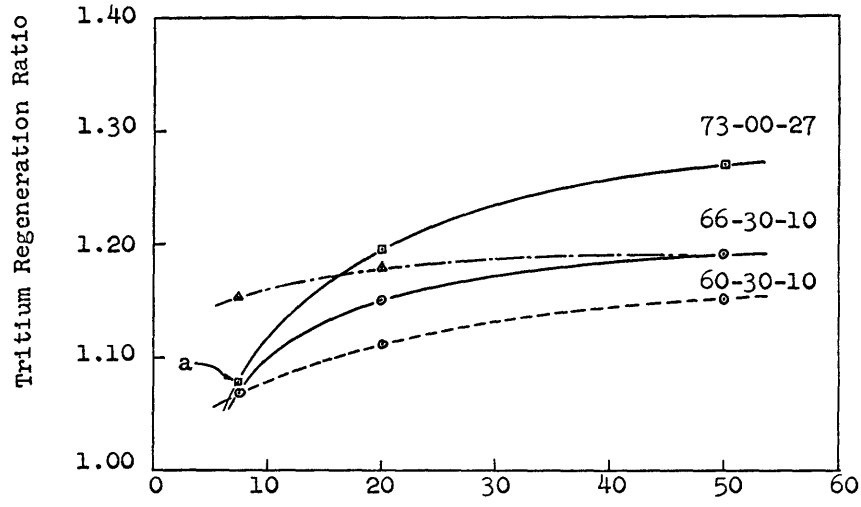

a) 73-00-27 (Nat. Li^6) With 6.68 cm Coolant Region

——— Enrichment of Whole Blanket
- - - - - - - - Enrichment of Coolant Region (Natural Li Attenuator)
—·—·— Enrichment of Attenuator (50% Li^6 Coolant)

Fig. 13. Net worth of Li^6 in the standard blanket.

Table 5. Results of calculations for standard blankets with varying U^{238} content with natural and 20% Li^6 concentration.

Coolant Salt	73 LiF - 27 UF_4		71LiF - 09BeF_2 -20UF_4		67 LiF - 16BeF_2 - 17UF_4	
Run Number	3-506[a]	3-514	3.537	3.538	3-534	3-535
Li^6 Enrichment	Natural	20%	Natural	20%	Natural	20%
Total Multiplication	0.5196	0.5126	0.4649	0.4690	0.4438	0.4479
U^{238} Multiplication	0.2907	0.2577	0.2240	0.2239	0.1946	0.1945
Be Multiplication	0.0556	0.0575	0.0676	0.0674	0.0756	0.0755
Total Fission	0.0660	0.0630	0.0505	0.0506	0.0438	0.0438
Total Absorption	1.4223	1.4498	1.3655	1.4059	1.3440	1.3841
U^{238} Absorption	0.2317	0.1442	0.1736	0.1125	0.1527	0.0980
Total Tritium	1.0773	1.1968	1.0806	1.1861	1.0772	1.1762
$Li^6(n,t)$	0.9800	1.1117	0.9786	1.0979	0.9754	1.0883
Leakage < 0.4 Mev	0.0558	0.0303	0.0570	0.0303	0.0570	0.0304
Leakage > 0.4 Mev	0.0327	0.0332	0.0342	0.0335	0.0345	0.0338

a) 6.68 cm Wide Coolant Region

Results are per unit incident neutron.

Table 6. Results of calculations for standard blankets with varying U^{238} content with natural and 20% Li^6 concentration.

Coolant Salt	71 LiF - 16BeF_2 - 13UF_4		74LiF - 16BeF_2 - 10UF_4		60LiF-30BeF_2-10UF_4	
Run Number	3-509	3-524	3-532	3-533	3-508	3-512
Li^6 Enrichment	Natural	20%	Natural	20%	Natural	20%
Total Multiplication	0.4100	0.4143	0.3778	0.3823	0.3882	0.3924
U^{238} Multiplication	0.1586	0.1585	0.1238	0.1237	0.1204	0.1205
Be Multiplication	0.0777	0.0776	0.0803	0.0802	0.0938	0.0937
Total Fission	0.0356	0.0356	0.0277	0.0277	0.0269	0.0270
Total Absorption	1.3109	1.3507	1.2775	1.3173	1.2887	1.3275
U^{238} Absorption	0.1223	0.0758	0.0939	0.0563	0.1010	0.0621
Total Tritium	1.0817	1.1716	1.0824	1.1625	1.0700	1.1518
$Li^6(n,t)$	0.9737	1.0783	0.9694	1.0649	0.9672	1.0630
Leakage < 0.4 Mev	0.0570	0.0305	0.0582	0.0314	0.0572	0.0308
Leakage > 0.4 Mev	0.0350	0.0343	0.0362	0.0355	0.0355	0.0348

Results are per unit incident neutron.

Table 7. Results of calculations for standard blanket with varying Li^6 enrichment.

Coolant Salt	$60LiF-30BeF_2-10UF_4$				$73LiF-27UF_4$
Run Number	3-511	3-522	3-525	3-523	3-518
Li^6 in Coolant	20%	50%	50%	50%	50%
Li^6 in Attenuator	Natural	Natural	20%	50%	50%
Total Multiplication	0.3897	0.3932	0.3959	0.4021	0.5217
U^{238} Multiplication	0.1203	0.1201	0.1202	0.1203	0.2775
Be Multiplication	0.0938	0.0936	0.0936	0.0934	0.0571
Total Absorption	1.2976	1.3070	1.3352	1.3570	1.4797
U^{238} Absorption	0.0747	0.0480	0.0419	0.0348	0.0841
Total Tritium	1.1131	1.1523	1.1802	1.1912	1.2708
Li^6 (n,t)	1.0152	1.0659	1.1029	1.1353	1.2176
Leakage < 0.4 Mev	0.0561	0.0542	0.0303	0.0145	0.0139
Leakage > 0.4 Mev	0.0354	0.0352	0.0346	0.0331	0.0316

Results are per unit incident neutron.

indicates that the UF_4 blankets with natural Li are less efficient tritium breeders than the nonfissile configuration. The reason is simple: U^{238} competes with Li^6 for neutron capture, and Li^6 enrichment is necessary to overwhelm the U^{238} competition; once this is done, the additional U^{238} neutrons are useful in breeding tritium.

The net (tritium production) worth of Li^6 for several enrichment schemes is shown in Fig. 13 (see also Table 7). Adequate tritium regeneration may be achieved in a fissile blanket either with approximately 50% Li^6 enrichment in the first-wall coolant alone or approximately 15-20% Li^6 enrichment in both the coolant and the primary attenuator regions. The last method seems to be more effective.

The typical reaction rate distributions in a fissile coolant blanket with natural Li and with 50% Li^6 enrichment are shown in Figs. 14 and 15. The effects of the increased Li^6 concentration are evident, and a strong similarity to the corresponding diagrams for the fissile first-wall blanket (Figs. 4 and 6) is observed.

The effects of increasing the beryllium content of the primary attenuator were investigated for two cases. The equivalent of a 5-cm slab of Be metal was homogenized throughout the attenuator region of a standard blanket with the 60-30-10 fused-salt coolant and natural Li^6 concentration, and similarly for the 73-00-27 configuration with 50% Li^6 enrichment. The results of the calculations are presented in Table 8. The total neutron multiplication in both blankets is increased approximately 0.07 neutron per incident neutron, and the resulting gain in tritium production is approximately 7 per cent. In the low-uranium blanket, the tritium regeneration appears to be marginal, but further addition of Be (or Li^6 enrichment) would give satisfactory results. In the Li^6 enriched 73-00-27 blanket, the production of 1.332 tritons per incident neutrons is certainly adequate to ensure continuous reactor operation.

Figure 16 shows the reaction rates in the natural Li^6 blanket with Be enrichment. The negligible increase of the tritium regeneration rate toward the back of the primary attenuator indicates that for maximum benefit the beryllium should be concentrated near the coolant-attenuator interface. Impink's five-region analysis shows that the homogeneous treatment of Be enrichment in the primary attenuator gives conservative results. The gain in tritium production may be as high as 20% for a 5-cm Be slab.

c. Blankets with UF_4 in the Primary Attenuator

Now we shall investigate a blanket containing a uranium salt in the primary attenuator region. The physical configuration is shown in Fig. 17. Both the first wall and the coolant region are made as narrow as possible to reduce the attenuation of the incident 14-Mev neutron flux. Even so, a large fraction of the uranium near the back of the attenuator will be exposed predominantly to low-energy neutron fluxes; consequently, a high rate of neutron multiplication must be provided to offset the U^{238} neutron capture. Therefore, only high UF_4 constituent salts will be considered in this analysis. The nonfissile salt was chosen as the first-wall coolant in order to maintain a low energy density region between the high-temperature Mo wall and the fissioning attenuator region.

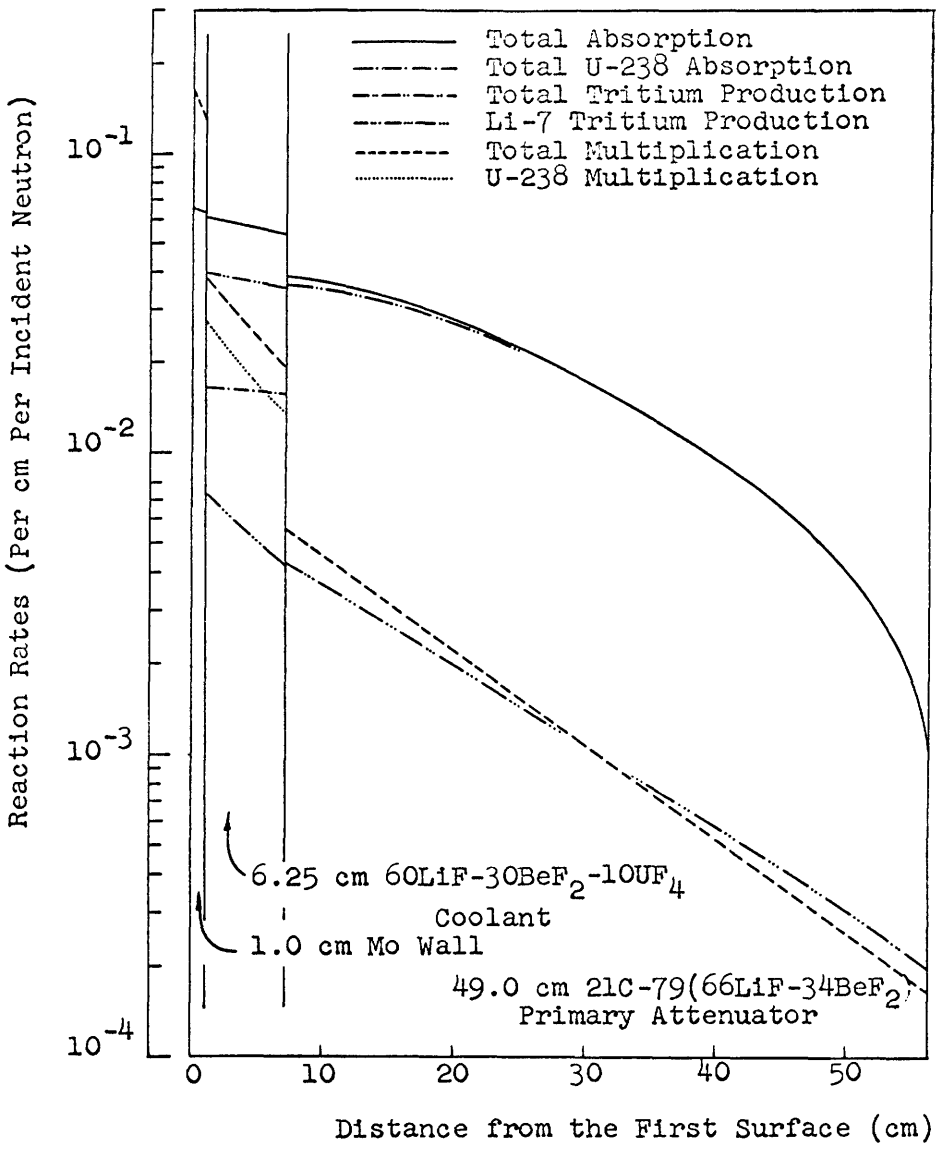

Fig. 14. Reaction distributions in a fissile-coolant blanket with natural Li (60-30-10 fused salt).

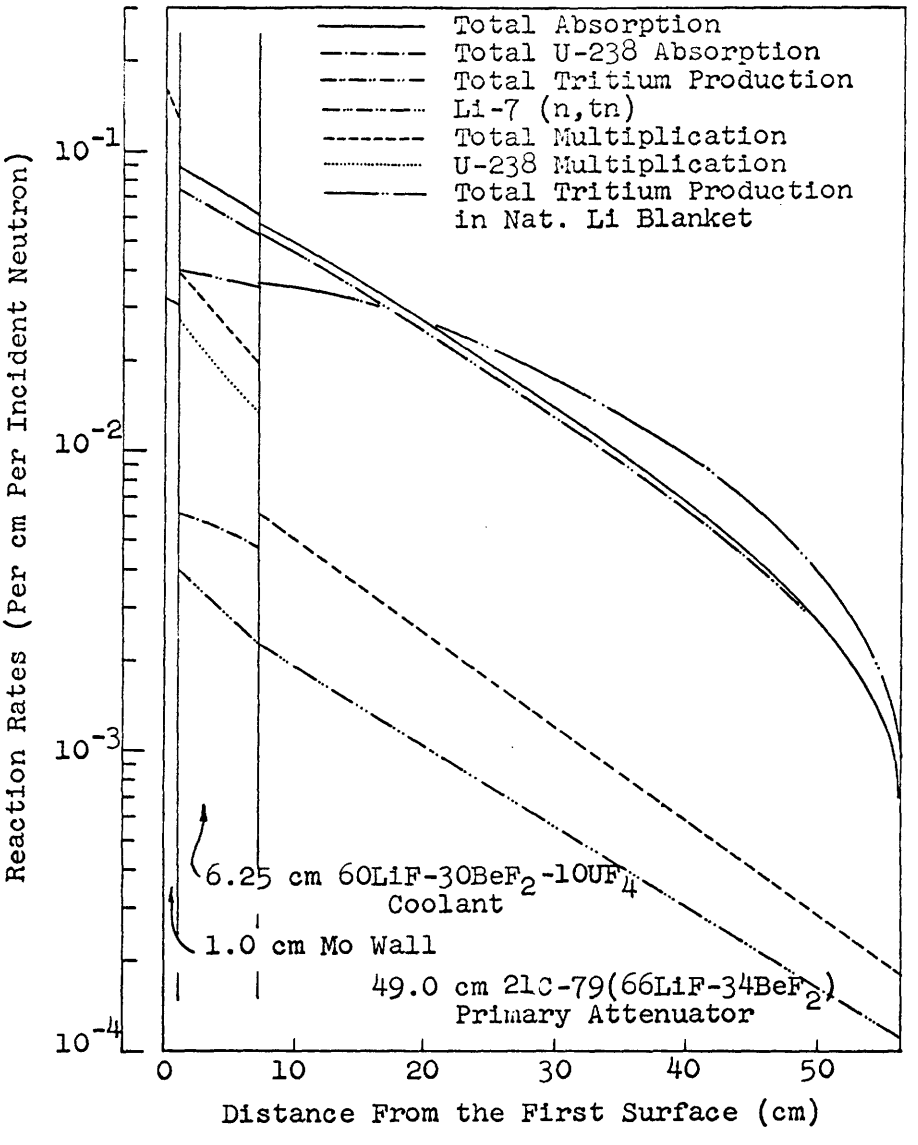

Fig. 15. Reaction distributions in a fissile-coolant blanket with 50% Li^6 (60-30-10 fused salt).

Table 8. Analysis of the effects of homogenizing the equivalent of 5 cm of Be throughout the primary attenuator of a standard blanket.

Coolant Salt	$60LiF-30BeF_2-10UF_4$	$73LiF-27UF_4$
Run Number	3-513	3-526
Li^6 Enrichment	Natural	50%
Total Multiplication	0.4635	0.5912
U^{238} Multiplication	0.1204	0.2775
Be Multiplication:		
In Coolant	0.0328	--
In Attenuator	0.1381	0.1290
Total Absorption	1.3689	1.5476
U^{238} Absorption	0.1054	0.0877
Total Tritium	1.1406	1.3320
Li^6 (n,t)	1.0415	1.2806
Leakage < 0.4 Mev	0.0504	0.0153
Leakage > 0.4 Mev	0.0360	0.0324

Results are per unit incident neutron.

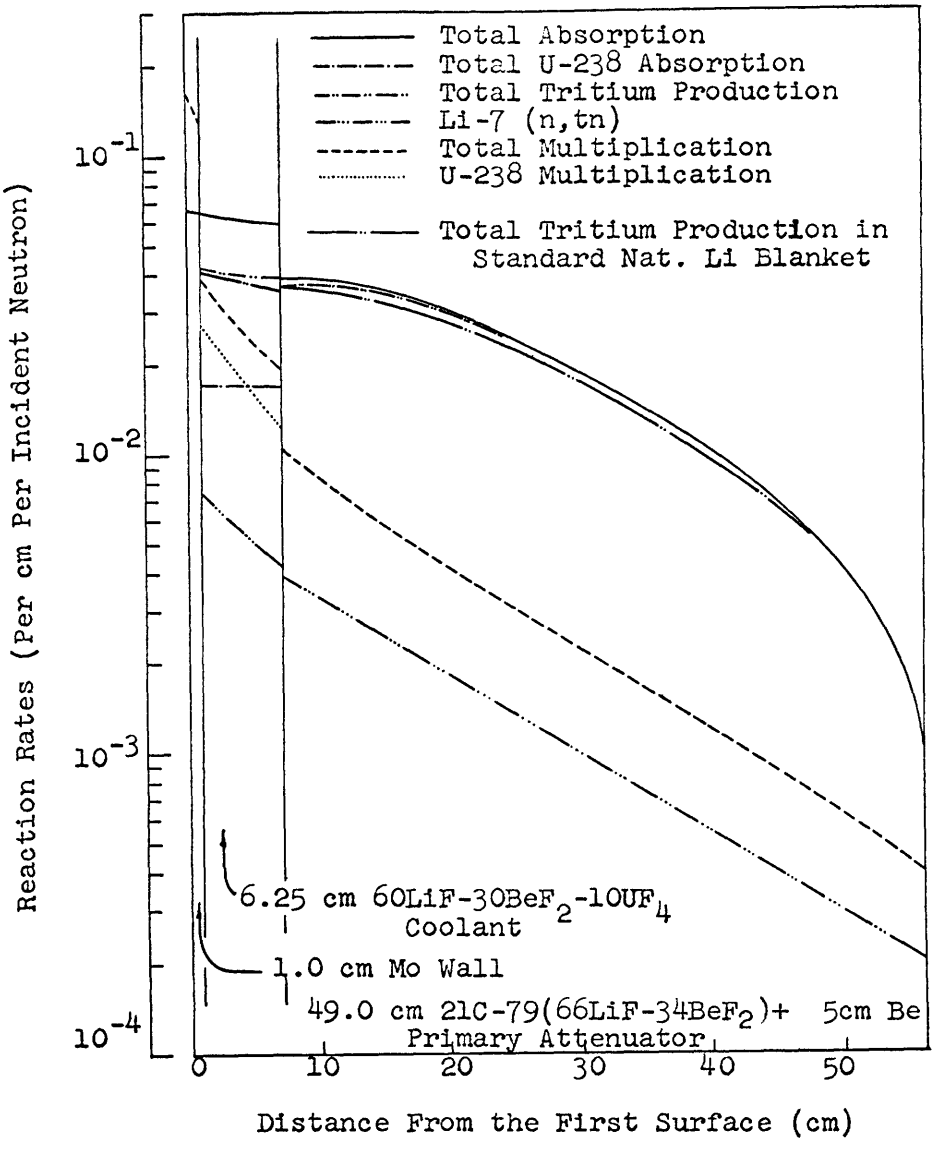

Fig. 16. Reaction distributions in a fissile-coolant blanket with 5 cm Be in the primary attenuator (60-30-10 fused salt).

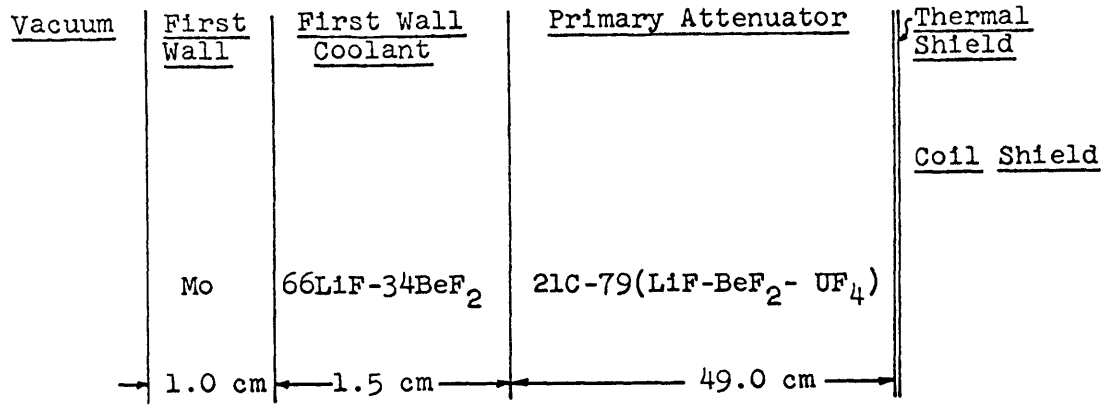

Fig. 17. Fissile attenuator blanket configuration.

Table 9. Effects of Li^6 enrichment.

Run Number	3-519	3-520	3-521
Li^6 Enrichment	Natural	50%	90%
Total Multiplication	0.6330	0.6396	0.6457
U^{238} Multiplication	0.4493	0.4439	0.4388
Total Fission	0.1100	0.1090	0.1081
Total Absorption	1.5278	1.5941	1.6131
U^{238} Absorption	0.6549	0.2222	0.1306
Total Tritium	0.7506	1.2483	1.3338
Li^6 (n,t)	0.6700	1.2046	1.3248
Leakage < 0.4 Mev	0.0841	0.0273	0.0153
Leakage > 0.4 Mev	0.0363	0.0343	0.0325

Results are per unit incident neutron.

The results of the calculations for the 73-00-27 fused salt are shown in Table 9. The natural lithium blanket configuration is definitely inadequate for tritium regeneration even if the entire leakage were overcome; Li^6 enrichment is necessary. Blankets with 50% and 90% Li^6 isotopic concentration show drastic reduction of uranium neutron capture and yield satisfactory tritium production. Figures 18 and 19 show the reaction rate distributions in the natural and 50% Li^6 blankets. In both cases, the major portion of the neutron multiplication in the primary attenuator comes from the U^{238} reactions. The neutron capture in uranium for the natural Li blanket, however, is comparable to the total tritium regeneration in the attenuator region. Increasing the Li^6 content in the fused salts to 50% reduces the U^{238} absorption approximately two-thirds, and increases the tritium production correspondingly. Rapid attenuation of the low-energy neutron fluxes is evident in the enriched attenuator, but the total tritium regeneration rate remains above that of the natural Li blanket throughout the whole attenuator region.

The net worth of Li^6 in the 27% UF_4 blanket is shown in Fig. 20. The minimum Li^6 enrichment is ~35% for this blanket; blankets with a lower UF_4 content will require more enrichment (however, there is a critical uranium concentration, below which the U^{238} absorption rate becomes a minor effect and high Li^6 enrichment is not needed). Increasing the Li^6 isotopic concentration above 50% results in relatively small additional tritium production, and therefore, it seems to be impractical.

Calculations for the 17% and the 20% UF_4 salts with 50% Li^6 enrichment indicate that these systems also yield sufficient tritium regeneration (see Table 10). The net worth of U^{238} in the attenuator region (with 50% Li^6 enrichment) is shown in Fig. 21. The curve is assumed to be linear by analogy with Fig. 12, and the deviation of the calculated points is attributed to the variation of the ratio of BeF_2 To LiF. From this diagram it appears that much lower uranium compositions will be adequate than what were initially anticipated.

The effects of adding the equivalent of 5 cm of metallic beryllium to the attenuator region of the 27% UF_4 blanket with 50% Li^6 were investigated. The increase in the tritium production is ~0.054 triton per incident neutron. As can be seen in Table 11, the U^{238} multiplication reactions are reduced approximately 10%, owing to the decrease in the volume of fused salt in the primary attenuator. Since it appears that an acceptable tritium regeneration cannot be achieved with reasonable Be enrichment alone, we conclude that the addition of metallic beryllium to this blanket configuration is of no advantage.

d. Evaluation of Results

The two preceding sections were mainly concerned with the optimization of tritium regeneration. Based on tritium production, both the fissile first-wall coolant and the fissile primary attenuator configurations are of satisfactory design, though neither offers a clear-cut advantage over the nonfissile blanket systems. The two other neutronic

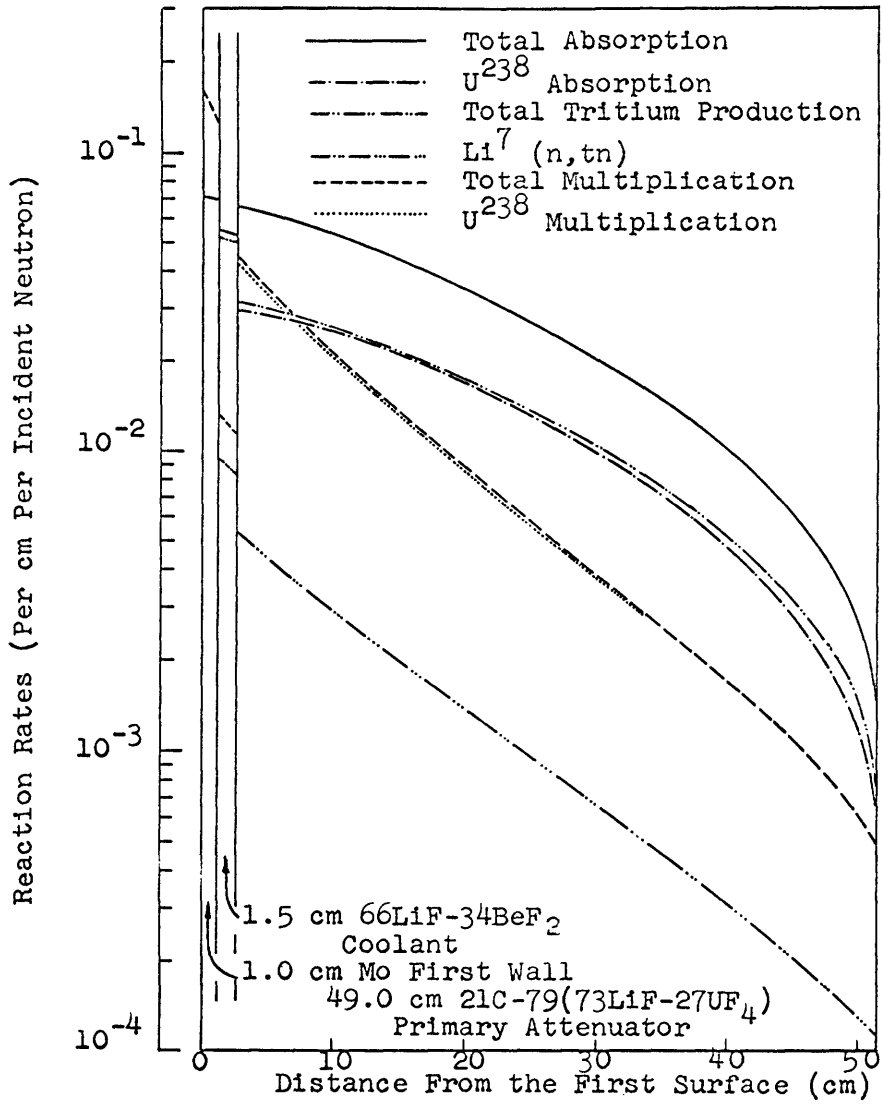

Fig. 18. Reaction distributions in a fissile attenuator blanket with natural Li (73-00-27 fused salt).

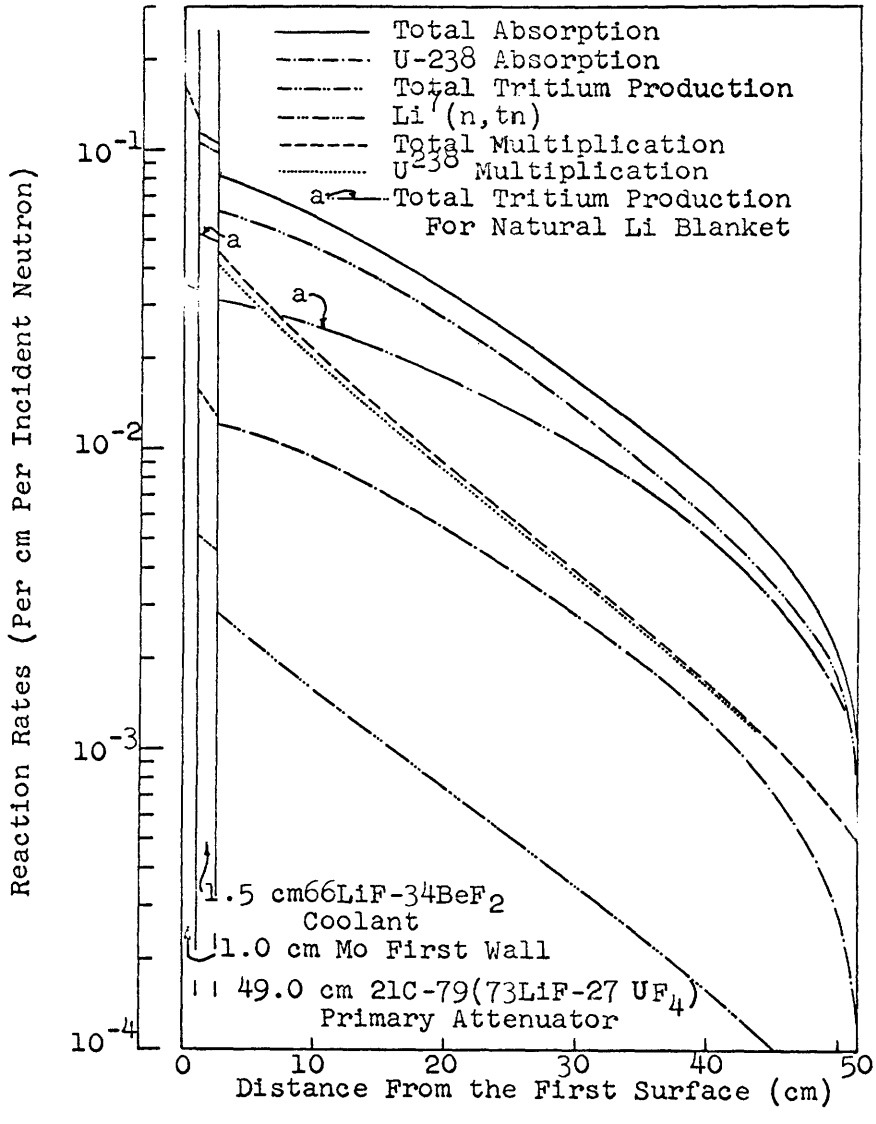

Fig. 19. Reaction distributions in a fissile attenuator blanket with 50% Li^6 enrichment (73-00-27 fused salt).

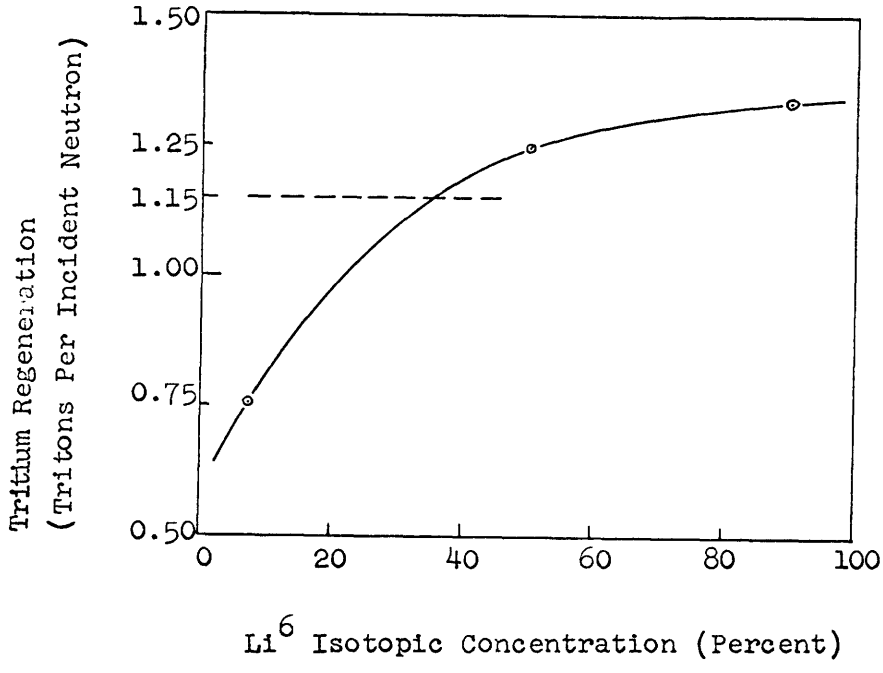

Fig. 20. Net worth of Li^6 enrichment in the 73-00-27 blanket.

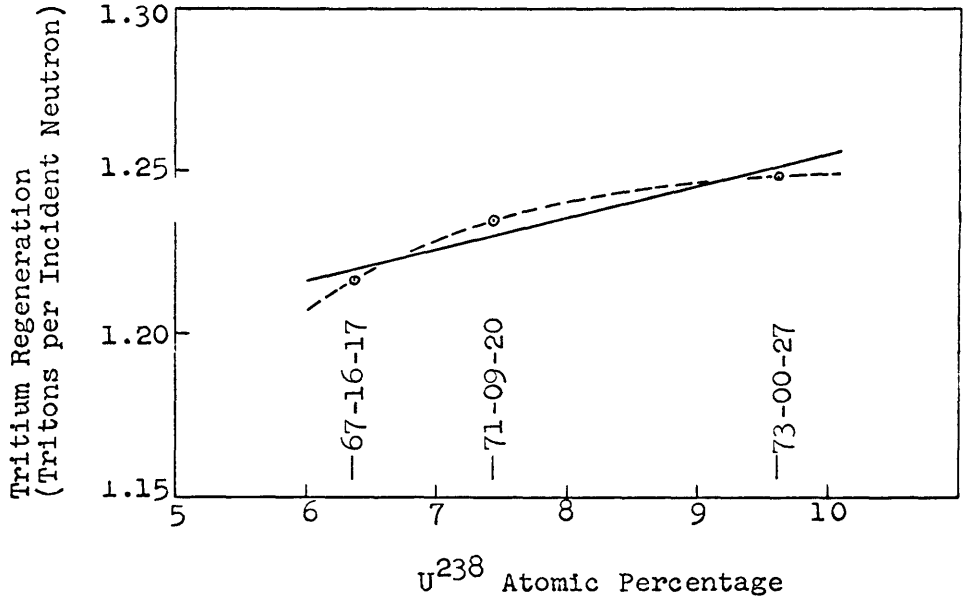

Fig. 21. Net worth of U^{238} in the primary attenuator.

Table 10. Comparison of the effects of fused-salt composition in a 50% Li^6 enriched fissile attenuator blanket.

Uranium Salt	$73LiF-27UF_4$	$71LiF-9BeF_2-20UF_4$	$67LiF-16BeF_2-17UF_4$
Run Number	3-520	3-515	3-536
Total Multiplication	0.6396	0.5738	0.5421
U^{238} Multiplication	0.4439	0.3602	0.3152
Total Fission	0.1090	0.0883	0.0771
Total Absorption	1.5941	1.5269	1.4924
U^{238} Absorption	0.2222	0.1669	0.1468
Total Tritium	1.2483	1.2357	1.2166
Li^6 (n,t)	1.2046	1.1888	1.1705
Leakage < 0.4 Mev	0.0273	0.0252	0.0257
Leakage > 0.4 Mev	0.0343	0.0354	0.0367

Results are per unit incident neutron.

Table 11. Effects of Be enrichment in the fissile attenuator blanket with the 73-00-27 salt and 50% Li^6 enrichment.

Be Enrichment	None	5 cm
Run Number	3-520	3-527
Total Multiplication	0.6396	0.7010
U^{238} Multiplication	0.4439	0.4030
Be Multiplication:		
In Coolant Region	0.0131	0.0131
In Attenuator Region	-	0.1058
Total Fission	0.1090	0.0997
Total Absorption	1.5941	1.6532
U^{238} Absorption	0.2222	0.2208
Total Tritium	1.2483	1.3027
Li^6 (n,t)	1.2046	1.2599
Leakage < 0.4 Mev	0.0273	0.0276
Leakage > 0.4 Mev	0.0343	0.0358

Results are per unit incident neutron.

considerations that bear directly on the choice of system are the fast fission rate and the U^{238} (n, γ) Pu^{239} reaction rate in the blanket. The benefits that may be derived from the fission energy in terms of total reactor power output will be analyzed in Section IV. It may be pointed out now that the fissile attenuator scheme maximizes the total number of fission reactions, yet maintains a reasonably low fission density in the wide attenuator region. Blankets with a high uranium content salt-coolant region yield half the fissions of the fissile attenuator system, but here the reactions occur in a narrow region and the fission density is high. Therefore, it appears that the blankets with a UF_4 primary attenuator region are more advantageous.

Assuming that the demand for fission reactor fuel will be sufficiently high to warrant the extraction of the Pu^{239} by-product from the blanket, the efficient manufacture of plutonium may possess tangible economic advantages. Pu^{239} and tritium production are opposite effects and a balance may be struck by proper choice of Li^6 enrichment. Figure 22 shows the inverse relationship between Pu^{239} production and tritium regeneration in standard fissile attenuator and fissile coolant configurations with the 27% UF_4 fused salt. The maximum plutonium breeding in the blanket with the fissile coolant region is only ~0.18 Pu atom per D-T fusion reaction, if reasonable tritium production is to be achieved also. In the case of the UF_4 attenuator region it is near 0.32 Pu atom per fusion

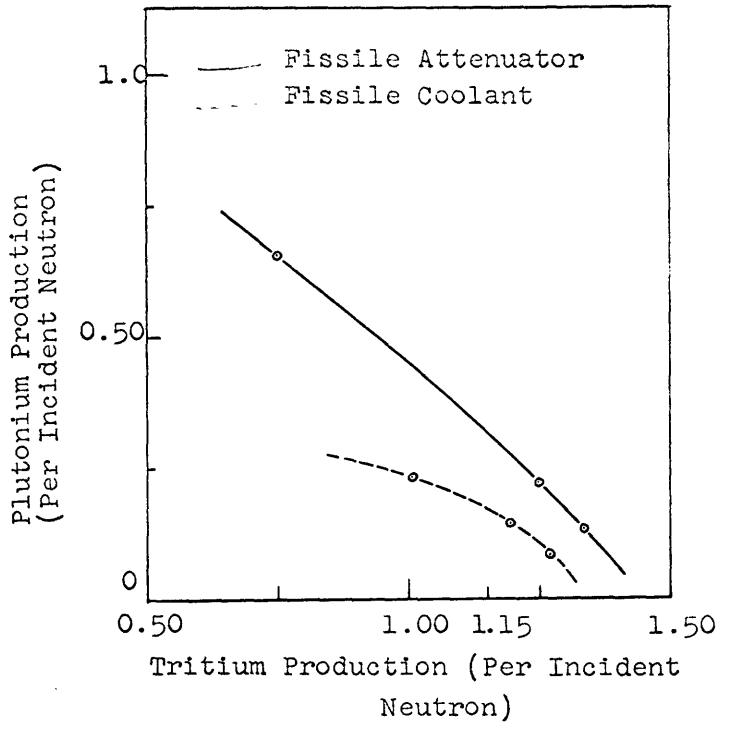

Fig. 22. Pu^{239} versus tritium production for standard fissile attenuator and fissile-coolant blankets with the 73-00-27 fused salt.

for similar tritium production. Under operating conditions with, say, 45% Li^6 enrichment, the latter blanket configuration will produce ~0.25 Pu atom for each D-T fusion; this represents a potential gain in ultimate power generation of approximately 250%. The fissile primary attenuator blanket is superior from the point of economic and ultimate power gain through plutonium recovery.

IV. NUCLEAR HEATING RATES

4.1 METHOD OF ANALYSIS AND SOURCE OF DATA

The mathematical models, calculational techniques, and computer codes developed by W. G. Homeyer for investigating the heating rates in nonfissile blankets were applicable without modification to the present study. The integral-spectrum model of gamma-ray transport was used for most of the calculations. The comparison of the results of the build-up factor and the integral-spectrum calculations for a number of cases showed that the difference in total heat generation does not exceed 3%. Furthermore, as Homeyer points out, the integral-spectrum method conserves gamma energy and its difference from the build-up factor calculations tends to cancel the known errors of the method.

All γ-ray energy spectrum and local heating data for the nonfissile nuclides used in this investigation were derived from Homeyer's work. The γ-ray spectra resulting from the various nuclear reactions in U^{238} and Th^{232} were obtained from experimental sources or calculated. The prompt fission γ-ray spectrum of U^{235} was used for both U^{238} and Th^{232} on the strength of the findings of Protopopov and Shiryaev[13] and of Kirkbride,[14] which show no significant difference in the spectral distribution for other fissile elements, and that the fission γ energy is independent of the bombarding neutron energy. The delayed γ-ray spectrum from the de-excitation of the fission fragments was approximated by the same distribution as the prompt γ-rays (a reasonable assumption up to 200-sec decay time,[15]) and the total fission γ energy was taken as the sum of these two sources of γ energy. The numerical values were taken from Blizard.[15]

The neutron-capture gamma spectra were given by Campion et al.[16] for U^{238}, and by Groshev et al.[17] for Th^{232}. The total capture γ energy was derived from the calculated binding energy of the captured neutron.[18] The inelastic scattering γ energy spectrum at high (>1.9 Mev) incident energies and the (n, 2n) γ spectrum were calculated with the statistical model from measured nuclear temperature data.[19] The (n, 3n) reaction was neglected, since the sum of the binding energies of the emitted neutrons and their most probable energy approximately equals the incident neutron energy. The (n, n') γ spectrum was calculated from the Gaussian model in the 1.4-1.9 Mev incident energy range, and for lower energies measured nuclear level energies[20] and excitation functions[21,22] were used.

The values for the fission fragment energies for Th^{232} were taken from Smith, Nobles and Friedman,[23] and for U^{238} from Stevenson et al.[24] The total β-particle energy released in both thorium and uranium fission was assumed to be 6 Mev.[15] The β energy emitted in the (n, γ), (n, 2n) and (n, 3n) reactions were calculated from the data given by Hellwege.[20] Since the probability of heavy charged-particle emission is very small for both Th^{232} and U^{238}, such reactions were neglected. Table 12 summarizes the reaction energetics of the two fissile nuclides.

Table 12. Reaction energetics of Th^{232} and U^{238}.

Reaction	Charged Particle Kinetic Energy	Gamma Ray Energy	Total Energy (Mev/Reaction
(n,f)			
Th^{232}	163	12.7	175.7
U^{238}	181	12.7	193.7
(n,γ)			
Th^{232}	1.56	5.09	6.65
U^{238}	1.53	4.71	6.24
(n,2n)			
Th^{232}	0.32	-	-
U^{238}	0.25	-	-

Note:

a) (n,n') and (n,2n) gamma energy is a function of incident neutron energy.

b) (n,3n) reaction is assumed to go directly to the ground state of the stable residual nucleus.

The gamma-ray absorption and attenuation coefficients for the fissile nuclides were taken from published tables of calculated values.[25] In determining the equivalent atomic charge (Z) for the build-up factor calculations the same tables were used. The neutron reaction cross sections of Th^{232} and U^{238} listed in Appendix B were employed in the heating-rate calculations.

4.2 BLANKET WITH A FISSILE FIRST WALL

The analysis of the thorium first-wall blankets (described in section 3.2) indicates excessively high heat generation in the first wall. The 2.0-cm Th wall configuration with natural Li yields approximately 24.2 Mev of recoverable energy for each incident 14.2-Mev neutron; 10.4 Mev of this is liberated in the first wall. Approximately 52% of the first-wall heating is caused by the thorium fission fragment and β-particle kinetic energies; approximately 30% results from the absorption of thorium gamma rays. The thorium reactions contribute 30% of the total heat generation in the blanket.

The calculations for the blanket configuration with 50% Li^6 enrichment show only a negligible decrease in the total heat generation. Reduction of the Th neutron capture rate lowers the first-wall heating approximately 8.3%, but the gain in Li^6 (n, t) reactions in the adjacent fused-salt region compensates for this loss. Figure 23 compares the heating rates in the natural and 50% Li^6 blankets. The sharp peak in the total heating curve of the first wall at the coolant-wall interface is caused by the absorption of the high γ flux originating in the fused salt. The thorium gamma radiation is absorbed for the most part in the first wall, and its effect on the heating in the other regions is very small.

Investigation of the effects of varying the Th wall thickness indicates that the total heat generation in the blanket changes directly with the first-wall width roughly at the rate of 1.5 Mev per cm change in Th (per 14.2 Mev incident neutron). The variation of the first-wall heating is approximately 1.25 times that of the whole blanket.

The results of the Th blanket heating-rate calculations are compared with a nonfissile blanket in Table 13. It is seen that in the identical 2 cm first wall configuration, the heat generation in the coolant and primary attenuator regions is almost equal for the Mo and the Th blanket. The heating in the Th wall, however, is nearly three times that in the Mo wall. Reduction of the Th thickness to 1 cm (and 50% Li^6 enrichment) decreases this ratio to ~1.6. For this case, the thorium blanket yields only 21% more energy recovery than the nonfissile assembly.

The thermal stress in the Th^{232} wall was calculated by the method indicated in Appendix C. The maximum reactor power (neutron energy flux) is evaluated by setting the thorium yield strength as the design limit. Therefore the results shown in Table 14 are obtained. Since the maximum power for the nonfissile blanket is approximately

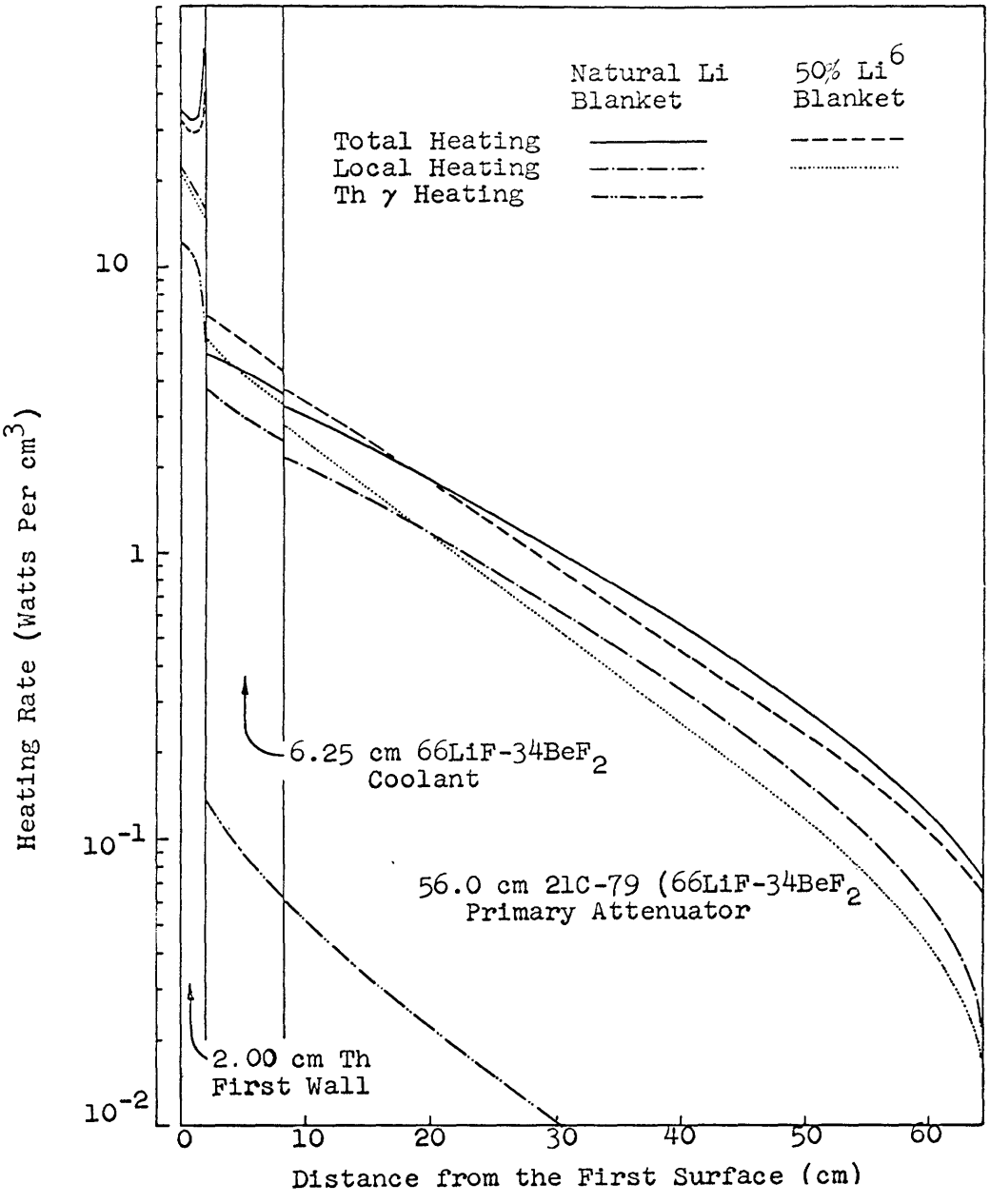

Fig. 23. Heating rate distribution in a Th^{232} first-wall blanket configuration. (Incident energy flux, 100 watts/cm^2.)

Table 13. Heat generation in Th^{232} first-wall blankets.

Run Number	3-531	3-530	3-517	3-503	3-113[a]
First Wall Material	Th	Th	Th	Th	Mo
First Wall Thickness	1.00 cm	1.50 cm	2.00 cm	2.00 cm	2.00 cm
Li^6 Concentration	50%	50%	50%	Natural	Natural
First Wall Heating:					
Total	41.2	54.6	67.4	73.5	25.0
Gamma	21.1	25.8	30.7	35.5	24.0
Coolant Heating:					
Total	35.3	35.4	35.4	28.0	28.3
Gamma	8.6	8.0	7.5	8.0	8.5
Attenuator Heating:					
Total	72.4	69.8	67.2	69.3	69.5
Gamma	27.5	25.7	24.0	25.3	26.4
Total Fission Energy	24.9	35.5	41.0	41.0	
Blanket Heating (Total)	148.9	159.8	170.0	170.8	122.8

All results are percent of neutron energy flux incident on first surface.
All calculations are for: 6.25 cm 66LiF-34BeF_2 coolant region
and 56.0 cm 21C-79(66LiF-34BeF_2) primary attenuator.

a) Calculations made by W. G. Homeyer

Table 14. Thermal stress in the Th first wall (50% Li^6 enrichment).

Th Wall Width (cm)	$(\sigma_{Max})_T$ at 1 Mw/m^2 (psi)	Maximum Power (Mw/m^2)
1.0	8040	4.36
1.5	14750	2.37
2.0	23100	1.53

5 Mw/m^2 (with a safety factor of two), it is clear that the metallic Th wall blankets are not competitive. (At high temperatures, the strength of thorium decreases rapidly, and the reactor power is limited even more.) Therefore, the fissile first-wall blanket is impractical on the basis of excessive thermal stresses in the first wall.

4.3 BLANKETS WITH URANIUM FUSED SALTS

a. Blankets with UF_4 in the First-Wall Coolant

The heating analysis of the blankets with a UF_4 salt coolant region (refer to section 3.3b) will be discussed briefly. Investigation of the 60-30-10 fused-salt blanket (see Table 15) indicates that the reduction of the first-wall thickness from 2.5 cm to 1.0 cm results in a 5% increase of the total heat generation. A 20% Li^6 enrichment in the 1-cm Mo wall configuration yields a 2% gain in heating (for higher UF_4 content the gain will be less), and the addition of 5 cm of metallic Be to the primary attenuator increases the heat generation nearly 3%. Calculations show that the various uranium reactions are responsible for approximately 24% of the total blanket heating, and that nearly 97% of the uranium energy is deposited in the first-wall coolant region. The heating-rate distributions in a 60-30-10 fissile coolant blanket are shown in Fig. 24 (the total heating curve in the 73-00-27 system is shown for comparison).

Table 16 shows the results of the heating calculations for several uranium salt systems. Heat goes up with increasing uranium concentration. The first-wall heating varies inversely with the UF_4 content in the coolant, owing to the high γ-ray absorption cross section for uranium. Comparison with a nonfissile blanket of similar design

Table 15. Heat generation in 60-30-10 coolant blankets.

Run Number	3-507	3-529	3-508	3-512	3-513
First Wall Thickness (Mo)	2.50 cm	1.75 cm	1.00 cm	1.00 cm	1.00 cm
Li^6 Concentration	Natural	Natural	Natural	20%	Natural
Be Addition to Attenuator	0	0	0	0	~5 cm
First Wall Heating:					
Total	24.5	18.2	11.5	10.8	11.4
Gamma	23.5	17.4	11.0	10.3	10.9
Coolant Heating:					
Total	63.8	69.7	77.0	78.7	77.2
Gamma	23.5	25.5	28.0	27.0	37.5
Attenuator Heating:					
Total	57.4	61.0	64.9	67.6	69.0
Gamma	18.2	20.3	22.6	22.3	20.9
Total Fission Energy	28.1	32.1	36.8	36.9	36.9
Blanket Heating (total)	145.8	148.9	153.4	157.1	157.6

All results are percent of neutron energy flux incident on first surface.
All calculations are for: 6.25 cm 60LiF - 30BeF_2-10UF_4 Coolant Region
and 49.0 cm 21C - 79(66LiF - 34BeF_2) primary attenuator

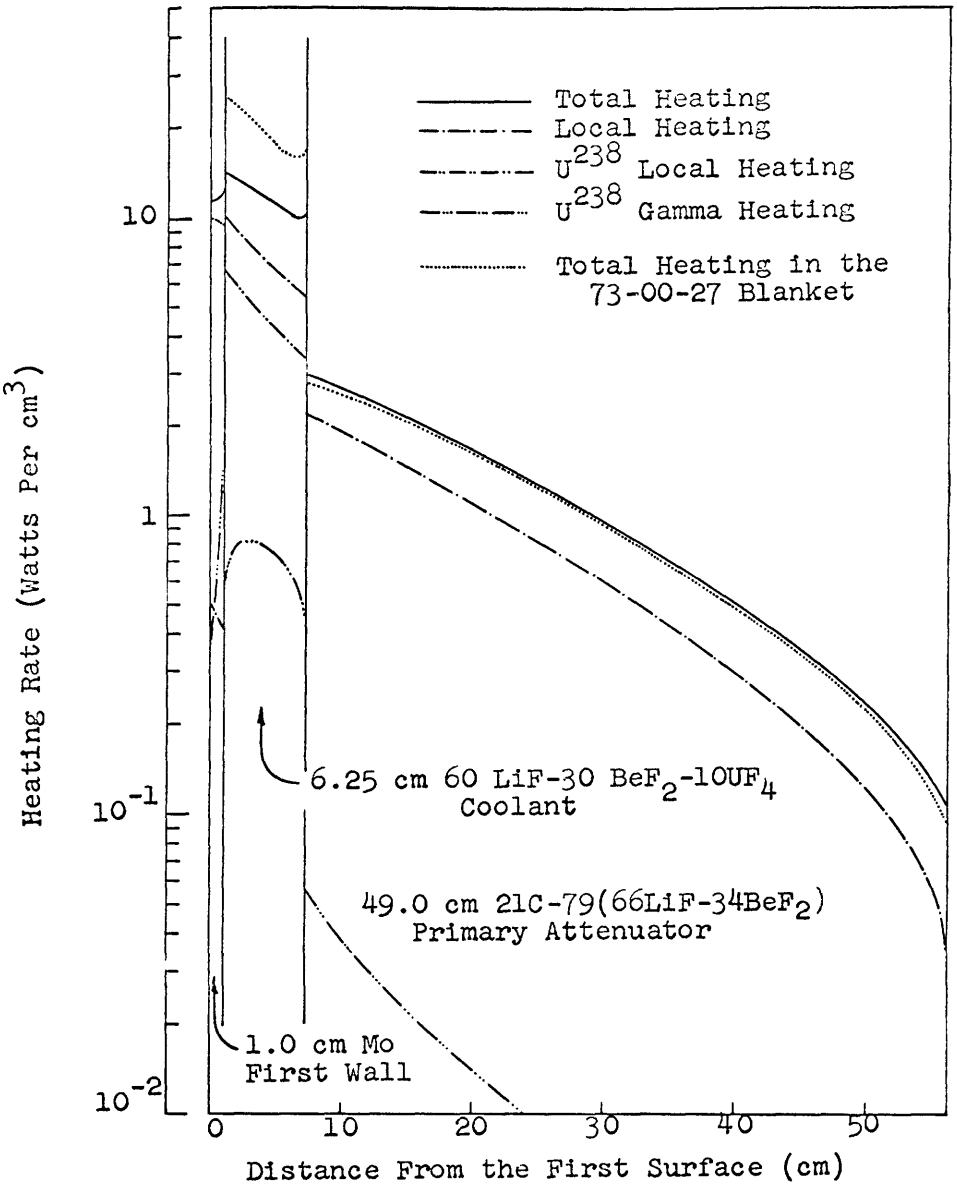

Fig. 24. Heating rate distribution in a fissile coolant (60-30-10) blanket with natural Li. (Incident energy flux, 100 watts/cm^2.)

Table 16. Heat generation in fissile coolant blankets.
(Natural Li composition)

Run Number	3-506[a]	3-537	3-509	3-532	3-508	3-111[b]
$LiF-BeF_2-UF_4$ Coolant Composition	73-00-27	71-09-20	71-16-13	74-16-10	60-30-10	66-34-00
First Wall Heating:						
Total	9.9	10.2	10.8	11.2	11.5	15.7
Gamma	9.2	9.8	10.4	10.8	11.0	15.2
Coolant Heating:						
Total	135.0	112.0	90.7	77.6	77.0	31.9
Gamma	41.7	36.3	31.1	27.3	28.0	10.5
Attenuator Heating:						
Total	62.9	62.3	65.7	65.1	64.9	75.7
Gamma	19.1	20.4	21.7	23.0	22.6	29.5
Total Fission Energy	89.5	69.0	48.6	37.8	36.8	
Blanket Heating (Total)	207.8	184.6	167.1	153.9	153.4	123.3

All results are percent of neutron energy flux incident on first surface.
All calculations are for: 6.25 cm coolant region
and 49.0 cm 21C-79 ($66LiF-34BeF_2$) primary attenuator.

a) Calculations made with 6.68 cm coolant region.

b) Calculations made by W. G. Homeyer (with 56.0 cm primary attenuator)

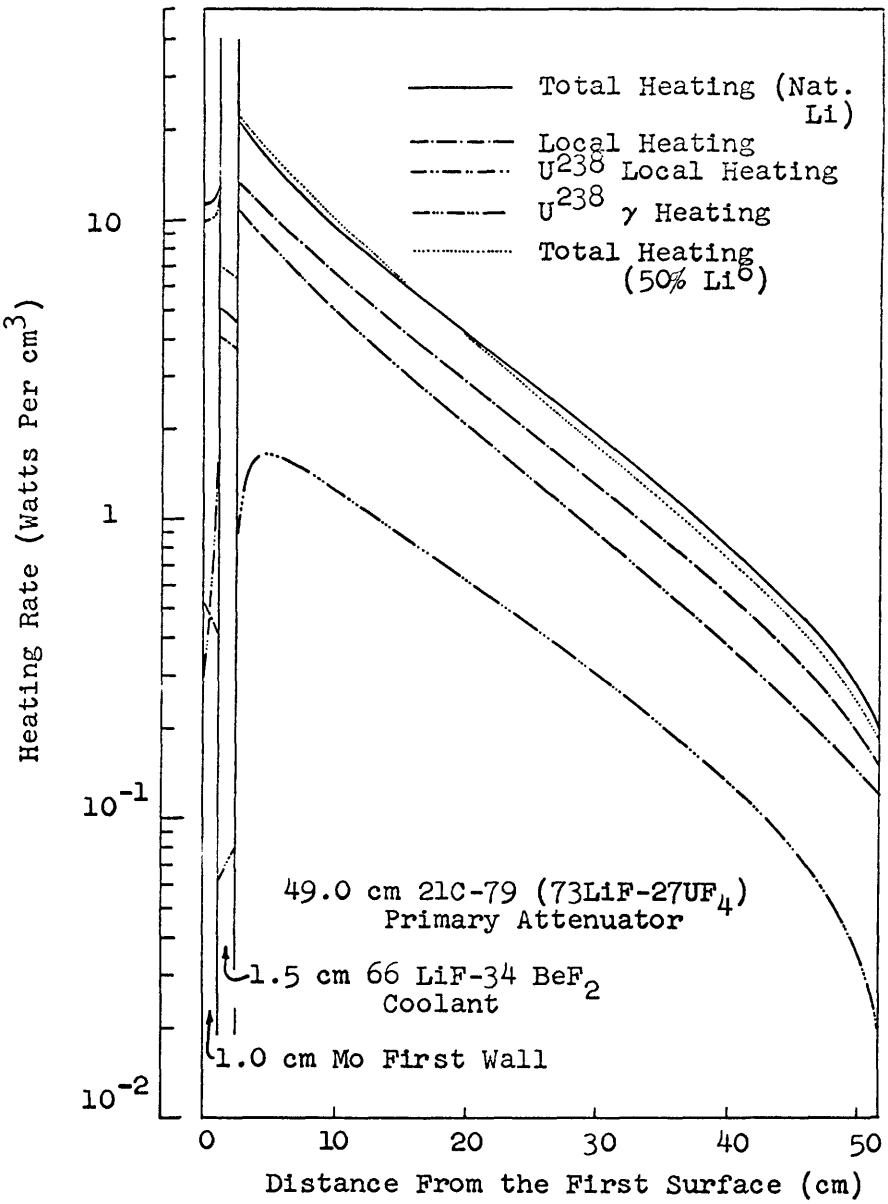

Fig. 25. Heating rate distribution in a fissile attenuator (73-00-27) blanket. (Incident energy flux, 100 watts/cm^2.)

Table 17. Heat generation in fissile attenuator blankets.

Run Number	3-519	3-520	3-515	3-536	3-111[a]
$LiF-BeF_2-UF_4$ (Attenuator) Composition	73-00-27	73-00-27	71-09-20	67-16-17	66-34-00
Li^6 Concentration	Natural	50%	50%	50%	Natural
First Wall Heating:					
Total	11.7	10.2	10.4	10.5	15.7
Gamma	11.2	9.7	9.9	10.0	15.2
Coolant Heating:					
Total	7.3	10.2	10.0	10.0	31.9
Gamma	1.4	1.2	1.3	1.3	10.5
Attenuator Heating:					
Total	244.5	244.3	217.3	202.6	75.7
Gamma	75.8	63.8	58.8	56.7	29.5
Total Fission Energy	150.2	148.8	120.2	105.2	
Blanket Heating (total)	263.5	264.7	237.7	223.1	123.3

All results are percent of neutron energy flux incident on first surface.
All calculations are for: 1.5 cm $66LiF-34BeF_2$ coolant region
and 49 cm 21C - $79(LiF-BeF_2-UF_4)$ primary attenuator

a) Calculations made by W. G. Homeyer (for standard configuration)

indicates that a maximum increase in total heat generation of approximately 89% may be gained by the use of a fissile coolant salt.

b. Blankets with UF_4 in the Primary Attenuator

Heat recovery is optimized in the fissile attenuator configuration (see section 3.3c). Figure 25 shows the heating rates for the 27% UF_4 attenuator system. Approximately 90% of the total heat generation takes place in the attenuator region where nearly all of the energy of the uranium reactions is deposited. Uranium reactions contribute 60% of the blanket heating. Comparison with the Th first-wall blanket and the UF_4 coolant blanket heating rates (Figs. 23 and 24) shows more even heat distribution, hence more efficient utilization of the primary attenuator region.

The results given in Table 17 indicate that both the first wall and the first-wall coolant heating are only slightly dependent on the UF_4 content of the primary attenuator. The total heat generation in the first two regions is nearly constant for the various salt compositions (as will be seen, this is an important property of the system). Li^6 enrichment has negligible effect on the total blanket heat recovery; however, the decrease of the first-wall heating and the increase of the coolant heating, owing to Li^6 enrichment, are significant. Comparison with a nonfissile blanket assembly shows that the use of a UF_4 fused salt in the primary attenuator region increases the total heat recovery as much as 110%.

c. Evaluation of Results

The results of the first-wall coolant heat-transfer calculations (see Appendix C) for the two uranium fused-salt blanket configurations are shown in Table 18. The incident neutron energy flux was taken to be 5 Mw/m^2, and a 30 inch long cooling channel was

Table 18. Heat-transfer results.

	Blanket Configuration		
	Fissile Coolant Region		Fissile Primary Attenuator
Coolant Salt (LiF-BeF_2-UF_4)	71-09-20	71-16-13	66-34-00
Mo Wall Temp. Drop (^oC)	95	82	82
Film Temp. Drop (^oC)	62	60	27
Coolant Velocity (m/sec)	10.3	8.6	6.1
Pumping Power to Heat Transfer Ratio	1.35%	0.56%	0.09%

considered. The coolant inlet-outlet bulk temperature rise was assumed to be 70°C for the uranium salts and 100°C for the nonfissile salt. The thermal stress in the first wall is about 12,000 psi for both configurations.

The heating-rate and the heat-transfer calculations bring out the following points.

1. For a given D-T fusion rate, the thermal power output of a fissile attenuator blanket is approximately 27% higher than that of a fissile coolant region blanket with the same uranium salt system.

2. In a fissile attenuator configuration the heat-transfer characteristics of the first wall and the wall-coolant region are approximately constant for all uranium salt compositions and depend only on the nuclear power level. In fissile coolant blankets the heat-transfer characteristics deteriorate with increasing uranium content.

3. For a reasonable nuclear power level (5 Mw/m^2 incident neutron energy flux), and at comparable thermal power output (10 Mw/m^2 or more), the fused-salt velocity in the first-wall coolant region is approximately 2 times higher in a fissile coolant assembly than in a fissile attenuator blanket; the corresponding pumping loss is 20 times greater; and the film temperature differential at the first wall-coolant interface is more than 2 times greater. Therefore, the blanket configuration with the uranium fused-salt primary attenuator appears to be definitely the better design.

V. CONCLUSIONS

The sources of error in this investigation result from the approximate nature of the theoretical methods and uncertainties in the experimental data. Impink showed that there is reasonable correlation between experimental measurements and his calculated results. The errors in the neutronic calculations arising from the computational methods and the nuclear cross section data are estimated to be less than 10%. The errors in the heating-rate calculations arising from the γ transport and γ spectrum assumptions are estimated by Homeyer to be less than 5%. In the present work there is an uncertainty of approximately 5% in the estimation of some UF_4 fused-salt densities. Therefore, the absolute error for both the nuclear reaction rate and the heating rate results should not exceed 15%. Care was excercised to preserve internal consistency throughout the study and the relative errors in the results are probably less than 5%.

Based on the foregoing analyses, the following conclusions may be drawn with reasonable certainty.

1. Blankets with a $LiF\text{-}BeF_2\text{-}UF_4$ salt primary attenuator region containing a high concentration of U^{238} (17 to 27 mole percent UF_4), and with approximately 50% Li^6 enrichment appear to be feasible and practical. This configuration optimizes the benefits that may be derived from the use of fissile nuclides, and utilizes the large primary attenuator volume as the main heat-recovery region. The heat generation in the first wall and the first-wall coolant region depends only on the thermonuclear fusion power level; this leads to a significant design consideration that the first wall and the coolant temperatures and heat-transfer characteristics are independent of the final fission thermal power output (UF_4 content) of the blanket.

The calculated tritium regeneration ratios are in excess of 1.2 tritons per incident neutron; thus a self-sustained tritium cycle is ensured. The heating rates in the Mo first wall and the nonfissile coolant region are comparable to that in fission-free blankets, and operation at an incident neutron energy flux of ~5 Mw/m^2 is possible. The fast fission reaction almost doubles the recoverable energy liberated in the blanket, and approximately 90% of the heat is generated in the primary attenuator. Substantial production of Pu^{239} (one atom per five D-T fusion reactions) may have considerable economic implications in terms of fission reactor fuel. If fission of this Pu^{239} is also accomplished (in some other device), the output of the entire combined system is approximately doubled again.

2. The performance of the blanket systems with a UF_4 fused-salt first-wall coolant is considered to be marginal. The total heat recovery is approximately 20% less than that in a fissile attenuator configuration with the same UF_4 salt mixture. More than half of the blanket heat generation occurs in the narrow first-wall coolant region, and a high coolant velocity with a correspondingly high pumping power expenditure is required.

3. The fissile first-wall blanket configuration is not feasible. Uranium metal is unsuited because of its low melting point. A thorium first-wall blanket is limited to

impractically low operating power levels, owing to excessive thermal stress in the first wall.

It is recommended that in future work on the blanket problem the limitations imposed by the corrosive properties of the fused salts should be explored. The problems associated with long-lived radioactive isotope build-up in the fissile blankets require thorough investigation. The state of the study at present is sufficiently far advanced that a comprehensive economic appraisal of the various nonfissile and fissile blanket configurations is possible and is definitely desirable.

APPENDIX A

Resonance Capture in a Homogeneous Mixture of Nuclides

Accurate calculation of resonance absorption is essential in the neutronic analysis of plasma blankets. The low-energy neutron fluxes in a blanket cannot be described by an inverse energy dependence (owing to high neutron absorption rates in the first wall and in the Li salts); consequently, the effective resonance integral concept does not apply. Therefore, a multigroup treatment of neutron downscattering and the use of group effective absorption cross sections are required.

A. J. Impink, following the approach of Wigner et al.,[26] formulated a resonance absorption model for a medium containing a single nuclide. The extension of this model (by using a procedure suggested by Impink), in order to treat the general case of a homogeneous mixture of nuclides, is presented here. For the LiF-BeF_2-UF_4 salts, the general model reduces to a particularly convenient form and allows a graphical evaluation of the group cross sections for the various salt compositions.

A.1 GENERAL DERIVATION

Several terms need to be defined.

1. The effective energy width of a resonance is the energy difference between those two points on the resonance peak where the resonance capture cross section is equal in magnitude to the potential scattering cross section of the medium.

2. A narrow resonance is one whose effective width is less than or equal to the average energy lost by a neutron in an elastic collision with a nuclide in the medium.

3. A wide resonance is one whose effective width is greater than the average energy lost by a neutron in an elastic collision.

4. The volume contribution to resonance capture results from the downscattering of neutrons (within the medium) into a resonance.

5. The surface contribution to resonance capture results from neutrons that are incident on the surface of the medium with energies within the width of a resonance.

Impink derived the following relationships for the group effective resonance capture cross sections and the surface-resonance weighting terms for a single nuclide medium. (Notation is defined in a glossary appended to this section.)

Effective Cross Section

(i) Narrow Resonance

$$\hat{\Sigma}_a|_i = \Sigma_s|_i \left[\frac{1}{(1-\alpha)\,\Delta E)_i} \left\{ (E_o - \epsilon) \ln \left\{ \frac{E_o + \epsilon}{E_o - \epsilon} \right\} - 2\epsilon(1 - \ln \alpha) \right\} \right] \left(\frac{\Gamma_\gamma}{\Gamma} \right) \qquad \text{(A.1)}$$

(ii) Wide Resonance

$$\hat{\Sigma}_a\big|_i = \Sigma_s\big|_i \left[\frac{E_o + \epsilon}{\Delta E)_i}\left\{\frac{1}{1-\alpha}\ln\frac{1}{\alpha} - 1\right\}\right]\left(1 - \left\{\frac{\Gamma_n}{\Gamma}\right\}^{\frac{\Delta u)_r}{\xi}}\right), \tag{A.2}$$

where the term in brackets is the probability of a neutron in group i scattering into resonance r (within group i), and the term in parentheses is the probability of capture within the resonance.

Surface Effect

(i) Narrow Resonance

$$\text{Weight term} \approx \left[\frac{\Delta E)_r}{\Delta E)_i}\frac{\Gamma_\gamma}{\Gamma}\frac{1}{4\Sigma_r}\right]. \tag{A.3}$$

(ii) Wide Resonance

$$\text{Weight term} \approx \left[\left(\frac{1}{2}\left\{\frac{1-\frac{\Gamma_n}{\Gamma}}{1-\frac{\Gamma_n}{2\Gamma}}\right\}\left\{1-\left(\frac{\Gamma_n}{2\Gamma}\right)^{\frac{\Delta u)_r}{4\xi}}\right\} + \frac{1}{2}\left\{1-\left(\frac{\Gamma_n}{2\Gamma}\right)^{\frac{3\Delta u)_r}{4\xi}}\right\}\right)\frac{1}{4\Sigma_r}\right]. \tag{A.4}$$

(The surface resonance is defined as $[\ ]\, S_i(0^+)$, where $S_i(0^+)$ is the group (neutron) source strength per unit volume at point 0^+, just outside the boundary of the absorbing medium.)

Consider a medium that contains a homogeneous mixture of K nuclides, the k^{th} nuclide having an atomic density of N_k. Now, let us look at a resonance of nuclide 1 in an energy group i. The macroscopic potential scattering cross section of the medium is

$$\Sigma_s\big|_i = \sum_{k=1}^{K} N_k \sigma_s\big|_{i)_k}. \tag{A.5}$$

The effective energy width of the resonance, $\Delta E)_r$, is evaluated at the total potential scattering cross section per atom of nuclide 1 (that is, $\frac{1}{N_1}\Sigma_s\big|_i$). The absolute resonance parameters Γ_γ, Γ_n, and Γ are not functions of the composition of the mixture; α and ξ are properties of the individual nuclides and are also independent of the relative ratio of the nuclides. Therefore, the equations for a homogeneous mixture, corresponding to Eqs. (A.1) to (A.4) may be obtained by summing over all nuclide species.

Effective Cross Section

(i) Narrow Resonance

$$\Sigma_a|_i = \Sigma_s|_i \frac{1}{\Delta E)_i}\left(\frac{\Gamma_\gamma}{\Gamma}\right)\sum_{k=1}^{K}\frac{1}{(1-a_k)}\left\{(E_o-\epsilon)\ln\left\{\frac{E_o+\epsilon}{E_o-\epsilon}\right\}-2\epsilon(1-\ln a_k)\right\}\frac{N_k}{N_T}. \qquad \text{(A. 6)}$$

(ii) Wide Resonance

$$\hat{\Sigma}_a|_i = \Sigma_s|_i \frac{E_o+\epsilon}{\Delta E)_i}\sum_{k=1}^{K}\left\{\frac{1}{1-a_k}\ln\frac{1}{a_k}-1\right\}\left(1-\left\{\frac{\Gamma_n}{\Gamma}\right\}^{\frac{\Delta u)_r}{\xi_k}}\right)\frac{N_k}{N_T}. \qquad \text{(A. 7)}$$

Surface Effect

(i) Narrow Resonance

The weight term is given by (A. 3).

(ii) Wide Resonance

$$\text{Weight term} \approx \frac{1}{8\Sigma_r}\left[\left\{\frac{1-\frac{\Gamma_n}{\Gamma}}{1-\frac{\Gamma_n}{2\Gamma}}\right\}\left\{1-\sum_{k=1}^{K}\left(\frac{\Gamma_n}{2\Gamma}\right)^{\frac{\Delta u)_r}{4\xi_k}}\frac{N_k}{N_T}\right\}+1-\sum_{k=1}^{K}\left(\frac{\Gamma_n}{2\Gamma}\right)^{\frac{3\Delta u)_r}{4\xi_k}}\frac{N_k}{N_T}\right]. \qquad \text{(A. 8)}$$

For neutron groups with several resonances (not necessarily all of one nuclide), both the groups' effective resonance capture cross section, given by (A. 6) or (A. 7), and the surface weight term, given by (A. 3) or (A. 8), for each resonance are additive. In computer calculations, it is convenient to assign all of the resonances in the mixture to one particular nuclide; and the microscopic group effective cross section is then expressed as "per atom of absorber nuclide."

A. 2 LiF-BeF_2-UF_4 SYSTEMS

The potential scattering cross section for a fused salt is given by (A. 5). Elastic neutron scattering, however, must be considered on a molecular scale, since the atoms are bound. The average maximum fractional neutron energy loss per collision with a salt molecule is approximated by

$$(1-\bar{a})_i = \frac{\sum_{j=1}^{m}\sigma_s|_{i)_j} n_j\left[\frac{A_j-1}{A_j+1}\right]^2}{\sum_{j=1}^{m}\sigma_s|_{i)_j} n_j}, \qquad \text{(A. 9)}$$

where m is the number of elements in the molecule, n_j is the number of atoms of element j per molecule, A_j is the mass number of element j, and $\sigma_s|_i)_j$ is the microscopic potential scattering cross section of element j (for energy group i). It may be assumed that $\sigma_s|_i)_j$ is constant in the resonance energy region, and then the subscript i may be deleted from (A. 9).

For the LiF-BeF_2-UF_4 salts, the average neutron energy loss in an elastic collision with a constituent molecule is greater than the effective width of the pertinent U^{238} resonances. Therefore, only narrow resonance calculations are of interest. From (A. 9), we find that $(1-\bar{\alpha})$ for LiF is only approximately 2% lower than that of BeF_2; consequently, by use of properly averaged values of $(1-\bar{\alpha})$ and $\ln \bar{\alpha}$, the two molecules may be treated as identical scatterers. From (A. 6), it follows that for a single resonance

$$\hat{\Sigma}_a|_i = \Sigma_s \frac{1}{\Delta E_i}\left(\frac{\Gamma_\gamma}{\Gamma}\right)\left[\frac{1}{(1-\bar{\alpha})_{ave}}\left\{(E_o-\epsilon)\ln\left\{\frac{E_o+\epsilon}{E_o-\epsilon}\right\} - 2\epsilon(1-(\ln\bar{\alpha})_{ave})\right\}\left(1-\frac{M_u}{M_T}\right)\right.$$

$$\left. + \frac{1}{\left(1-\bar{\alpha}_{UF_4}\right)}\left\{(E_o-\epsilon)\ln\left\{\frac{E_o+\epsilon}{E_o-\epsilon}\right\} - 2\epsilon\left(1-\ln\bar{\alpha}_{UF_4}\right)\right\}\left(\frac{M_{UF_4}}{M_T}\right)\right], \qquad \text{(A. 10)}$$

where Σ_s is obtained from (A. 5) by assuming $\sigma_s|_i$ to be constant throughout the resonance energy range, $(1-\bar{\alpha})_{ave}$ and $(\ln\bar{\alpha})_{ave}$ refer to LiF and BeF_2, $\left(1-\bar{\alpha}_{UF_4}\right)$ and $\ln\bar{\alpha}_{UF_4}$ refer to UF_4, and M_{UF_4} and M_T are UF_4 and total molecular densities, respectively.

Division of both sides of (A. 10) by N_U, the atomic density of U^{238} in the mixture, eliminates the density dependence, and the equation reduces to the form

$$\frac{\hat{\Sigma}_a|_i}{N_U} = F_i\left(\frac{\Sigma_s}{N_U}, \frac{M_{UF_4}}{M_T}\right), \qquad \text{(A. 11)}$$

where F_i indicates the functional form of (A. 10). (Note that ϵ is a function of $\frac{1}{N_U}\Sigma_s$.) For a group with several resonances, (A. 11) may be summed to yield the total group cross section. Therefore, the group effective resonance capture cross section of the salt (per U^{238} atom) is a function only of the potential scattering cross section of the salt (per U^{238} atom) and of the mole percentage of UF_4 in the salt. A plot of $F_i)_{total}$ versus Σ_s/N_U for several UF_4 compositions results in a set of curves from which the group effective cross section for any mixture may be estimated.

The surface-resonance weight term may be approached similarly. From (A. 3) we see that the weight term is a direct function of $\Delta E)_r$, which in turn depends on Σ_s/N_U. (The functional dependence on Σ_s/N_U also includes the effects of composition, as is seen in (A. 5).) The total surface-resonance weight per group i is obtained by summing over all resonances in group i. The plot of the total surface weighting term versus Σ_s/N_U gives, then, a single curve for all salt mixtures.

GLOSSARY

Symbol	Definition	Units
A	Atomic mass number	
E_o	Resonance energy	ev, kev
$\Delta E)_i$	Neutron energy group width	ev, kev
$\Delta E)_r$	Resonance energy width	ev, kev
m	Number of elements per molecule	
n	Number of atoms of an element per molecule	
M	Molecular density	cm^{-3}
N	Atomic density	cm^{-3}
$S(0^+)$	Surface source strength	$cm^{-3}\ sec^{-1}$
$\Delta u)_r$	Resonance lethargy width	
α	Maximum fractional energy loss (atom)	
$\bar{\alpha}$	Maximum fractional energy loss (molecule)	
Γ_γ	Resonance gamma emission width	ev, kev
Γ_n	Resonance neutron emission width	ev, kev
Γ	Resonance total width	ev, kev
ϵ	Resonance energy half width	ev, kev
ξ	Logarithmic mean energy decrement	
σ_s	Microscopic potential scattering cross section	cm^2
$\hat{\Sigma}_a$	Effective macroscopic absorption cross section	cm^{-1}
Σ_r	Macroscopic removal cross section	cm^{-1}
Σ_s	Macroscopic potential scattering cross section	cm^{-1}

Subscripts	Reference
i	Neutron group
j	Element in molecule
k	Nuclide in mixture
l	Resonance absorber
T	Total

APPENDIX B

Neutron Cross Sections and Scattering Matrices

B. 1 INTRODUCTION

The purpose here is to summarize and document the nuclear reaction data for Th^{232} and U^{238}. This section may be considered a continuation of A. J. Impink's Appendix D, in which he treats the nonfissile nuclides of interest in the blanket problem.[2] Therefore, we shall retain the format used by Impink.

The 50 group (see Table B. 1) cross sections and the nonelastically scattered neutron and fission neutron spectra of Th^{232} and U^{238} are discussed in sections B. 2 and B. 3. The group cross sections are tabulated and the complete nuclide decks are listed. (The nuclide decks are part of the computer input data, and reference is made to Impink's Appendix C for a detailed description.[2])

Section B. 4 deals with the cases in which U^{238} is a constituent of a fused salt. The high energy cross sections are not altered by the presence of other nuclides and the high energy nuclide decks are identical to that for U^{238} metal. Therefore, only the group cross sections for groups 35 to 50, and the corresponding low-energy nuclide decks are tabulated.

B. 2 Thorium 232

a. High Energy Cross Sections

(i) Total cross section

Good agreement is found between the total cross section curves given by Hughes and Schwartz[27] and by Buckingham, Parker and Pendlebury.[28] The Buckingham curve extends up to 15 Mev and therefore it is used.

(ii) Nonelastic cross section

The nonelastic cross section curve given by Buckingham et al.[28] is not consistent with the sum of the various nonelastic reaction cross sections given by other sources. Values obtained from the sum of the measured individual nonelastic reaction cross sections are used.

(iii) Elastic cross section

For consistency, the elastic cross section is determined from the difference between the total and the nonelastic cross sections. These values are in agreement with experimental values given by Smith[21] in the range 0. 5-1. 5 Mev.

(iv) Radiative capture cross section

There is fair agreement between the experimental values given by Stavisskii and Tolstikov,[29] Barry, O'Connor and Perkin[30] and Lindner and Miskel[31] near 1 Mev; the

TABLE B.1 NEUTRON ENERGY GROUPS

GROUP	MAXIMUM ENERGY MEV	MEAN ENERGY MEV	MINIMUM ENERGY MEV	ENERGY WIDTH MEV	LETHARGY WIDTH
01	14.930	14.200	13.470	1.460	0.1053
02	13.470	12.780	12.120	1.350	0.1053
03	12.120	11.500	10.910	1.210	0.1053
04	10.910	10.350	9.820	1.090	0.1053
05	9.820	9.310	8.830	0.990	0.1053
06	8.830	8.380	7.950	0.880	0.1053
07	7.950	7.540	7.160	0.790	0.1053
08	7.160	6.790	6.440	0.720	0.1053
09	6.440	6.110	5.800	0.640	0.1053
10	5.800	5.500	5.220	0.580	0.1053
11	5.220	4.950	4.690	0.530	0.1053
12	4.690	4.450	4.220	0.470	0.1053
13	4.220	4.010	3.800	0.420	0.1053
14	3.800	3.610	3.420	0.380	0.1053
15	3.420	3.250	3.080	0.340	0.1053
16	3.080	2.920	2.770	0.310	0.1053
17	2.770	2.630	2.490	0.280	0.1053
18	2.490	2.370	2.240	0.250	0.1053
19	2.240	2.130	2.020	0.220	0.1053
20	2.020	1.917	1.818	0.202	0.1053
21	1.818	1.725	1.636	0.182	0.1053
22	1.636	1.553	1.473	0.163	0.1053
23	1.473	1.397	1.325	0.148	0.1053
24	1.325	1.258	1.193	0.132	0.1053
25	1.193	1.132	1.073	0.120	0.1053
26	1.073	1.019	0.966	0.107	0.1053
27	0.966	0.917	0.869	0.097	0.1053
28	0.869	0.825	0.782	0.087	0.1053
29	0.782	0.742	0.704	0.078	0.1053
30	0.704	0.668	0.634	0.070	0.1053
31	0.634	0.601	0.570	0.064	0.1053
32	0.570	0.541	0.513	0.057	0.1053
33	0.513	0.487	0.462	0.051	0.1053
34	0.462	0.440	0.420	0.042	0.1053
35	0.420000	0.364000	0.320000	0.100000	0.2719
36	0.320000	0.265000	0.220000	0.100000	0.3747
37	0.220000	0.162000	0.120000	0.100000	0.6061
38	0.120000	0.091600	0.070000	0.050000	0.5390
39	0.070000	0.045800	0.030000	0.040000	0.8473
40	0.030000	0.017300	0.010000	0.020000	1.0986
41	0.010000	0.006813	0.004641	0.005359	0.7677
42	0.004641	0.003162	0.002154	0.002487	0.7677
43	0.002154	0.001468	0.001000	0.001154	0.7677
44	0.001000	0.000681	0.000464	0.000536	0.7677
45	0.000464	0.000316	0.000215	0.000249	0.7677
46	0.000215	0.000147	0.000100	0.000115	0.7677
47	0.000100	0.000068	0.000046	0.000054	0.7677
48	0.000046	0.000032	0.000021	0.000025	0.7677
49	0.000021	0.000015	0.000010	0.000011	0.7677
50	0.000010	0.000003	THERMAL	0.000010	5.9915

values given by Hanna and Rose[32] are somewhat lower than the other results. The (n, γ) cross-section curve given by Buckingham et al.[28] differs considerably from the experimental data in the range 0.5-2 Mev. Hughes and Schwartz[27] give a curve that is consistent with the available data below 7 Mev and agrees with the value given by Perkin, O'Connor and Coleman[33] at 14.5 Mev. The Hughes and Schwartz curve was used.

(v) Charged-particle emission cross section

There are no available experimental data on (n, p), (n, d), (n, t), and (n, α) cross sections for Th^{232}. We infer from the 14.5-Mev (n, α) cross sections for U^{238} and Th^{230} (1.5 and 4.6 mb, respectively) and the (n, p) cross section for U^{235} (1.86 mb) reported by Coleman, Howker, O'Connor and Perkin[34] that the Th^{232} charged-particle emission cross sections are also small and may be ignored.

(vi) (n, 3n) cross section

The (n, 3n) cross section has been plotted by Buckingham et al.[28] and is used.

(vii) (n, 2n) cross section

The measured (n, 2n) cross sections reported by Butler and Santry,[35] Prestwood and Bayhurst,[36,37] Perkin and Coleman,[38] Tewes, Caretto, Miller, and Methaway,[39] Cochran and Henkel,[40,41] and Halperin, Schmitt and Druschel[42] are generally in fair agreement; the value given by Rysin, Korrizkhykh, Lbov and Sel'chenko[43] at 14.7 Mev is much lower than the other results. The curve given by Buckingham et al.[28] agrees well with the measured values up to ~9 Mev, but thereafter it is lower than most of the experimental points. The cross section curve plotted by Kalos and Troubetzkoy[44] is in good agreement with most of the measured data below ~8 Mev and above ~11 Mev, but is too low in the range 8-11 Mev. Therefore, the (n, 2n) cross sections are obtained from the Buckingham curve below 8 Mev, from a curve based on the available experimental values between 8 and 11 Mev, and from the Kalos curve above 11 Mev.

(viii) (n, n') cross section

The (n, n') total cross section curve plotted by Buckingham et al.[28] is somewhat higher than the experimental values given by Smith.[21] The curve given by Howerton[45] is not consistent with the other results at energies below ~1.5 Mev. The measured values were used when applicable, and the curve was extrapolated to the Buckingham values at the higher and lower energies. There is at least qualitative agreement between the relative magnitudes of the level excitation functions for Th^{232} given by Smith[21] and the corresponding excitation functions for U^{238} given by Yiftah, Okrent and Moldauer.[22] Since the level excitation functions need to be renormalized to the total (n, n') cross section, it is convenient to use the Yiftah values for U^{238} scaled by the ratio of the (n, n') cross section of Th^{232} to that of U^{238}. The nuclear level energies for Th^{232} are taken from Hellwege,[20] and a direct correspondence is found with the U^{238} level energies; the

Th^{232} 0.820, 0.790, and 0.773-kev levels are assumed to correspond to the U^{238} 0.790-kev level, and their excitation probabilities are taken to be identical.

(ix) (n, f) cross section

The fast-fission cross-section curves plotted by Hughes and Schwartz[27] and by Buckingham et al.[28] are nearly identical in shape, but the Buckingham curve is consistently higher than the Hughes values. The curve given by Hughes is used because it is documented and is considered more reliable. Independent measurements by Protopopov et al.[46] and by Berezin et al.[47] at 14.6 Mev both agree with the Hughes curve.

b. Low Energy Cross Sections

(i) Total cross section

The total cross section curve plotted by Buckingham et al.[28] is used down to ~30 kev. For energies below 30 kev the total cross section is attained as the sum of the elastic cross section and the nonelastic cross section.

(ii) Nonelastic cross section

The nonelastic cross sections are obtained as the sum of the (n, n') and the (n, γ) cross sections.

(iii) Elastic cross section

Above 30 kev the elastic cross section is determined from the difference of the total cross section and the nonelastic cross section. Between 30 kev and 2 kev, the cross section curve is extrapolated to the potential scattering cross section; and at energies below 2 kev, the potential scattering cross section is used. For thermal energy, the thermal scattering cross section given by Hughes and Schwartz[27] is used.

(iv) Radiative capture cross section

The Hughes and Schwartz[27] values are used down to 30 kev. Below 0.46 kev the group effective capture cross section is calculated as indicated in Appendix A. Between 30 and 0.46 kev, the capture cross section is estimated by an interpolated curve; at thermal energy, the Hughes and Schwartz[27] thermal absorption cross section is used. The v^{-1} absorption contribution was calculated and included for energies below 30 kev.

(v) (n, n') cross section

The total (n, n') cross section curve plotted by Buckingham et al.[28] is used at low energies. The level excitation functions for the two energetically allowed levels are determined from (renormalized) values given by Yiftah et al.[21] for U^{238}.

TABLE B.2 TH-232 REACTION CROSS SECTIONS (BARNS)

GP	TOTAL	N,N	N,F	N,3N	N,2N
01	5.600	2.285	0.340	1.000	1.500
02	5.200	2.167	0.332	0.500	1.700
03	4.800	2.051	0.322	0.050	1.850
04	4.900	2.142	0.310	0.000	1.900
05	5.250	2.506	0.305	0.000	1.850
06	5.700	3.054	0.306	0.000	1.550
07	6.100	3.554	0.335	0.000	0.900
08	6.700	4.167	0.320	0.000	0.200
09	6.850	4.175	0.150	0.000	0.010
10	7.100	4.296	0.137	0.000	0.000
11	7.300	4.456	0.145	0.000	0.000
12	7.500	4.633	0.145	0.000	0.000
13	7.600	4.711	0.143	0.000	0.000
14	7.600	4.679	0.141	0.000	0.000
15	7.500	4.508	0.138	0.000	0.000
16	7.200	4.218	0.134	0.000	0.000
17	7.000	4.036	0.120	0.000	0.000
18	6.800	3.845	0.115	0.000	0.000
19	6.700	3.742	0.120	0.000	0.000
20	6.650	3.722	0.092	0.000	0.000
21	6.600	3.734	0.090	0.000	0.000
22	6.600	3.834	0.100	0.000	0.000
23	6.620	3.972	0.052	0.000	0.000
24	6.650	4.144	0.010	0.000	0.000
25	6.700	4.343	0.000	0.000	0.000
26	6.850	4.623	0.000	0.000	0.000
27	7.000	4.914	0.000	0.000	0.000
28	7.050	5.077	0.000	0.000	0.000
29	7.200	5.330	0.000	0.000	0.000
30	7.300	5.525	0.000	0.000	0.000
31	7.530	5.870	0.000	0.000	0.000
32	7.800	6.255	0.000	0.000	0.000
33	8.000	6.532	0.000	0.000	0.000
34	8.250	6.880	0.000	0.000	0.000
35	8.700	7.353	0.000	0.000	0.000
36	9.700	8.490	0.000	0.000	0.000
37	11.000	9.950	0.000	0.000	0.000
38	12.150	11.240	0.000	0.000	0.000
39	13.100	12.510	0.000	0.000	0.000
40	13.639	13.050	0.000	0.000	0.000
41	13.265	12.600	0.000	0.000	0.000
42	12.797	12.100	0.000	0.000	0.000
43	12.712	12.000	0.000	0.000	0.000
44	12.642	12.000	0.000	0.000	0.000
45	12.646	12.000	0.000	0.000	0.000
46	12.710	12.000	0.000	0.000	0.000
47	12.382	12.000	0.000	0.000	0.000
48	12.413	12.000	0.000	0.000	0.000
49	12.320	12.000	0.000	0.000	0.000
50	20.160	12.600	0.000	0.000	0.000

TABLE B.2 CONTINUED

GP	N,N'				
KEV	(≥1000)	(820)	(790)	(773)	(330)
01	0.470	0.000	0.000	0.000	0.000
02	0.495	0.000	0.000	0.000	0.000
03	0.520	0.000	0.000	0.000	0.000
04	0.540	0.000	0.000	0.000	0.000
05	0.580	0.000	0.000	0.000	0.000
06	0.780	0.000	0.000	0.000	0.000
07	1.300	0.000	0.000	0.000	0.000
08	2.000	0.000	0.000	0.000	0.000
09	2.500	0.000	0.000	0.000	0.000
10	2.650	0.000	0.000	0.000	0.000
11	2.680	0.000	0.000	0.000	0.000
12	2.700	0.000	0.000	0.000	0.000
13	2.720	0.000	0.000	0.000	0.000
14	2.750	0.000	0.000	0.000	0.000
15	2.820	0.000	0.000	0.000	0.000
16	2.810	0.000	0.000	0.000	0.000
17	2.800	0.000	0.000	0.000	0.000
18	2.790	0.000	0.000	0.000	0.000
19	2.780	0.000	0.000	0.000	0.000
20	2.193	0.054	0.054	0.054	0.023
21	1.901	0.086	0.086	0.086	0.031
22	1.024	0.185	0.185	0.185	0.044
23	0.575	0.261	0.261	0.261	0.056
24	0.252	0.294	0.294	0.294	0.061
25	0.111	0.263	0.263	0.263	0.060
26	0.001	0.217	0.217	0.217	0.056
27	0.000	0.149	0.149	0.149	0.043
28	0.000	0.066	0.066	0.066	0.022
29	0.000	0.023	0.023	0.023	0.000
30	0.000	0.000	0.000	0.000	0.000
31	0.000	0.000	0.000	0.000	0.000
32	0.000	0.000	0.000	0.000	0.000
33	0.000	0.000	0.000	0.000	0.000
34	0.000	0.000	0.000	0.000	0.000
35	0.000	0.000	0.000	0.000	0.000
36	0.000	0.000	0.000	0.000	0.000
37	0.000	0.000	0.000	0.000	0.000
38	0.000	0.000	0.000	0.000	0.000
39	0.000	0.000	0.000	0.000	0.000
40	0.000	0.000	0.000	0.000	0.000
41	0.000	0.000	0.000	0.000	0.000
42	0.000	0.000	0.000	0.000	0.000
43	0.000	0.000	0.000	0.000	0.000
44	0.000	0.000	0.000	0.000	0.000
45	0.000	0.000	0.000	0.000	0.000
46	0.000	0.000	0.000	0.000	0.000
47	0.000	0.000	0.000	0.000	0.000
48	0.000	0.000	0.000	0.000	0.000
49	0.000	0.000	0.000	0.000	0.000
50	0.000	0.000	0.000	0.000	0.000

TABLE B.2 CONTINUED

GP	----- N,N' -----		CAPTURE	SURFACE
KEV	(180)	(50)		
01	0.000	0.000	0.005	0.00000
02	0.000	0.000	0.006	0.00000
03	0.000	0.000	0.007	0.00000
04	0.000	0.000	0.008	0.00000
05	0.000	0.000	0.009	0.00000
06	0.000	0.000	0.010	0.00000
07	0.000	0.000	0.011	0.00000
08	0.000	0.000	0.013	0.00000
09	0.000	0.000	0.015	0.00000
10	0.000	0.000	0.017	0.00000
11	0.000	0.000	0.019	0.00000
12	0.000	0.000	0.022	0.00000
13	0.000	0.000	0.026	0.00000
14	0.000	0.000	0.030	0.00000
15	0.000	0.000	0.034	0.00000
16	0.000	0.000	0.038	0.00000
17	0.000	0.000	0.044	0.00000
18	0.000	0.000	0.050	0.00000
19	0.000	0.000	0.058	0.00000
20	0.217	0.121	0.066	0.00000
21	0.299	0.210	0.076	0.00000
22	0.695	0.261	0.086	0.00000
23	0.784	0.301	0.096	0.00000
24	0.865	0.330	0.106	0.00000
25	0.917	0.363	0.117	0.00000
26	0.983	0.409	0.127	0.00000
27	1.005	0.455	0.136	0.00000
28	1.074	0.536	0.143	0.00000
29	1.065	0.586	0.150	0.00000
30	0.972	0.648	0.155	0.00000
31	0.812	0.688	0.160	0.00000
32	0.647	0.733	0.165	0.00000
33	0.515	0.785	0.168	0.00000
34	0.412	0.788	0.170	0.00000
35	0.283	0.887	0.177	0.00000
36	0.071	0.939	0.200	0.00000
37	0.000	0.770	0.280	0.00000
38	0.000	0.510	0.400	0.00000
39	0.000	0.100	0.490	0.00000
40	0.000	0.000	0.589	0.00100
41	0.000	0.000	0.665	0.00300
42	0.000	0.000	0.697	0.00510
43	0.000	0.000	0.712	0.00780
44	0.000	0.000	0.642	0.01384
45	0.000	0.000	0.646	0.01544
46	0.000	0.000	0.710	0.02035
47	0.000	0.000	0.382	0.01402
48	0.000	0.000	0.413	0.02623
49	0.000	0.000	0.320	0.00000
50	0.000	0.000	7.560	0.00000

TABLE B.3 TH-232 HIGH ENERGY NUCLIDE DECK

THORIUM						TH 001
2.28500	2.16700	2.05100	2.14200	2.50600	3.05400	TH 002
3.55400	4.16700	4.17500	4.29600	4.10900	4.27200	TH 003
4.34400	4.31500	4.15700	3.89000	3.72200	3.54600	TH 004
3.45100	3.43200	3.44300	3.53600	3.68165	4.04102	TH 005
4.23507	4.50382	4.78084	4.94693	5.17044	5.33568	TH 006
5.62810	5.93520	6.13179	6.34500			TH 007
0.00000	0.00000	0.00000	0.00000	0.00000	0.00000	TH 008
0.00000	0.00000	0.00000	0.00000	0.34700	0.36100	TH 009
0.36700	0.36400	0.35100	0.32800	0.31400	0.29900	TH 010
0.29100	0.29000	0.29100	0.31725	0.39525	1.12760	TH 011
1.09010	1.06096	0.98210	0.90054	0.77290	0.83732	TH 012
0.93023	1.05292	1.15482	0.00000			TH 013
0.00000	0.00000	0.00000	0.00000	0.00000	0.00000	TH 014
0.00000	0.00000	0.00000	0.00000	0.00000	0.00000	TH 015
0.00000	0.00000	0.00000	0.00000	0.00000	0.00000	TH 016
0.00000	0.00000	0.02014	0.08901	0.19143	0.19785	TH 017
0.29799	0.45008	0.61099	0.83906	0.87423	0.62487	TH 018
0.32974	0.04541	0.00000	0.00000			TH 019
0.00000	0.00000	0.00000	0.00000	0.00000	0.00000	TH 020
0.00000	0.00000	0.00000	0.00000	0.00000	0.00000	TH 021
0.00000	0.00000	0.00000	0.00000	0.00000	0.00000	TH 022
0.00000	0.02066	0.09315	0.19755	0.30447	0.03398	TH 023
0.05583	0.03621	0.01397	0.00000	0.16394	0.34713	TH 024
0.48193	0.00000	0.00000	0.00000			TH 025
0.00000	0.00000	0.00000	0.00000	0.00000	0.00000	TH 026
0.00000	0.00000	0.00000	0.00000	0.00000	0.00000	TH 027
0.00000	0.00000	0.00000	0.00000	0.00000	0.00000	TH 028
0.00000	0.00000	0.00000	0.00000	0.00000	0.00000	TH 029
0.00000	0.00000	0.00000	0.00000	0.00000	0.00000	TH 030
0.00000	0.00000	0.00000	0.00000			TH 031
0.00000	0.00000	0.00000	0.00000	0.00000	0.00000	TH 032
0.00000	0.00000	0.00000	0.00000	0.00000	0.00000	TH 033
0.00000	0.00000	0.00000	0.00000	0.00000	0.00000	TH 034
0.00000	0.00000	0.00000	0.00000	0.00000	0.00000	TH 035

TABLE B.3 CONTINUED

0.00000	0.00000	0.00000	0.00000	0.00000	0.00000	TH 036
0.00000	0.00000	0.00000	0.53500			TH 037
1.000	1.000	1.000	1.000	1.000	1.000	TH 038
1.000	1.000	1.000	1.000	0.970	0.910	TH 039
0.840	0.770	0.715	0.660	0.612	0.575	TH 040
0.535	0.500	0.470	0.442	0.417	0.395	TH 041
0.377	0.350	0.336	0.320	0.300	0.288	TH 042
0.275	0.260	0.246	0.237			TH 043
0.23230	0.18467	0.14397	0.13022	0.11506		TH 044
0.09442	0.07212	0.05723	0.05569	0.05086		TH 045
0.04387	0.03715	0.03105	0.02565	0.02115		TH 046
0.01664	0.18811	0.14768	0.11399	0.10101		TH 047
0.08724	0.07024	0.05327	0.04237	0.04051		TH 048
0.03602	0.03017	0.02478	0.02005	0.01601	0.01274	TH 049
0.27152	0.21810	0.17162	0.15817	0.14271		TH 050
0.11918	0.09166	0.07254	0.07169	0.06709		TH 051
0.05943	0.05175	0.04454	0.03794	0.03231		TH 052
0.02632	0.02104	0.15194	0.11782	0.08990		TH 053
0.07781	0.06553	0.05167	0.03890	0.03099		TH 054
0.02903	0.02505	0.02031	0.01612	0.01259	0.00968	TH 055
0.30428	0.24670	0.19561	0.18341	0.16863		TH 056
0.14310	0.11076	0.08740	0.08754	0.08375		TH 057
0.07597	0.06785	0.05994	0.05250	0.04603		TH 058
0.03866	0.03194	0.02600	0.11476	0.08765		TH 059
0.06593	0.05561	0.04552	0.03508	0.02620		TH 060
0.02088	0.01911	0.01594	0.01246	0.00951	0.00713	TH 061
0.33472	0.27370	0.21846	0.20804	0.19456		TH 062
0.16754	0.13047	0.10264	0.10401	0.10150		TH 063
0.09407	0.08594	0.07775	0.06981	0.06284		TH 064
0.05426	0.04618	0.03877	0.02074	0.08103		TH 065
0.06085	0.04511	0.03693	0.02930	0.02202		TH 066
0.01632	0.01299	0.01157	0.00929	0.00697	0.00510	TH 067
0.35128	0.28931	0.23241	0.22439	0.21310		TH 068
0.18597	0.14564	0.11423	0.11694	0.11617		TH 069
0.10978	0.10236	0.09459	0.08687	0.08006		TH 070

TABLE B.3 CONTINUED

0.07088	0.06195	0.05348	0.09591	0.09557		TH 071
0.05371	0.03967	0.02878	0.02284	0.01751		TH 072
0.01281	0.00941	0.00747	0.00645	0.00497	0.00357	TH 073
0.36596	0.30349	0.24508	0.23955	0.23068		TH 074
0.20376	0.16043	0.12545	0.12958	0.13080		TH 075
0.12577	0.11945	0.11253	0.10544	0.09927		TH 076
0.08989	0.08047	0.07124	0.21286	0.21210		TH 077
0.20674	0.03400	0.02458	0.01752	0.01340		TH 078
0.00990	0.00703	0.00512	0.00404	0.00337	0.00248	TH 079
0.36512	0.30366	0.24716	0.24430	0.23822		TH 080
0.21275	0.16834	0.13126	0.13664	0.13993		TH 081
0.13668	0.13198	0.12650	0.12071	0.11584		TH 082
0.10704	0.09791	0.08868	0.33858	0.33736		TH 083
0.32883	0.31422	0.01983	0.01402	0.00970		TH 084
0.00717	0.00508	0.00350	0.00252	0.00197	0.00158	TH 085
0.36236	0.30100	0.24774	0.24729	0.24387		TH 086
0.21997	0.17486	0.13597	0.14252	0.14784		TH 087
0.14646	0.14354	0.13974	0.13554	0.13234		TH 088
0.12453	0.11613	0.10735	0.41011	0.40863		TH 089
0.39831	0.38060	0.36880	0.01084	0.00750		TH 090
0.00506	0.00359	0.00241	0.00160	0.00114	0.00088	TH 091
0.34912	0.29343	0.24063	0.24243	0.24153		TH 092
0.21984	0.17549	0.13612	0.14353	0.15064		TH 093
0.15113	0.15013	0.14821	0.14590	0.14468		TH 094
0.13839	0.13134	0.12367	0.41374	0.41226		TH 095
0.40184	0.38398	0.37208	0.00000	0.00547		TH 096
0.00360	0.00237	0.00159	0.00103	0.00066	0.00046	TH 097
0.33027	0.27973	0.22937	0.23294	0.23422		TH 098
0.21493	0.17224	0.13328	0.14128	0.14983		TH 099
0.15205	0.15286	0.15282	0.15244	0.15328		TH 100
0.14880	0.14345	0.13731	0.36184	0.36054		TH 101
0.35143	0.33581	0.32540	0.00000	0.00453		TH 102
0.00241	0.00153	0.00097	0.00062	0.00038	0.00023	TH 103
0.30772	0.26168	0.21518	0.22016	0.22319		TH 104
0.20632	0.16594	0.12812	0.13643	0.14605		TH 105

TABLE B.3 CONTINUED

0.14973	0.15217	0.15385	0.15530	0.15813		TH 106
0.15554	0.15207	0.14774	0.28612	0.28509		TH 107
0.27789	0.26553	0.25730	0.00000	0.00000		TH 108
0.01995	0.00101	0.00062	0.00036	0.00022	0.00013	TH 109
0.28816	0.24591	0.20271	0.20874	0.21320		TH 110
0.19840	0.16010	0.12336	0.13190	0.14240		TH 111
0.14735	0.15122	0.15446	0.15759	0.16229		TH 112
0.16156	0.15997	0.15752	0.21448	0.21371		TH 113
0.20830	0.19905	0.19287	0.16705	0.00000		TH 114
0.00000	0.02793	0.00040	0.00022	0.00012	0.00007	TH 115
0.25938	0.22838	0.18353	0.19009	0.19546		TH 116
0.18300	0.14812	0.11392	0.12224	0.13298		TH 117
0.13876	0.14367	0.14811	0.15259	0.15875		TH 118
0.15975	0.16001	0.15947	0.12891	0.12844		TH 119
0.12520	0.11963	0.11592	0.38088	0.00000		TH 120
0.00000	0.00044	0.01392	0.00016	0.00006	0.00004	TH 121
0.23193	0.19915	0.16490	0.17168	0.17760		TH 122
0.16718	0.13569	0.10418	0.11214	0.12283		TH 123
0.12913	0.13476	0.14007	0.14555	0.15282		TH 124
0.15527	0.15713	0.15830	0.10089	0.10052		TH 125
0.09798	0.09363	0.09073	0.33410	0.00657		TH 126
0.00000	0.00000	0.00770	0.00000	0.00003	0.00002	TH 127
0.18897	0.16280	0.13495	0.14114	0.14677		TH 128
0.13881	0.11293	0.08658	0.09344	0.10295		TH 129
0.10893	0.11445	0.11981	0.12543	0.13273		TH 130
0.13599	0.13883	0.14117	0.06263	0.06241		TH 131
0.06083	0.05813	0.05632	0.00000	0.27623		TH 132
0.00000	0.00000	0.00000	0.00000	0.00000	0.00001	TH 133
0.43311	0.37334	0.31116	0.32774	0.34352	0.32723	TH 134
0.26722	0.20439	0.22148	0.24621	0.26307	0.27929	TH 135
0.29553	0.31295	0.33515	0.34776	0.35985	0.37116	TH 136
0.09038	0.09005	0.08778	0.08388	0.08128	0.00000	TH 137
0.50642	0.14014	0.00000	0.00000	0.00000	0.00000	TH 138
0.00000	0.60147	0.50503	0.78806			TH 139
0.38353	0.33234	0.27801	0.29565	0.31338	0.30156	TH 140

TABLE B.3 CONTINUED

0.24758	0.18874	0.20564	0.23150	0.25080	0.27018	TH 141
0.29027	0.31235	0.34020	0.35936	0.37898	0.39879	TH 142
0.03864	0.03850	0.03753	0.03586	0.03475	0.16196	TH 143
0.00000	0.51184	0.00000	0.00000	0.00000	0.00000	TH 144
0.00000	0.00000	0.04036	0.41194			TH 145
0.29309	0.25506	0.21430	0.23014	0.24669	0.23983	TH 146
0.19797	0.15042	0.16475	0.18781	0.20629	0.22550	TH 147
0.24600	0.26898	0.29796	0.32040	0.34438	0.36971	TH 148
0.00417	0.00416	0.00405	0.00387	0.00375	0.08956	TH 149
0.04870	0.00000	0.07386	0.04343	0.00000	0.00000	TH 150
0.00000	0.00000	0.00000	0.00000			TH 151
0.15348	0.13462	0.11341	0.12310	0.13359	0.13135	TH 152
0.10910	0.08258	0.09095	0.10512	0.11724	0.13023	TH 153
0.14446	0.16077	0.18143	0.19896	0.21837	0.23964	TH 154
0.00000	0.00000	0.00000	0.00000	0.00000	0.00000	TH 155
0.06156	0.00000	0.37387	0.15542	0.06849	0.00000	TH 156
0.00000	0.00000	0.00000	0.00000			TH 157
5.60000	5.20000	4.80000	4.90000	5.25000	5.70000	TH 158
6.10000	6.70000	6.85000	7.10000	7.30000	7.50000	TH 159
7.60000	7.60000	7.50000	7.20000	7.00000	6.80000	TH 160
6.70000	6.65000	6.60000	6.60000	6.62000	6.65000	TH 161
6.70000	6.85000	7.00000	7.05000	7.20000	7.30000	TH 162
7.53000	7.80000	8.00000	8.25000			TH 163
X.XXXX		THORIUM DENSITY CARD				
1.38000	1.26800	1.17200	1.07300	1.00300	0.96400	TH-FC 1
1.01200	0.92800	0.41900	0.37000	0.37800	0.36700	TH-FC 2
0.35200	0.33800	0.32900	0.30700	0.27000	0.25300	TH-FC 3
0.26000	0.19600	0.18900	0.20800	0.10700	0.02000	TH-FC 4
0.00000	0.00000	0.00000	0.00000	0.00000	0.00000	TH-FC 5
0.00000	0.00000	0.00000	0.00000			TH-FC 6
0.00000	0.00000	0.00000	0.00091	0.00198	0.00352	FSPCT 1
0.00552	0.00792	0.01024	0.01450	0.02014	0.02397	FSPCT 2
0.02940	0.03420	0.03740	0.04247	0.04536	0.04775	FSPCT 3
0.04774	0.04909	0.04823	0.04694	0.04558	0.04290	FSPCT 4
0.04080	0.03766	0.03502	0.03210	0.02909	0.02625	FSPCT 5
0.02394	0.02120	0.01877	0.01525	0.03510	0.03210	FSPCT 6
0.02720	0.01975					FSPCT 7

TABLE B.4 TH-232 LOW ENERGY NUCLIDE DECK

THORIUM						TH 164
7.64586	0.74708	0.13006	0.00000	0.002873	8.70000	TH 165
8.85501	0.61247	0.03252	0.00000	0.002873	9.70000	TH 166
10.27820	0.44180	0.00000	0.00000	0.002873	11.00000	TH 167
11.16520	0.54400	0.04080	0.00000	0.002873	12.15000	TH 168
12.42900	0.14220	0.02060	0.01790	0.002873	13.10000	TH 169
12.99400	0.05600	0.00000	0.00000	0.002873	13.63900	TH 170
12.50500	0.09500	0.00000	0.00000	0.002873	13.26500	TH 171
12.00900	0.09100	0.00000	0.00000	0.002873	12.79700	TH 172
11.91000	0.09000	0.00000	0.00000	0.002873	12.71200	TH 173
11.91000	0.09000	0.00000	0.00000	0.002873	12.64200	TH 174
11.91000	0.09000	0.00000	0.00000	0.002873	12.64600	TH 175
11.91000	0.09000	0.00000	0.00000	0.002873	12.71000	TH 176
11.91000	0.09000	0.00000	0.00000	0.002873	12.38200	TH 177
11.91000	0.09000	0.00000	0.00000	0.002873	12.41300	TH 178
11.91000	0.09000	0.00000	0.00000	0.002873	12.32000	TH 179
12.60000	0.00000	0.00000	0.00860	0.002873	20.16000	TH 180
0.00000	0.00000	0.00000	0.00000			TH-SR 1
0.00000	0.00100	0.00300	0.00510			TH-SR 2
0.00780	0.01384	0.01544	0.02035			TH-SR 3
0.01402	0.02623	0.00000	0.00000			TH-SR 4

c. Neutron Nonelastic Spectra

The (n, n'), (n, 2n) and (n, 3n) spectra are calculated with the multiparticle statistical model[25] for incident neutron energies above 2 Mev. (The threshold energies for the (n, 2n) and (n, 3n) reactions are approximately 6.4 and 11.5 Mev, respectively.) Between 1.3 and 2 Mev, the asymptotic empirical model[2] is used; for energies below 1.3 Mev, the isolated level model is applied. There is no inelastic scattering below about 50 kev.

d. Fission Neutron Spectrum

Owing to the lack of experimental measurements, the Th^{232} fast fission spectrum is approximated by the U^{235} thermal fission neutron spectrum given by Weinberg and Wigner.[48] The similarity observed in the thermal fission neutron spectra of several nuclides,[49] and the nearly identical fission γ spectra for thermal and fast fission reactions in fissile nuclides[50, 51] give some assurance that the approximation is valid. The neutron yield per fission for the range of incident neutron energies is given by Kuz'minov.[52]

B.3 Uranium 238

a. High Energy Cross Sections

(i) Total cross section

There is good agreement between the curves plotted by Hughes and Schwartz[27] and by Buckingham et al.[28] at energies up to 8 Mev; at higher energies the Hughes curve is somewhat higher. Experimental values given by Bratenahl et al.,[53] Galloway[54] and others[55-57] are consistent with the Hughes curve; it is used.

(ii) Nonelastic cross section

The values given by Hughes and Schwartz[27] at energies below 2.5 Mev and measurements at high energies (~14 Mev) by Cohen,[58] Degtyarev et al.[59] and others[57, 60] agree with the sum of the individual nonelastic reaction cross sections. The curve plotted by Buckingham et al.[28] is not consistent with the Hughes results below ~2 Mev. The nonelastic cross section is obtained as the sum of the various nonelastic reaction cross sections.

(iii) Elastic cross section

The elastic cross section is obtained from the difference of the total and the nonelastic cross sections. These results agree with the measured values given by Cranberg and Levin.[61]

(iv) Radiative capture cross section

There have been many measurements[61-66, 32, 33, 67] of (n,γ) cross sections at higher energies with varying degrees of agreement. The curve plotted by Hughes and Schwartz[27] appears to be consistent with most recent measurements, and it is used.

(v) Charged-particle emission cross section

Coleman et al.[34] give the (n, α) cross section at 14.5 Mev as 1.5 mb. Since at lower energies α emission is less probable, the reaction is ignored. By inference from the U^{235} (n, p) cross section,[34] this reaction is also negligible.

(vi) (n, 3n) Cross section

There is good agreement between the (n, 3n) cross-section curves plotted by Henkel[68] and by Buckingham et al.,[28] and the measured value at 14.1 Mev reported by Allen et al.[69] is in reasonable agreement with these curves. The (n, 3n) cross section given by Rosen and Stewart[60] is inconsistent with the other results. The Buckingham curve is used.

(vii) (n, 2n) Cross section

The (n, 2n) curves presented by Hughes and Schwartz,[27] by Buckingham et al.,[28] and by Henkel[68] are not in agreement above 8 Mev. The Hughes curve is based on measurements reported by Knight, Smith, and Warren[70]; the values given by Perkin and Coleman[71] and by Rosen and Stewart[60] near 14 Mev indicate somewhat higher cross sections that are more consistent with the curve plotted by Buckingham. The (n, 2n) cross section is obtained from the Hughes curve below 10 Mev, and from the Buckingham curve at higher energies.

(viii) (n, n') Cross section

Dresner[72] gives a summary of the experimental (n, n') cross-section data up to 1 Mev. Rosen et al.[60] and Allen et al.[69] both report measured values near 14 Mev; the last result is considered more reliable. The (n, n') cross-section curve presented by Buckingham et al.[28] is not consistent with the above-mentioned data, and is not usable beyond ~0.07 Mev. Howerton[45] plots a curve that gives very good correlation with the experimental results, and also agrees with the total nonelastic cross sections given by Hughes and Schwartz.[27] The Howerton curve is used above 0.1 Mev; at lower energies the (n, n') cross section is obtained by extrapolation to the Buckingham curve.

The nuclear-level excitation functions are obtained by renormalizing the curves given by Yiftah et al.[22]; these curves are based on measurements made by Cranberg and Levin.[73]

(ix) (n, f) Cross section

The fast-fission cross-section curves plotted by Hughes and Schwartz,[27] by Buckingham et al.[28] and by Hemmendinger[74] are in agreement. Experimental values reported by Adams et al.,[75] Knight et al.,[70] Cranberg and Levin,[61] and others[60, 76-78] are consistent and give good correlation with the above curves. (The Knight results are somewhat high in the range 9-10 Mev.) As a matter of convenience, the Buckingham curve is used.

b. Low Energy Cross Sections

(i) Total cross section

Down to about 30 kev, the total cross-section curve plotted by Buckingham et al.[28] is employed; for lower energies, the total cross section is derived from the sum of the elastic and the nonelastic cross sections.

(ii) Nonelastic cross section

The total nonelastic cross section for energies below 0.44 Mev is obtained as the sum of the (n, n') and (n, γ) cross sections.

(iii) Elastic cross section

The elastic cross section is determined from the difference of the total and the nonelastic cross sections for energies greater than 30 kev, and from a smoothly extrapolated curve that levels off at the potential scattering cross section in the energy range 2-30 Mev, and by assuming that below 2 Mev it equals the potential scattering cross section. At thermal energy the thermal scattering cross section given by Hughes and Schwartz[27] is used.

(iv) Radiative capture cross section

For energies above 30 kev, the Hughes and Schwartz[27] absorption cross section curve is used. The group effective resonance capture cross sections are calculated below 0.22 kev, and between 0.22 and 30 kev an estimated curve, joining the measured and the calculated results, is employed. The v^{-1} absorption contribution is computed for energies below 30 kev. The thermal absorption cross section given by Hughes is used at thermal energy.

(v) (n, n') Cross section

The total (n, n') cross section is obtained from a composite curve based on the curve plotted by Howerton; at energies below 0.07 Mev the Buckingham results are used, with an estimated segment (from 0.07 Mev to 0.15 Mev) joining the two curves. The nuclear-level excitation functions for the two lower energy levels are obtained from Yiftah et al.[22]

c. Nonelastic Spectra

The neutron spectra of the (n, n'), (n, 2n) and (n, 3n) reactions are calculated with the multiparticle statistical model[2] for incident neutron energies above 2 Mev. Between 1.3 Mev and 2 Mev, the asymptotic empirical model[2] is employed. The isolated-level model is used below 1.3 Mev. The threshold energies of the (n, n'), (n, 2n) and (n, 3n) reactions are approximately 0.045, 5.90 and 11.5 Mev.

d. Fission Neutron Spectrum

The U^{238} fast fission neutron spectrum is assumed to be identical to the U^{235} thermal fission spectrum. The validity of this approximation is inferred from the similarity of the thermal fission neutron spectra of several nuclides [48] and from the independence of the fission γ spectrum from the compound nucleus excitation before fission.[49, 50] The fission neutron yield is obtained from Kuz'minov.[52]

TABLE B.5 U-238 REACTION CROSS SECTIONS (BARNS)

GP	TOTAL	N,N	N,F	N,3N	N,2N
01	5.900	3.247	1.200	0.800	0.550
02	5.600	2.867	1.010	0.430	1.050
03	5.500	2.777	1.010	0.020	1.420
04	5.550	2.737	1.020	0.000	1.470
05	5.750	2.877	1.020	0.000	1.450
06	6.000	3.126	1.020	0.000	1.200
07	6.300	3.346	1.010	0.000	0.840
08	6.650	3.545	0.900	0.000	0.350
09	7.000	3.984	0.650	0.000	0.010
10	7.400	4.373	0.550	0.000	0.000
11	7.500	4.422	0.540	0.000	0.000
12	7.550	4.430	0.540	0.000	0.000
13	7.600	4.447	0.540	0.000	0.000
14	7.550	4.414	0.540	0.000	0.000
15	7.550	4.432	0.540	0.000	0.000
16	7.450	4.346	0.542	0.000	0.000
17	7.300	4.205	0.548	0.000	0.000
18	7.350	4.266	0.552	0.000	0.000
19	7.100	4.064	0.547	0.000	0.000
20	7.000	4.031	0.522	0.000	0.000
21	6.850	3.971	0.470	0.000	0.000
22	6.800	4.058	0.370	0.000	0.000
23	6.720	4.200	0.230	0.000	0.000
24	6.760	4.510	0.042	0.000	0.000
25	6.780	4.690	0.035	0.000	0.000
26	6.800	4.922	0.018	0.000	0.000
27	6.820	5.142	0.012	0.000	0.000
28	7.000	5.577	0.005	0.000	0.000
29	7.030	5.754	0.001	0.000	0.000
30	7.400	6.263	0.000	0.000	0.000
31	7.600	6.567	0.000	0.000	0.000
32	7.900	6.971	0.000	0.000	0.000
33	8.100	7.255	0.000	0.000	0.000
34	8.300	7.507	0.000	0.000	0.000
35	8.800	8.073	0.000	0.000	0.000
36	9.750	9.100	0.000	0.000	0.000
37	11.000	10.350	0.000	0.000	0.000
38	12.300	11.620	0.000	0.000	0.000
39	13.100	12.720	0.000	0.000	0.000
40	13.513	13.000	0.000	0.000	0.000
41	12.405	11.800	0.000	0.000	0.000
42	11.508	10.900	0.000	0.000	0.000
43	11.267	10.700	0.000	0.000	0.000
44	11.218	10.700	0.000	0.000	0.000
45	11.155	10.700	0.000	0.000	0.000
46	11.105	10.700	0.000	0.000	0.000
47	10.986	10.700	0.000	0.000	0.000
48	10.910	10.700	0.000	0.000	0.000
49	11.053	10.700	0.000	0.000	0.000
50	11.350	8.500	0.000	0.000	0.000

TABLE B.5 CONTINUED

GP	N,N'				
KEV	(≥1000)	(790)	(310)	(148)	(45)
01	0.200	0.000	0.000	0.000	0.000
02	0.240	0.000	0.000	0.000	0.000
03	0.270	0.000	0.000	0.000	0.000
04	0.320	0.000	0.000	0.000	0.000
05	0.400	0.000	0.000	0.000	0.000
06	0.650	0.000	0.000	0.000	0.000
07	1.100	0.000	0.000	0.000	0.000
08	1.850	0.000	0.000	0.000	0.000
09	2.350	0.000	0.000	0.000	0.000
10	2.470	0.000	0.000	0.000	0.000
11	2.530	0.000	0.000	0.000	0.000
12	2.570	0.000	0.000	0.000	0.000
13	2.600	0.000	0.000	0.000	0.000
14	2.580	0.000	0.000	0.000	0.000
15	2.560	0.000	0.000	0.000	0.000
16	2.540	0.000	0.000	0.000	0.000
17	2.520	0.000	0.000	0.000	0.000
18	2.500	0.000	0.000	0.000	0.000
19	2.450	0.000	0.000	0.000	0.000
20	1.900	0.140	0.020	0.235	0.105
21	1.655	0.225	0.027	0.260	0.183
22	0.913	0.495	0.039	0.620	0.233
23	0.506	0.690	0.049	0.690	0.265
24	0.221	0.775	0.054	0.760	0.290
25	0.095	0.680	0.052	0.790	0.313
26	0.000	0.534	0.046	0.805	0.335
27	0.000	0.349	0.033	0.783	0.355
28	0.000	0.138	0.015	0.745	0.372
29	0.000	0.045	0.000	0.700	0.385
30	0.000	0.000	0.000	0.600	0.400
31	0.000	0.000	0.000	0.487	0.413
32	0.000	0.000	0.000	0.375	0.425
33	0.000	0.000	0.000	0.285	0.435
34	0.000	0.000	0.000	0.230	0.440
35	0.000	0.000	0.000	0.145	0.455
36	0.000	0.000	0.000	0.035	0.465
37	0.000	0.000	0.000	0.000	0.440
38	0.000	0.000	0.000	0.000	0.400
39	0.000	0.000	0.000	0.000	0.010
40	0.000	0.000	0.000	0.000	0.000
41	0.000	0.000	0.000	0.000	0.000
42	0.000	0.000	0.000	0.000	0.000
43	0.000	0.000	0.000	0.000	0.000
44	0.000	0.000	0.000	0.000	0.000
45	0.000	0.000	0.000	0.000	0.000
46	0.000	0.000	0.000	0.000	0.000
47	0.000	0.000	0.000	0.000	0.000
48	0.000	0.000	0.000	0.000	0.000
49	0.000	0.000	0.000	0.000	0.000
50	0.000	0.000	0.000	0.000	0.000

TABLE B.5 CONTINUED

GP	CAPTURE	SURFACE
01	0.003	0.00000
02	0.003	0.00000
03	0.003	0.00000
04	0.003	0.00000
05	0.003	0.00000
06	0.004	0.00000
07	0.004	0.00000
08	0.005	0.00000
09	0.006	0.00000
10	0.007	0.00000
11	0.008	0.00000
12	0.010	0.00000
13	0.013	0.00000
14	0.016	0.00000
15	0.018	0.00000
16	0.022	0.00000
17	0.027	0.00000
18	0.032	0.00000
19	0.039	0.00000
20	0.047	0.00000
21	0.059	0.00000
22	0.072	0.00000
23	0.090	0.00000
24	0.108	0.00000
25	0.125	0.00000
26	0.140	0.00000
27	0.146	0.00000
28	0.148	0.00000
29	0.145	0.00000
30	0.137	0.00000
31	0.133	0.00000
32	0.129	0.00000
33	0.125	0.00000
34	0.123	0.00000
35	0.127	0.00000
36	0.150	0.00000
37	0.210	0.00000
38	0.280	0.00000
39	0.370	0.00000
40	0.513	0.00050
41	0.605	0.00150
42	0.608	0.00230
43	0.567	0.00350
44	0.518	0.00520
45	0.455	0.00740
46	0.405	0.01317
47	0.286	0.01128
48	0.210	0.01295
49	0.353	0.03991
50	2.750	0.03098

TABLE B.6 U-238 HIGH ENERGY NUCLIDE DECK

URANIUM						U 001
3.24700	2.86700	2.77700	2.73700	2.87700	3.12600	U 002
3.34600	3.54500	3.98400	4.37300	4.08700	4.09400	U 003
4.11000	4.07900	4.09600	4.01700	3.88600	3.94300	U 004
3.756000	3.72500	3.67000	3.75000	3.89841	4.36133	U 005
4.53223	4.74624	4.94597	5.33786	5.48582	5.93657	U 006
6.19806	6.53893	6.76470	6.93800			U 007
0.00000	0.00000	0.00000	0.00000	0.00000	0.00000	U 008
0.00000	0.00000	0.00000	0.00000	0.33500	0.33600	U 009
0.33700	0.33500	0.33600	0.32900	0.31900	0.32300	U 010
0.30800	0.30600	0.30100	0.32515	0.39390	1.04897	U 011
1.00402	0.94712	0.85777	0.77384	0.67113	0.72643	U 012
0.78194	0.85707	0.90824	0.00000			U 013
0.00000	0.00000	0.00000	0.00000	0.00000	0.00000	U 014
0.00000	0.00000	0.00000	0.00000	0.00000	0.00000	U 015
0.00000	0.00000	0.00000	0.00000	0.00000	0.00000	U 016
0.00000	0.00000	0.01752	0.07935	0.16845	0.17384	U 017
0.25675	0.36864	0.47626	0.58230	0.57435	0.38572	U 018
0.19784	0.02632	0.00000	0.00000			U 019
0.00000	0.00000	0.00000	0.00000	0.00000	0.00000	U 020
0.00000	0.00000	0.00000	0.00000	0.00000	0.00000	U 021
0.00000	0.00000	0.00000	0.00000	0.00000	0.00000	U 022
0.00000	0.01790	0.08108	0.17611	0.26794	0.02986	U 023
0.04810	0.02966	0.01089	0.00000	0.10770	0.21428	U 024
0.28916	0.00000	0.00000	0.00000			U 025
0.00000	0.00000	0.00000	0.00000	0.00000	0.00000	U 026
0.00000	0.00000	0.00000	0.00000	0.00000	0.00000	U 027
0.00000	0.00000	0.00000	0.00000	0.00000	0.00000	U 028
0.00000	0.00000	0.00000	0.00000	0.00000	0.00000	U 029
0.00000	0.00000	0.00000	0.00000	0.00000	0.00000	U 030
0.00000	0.00000	0.00000	0.00000			U 031
0.00000	0.00000	0.00000	0.00000	0.00000	0.00000	U 032
0.00000	0.00000	0.00000	0.00000	0.00000	0.00000	U 033
0.00000	0.00000	0.00000	0.00000	0.00000	0.00000	U 034
0.00000	0.00000	0.00000	0.00000	0.00000	0.00000	U 035

TABLE B.6 CONTINUED

0.00000	0.00000	0.00000	0.00000	0.00000	0.00000	U 036
0.00000	0.00000	0.00000	0.56900			U 037
1.000	1.000	1.000	1.000	1.000	1.000	U 038
1.000	1.000	1.000	1.000	0.970	0.910	U 039
0.840	0.770	0.715	0.660	0.612	0.575	U 040
0.535	0.500	0.470	0.442	0.417	0.395	U 041
0.377	0.350	0.336	0.320	0.300	0.288	U 042
0.275	0.260	0.246	0.237			U 043
0.11114	0.10587	0.09063	0.08365	0.09510		U 044
0.06288	0.05392	0.04942	0.04420	0.03940		U 045
0.03384	0.02838	0.02338	0.01858	0.01452		U 046
0.01113	0.08646	0.08186	0.06958	0.06280		U 047
0.05509	0.04535	0.03851	0.03524	0.03114		U 048
0.02698	0.02247	0.01823	0.01451	0.01113	0.00837	U 049
0.13473	0.12908	0.11114	0.10468	0.09600		U 050
0.08168	0.07067	0.06484	0.05857	0.05359		U 051
0.04735	0.04091	0.03476	0.02855	0.02309		U 052
0.01835	0.01430	0.06687	0.06284	0.05298		U 053
0.04665	0.03989	0.03223	0.02710	0.02473		U 054
0.02154	0.01807	0.01454	0.01138	0.00872	0.00642	U 055
0.15602	0.15025	0.12997	0.12467	0.11655		U 056
0.10064	0.08781	0.08063	0.07342	0.06876		U 057
0.06232	0.05530	0.04832	0.04087	0.03409		U 058
0.02800	0.02259	0.01793	0.04806	0.04478		U 059
0.03736	0.03200	0.02660	0.02106	0.01752		U 060
0.01592	0.01362	0.01102	0.00853	0.00640	0.00470	U 061
0.17684	0.17109	0.14855	0.14487	0.13782		U 062
0.12063	0.10609	0.09745	0.08932	0.08543		U 063
0.07921	0.07201	0.06453	0.05605	0.04807		U 064
0.04066	0.03385	0.02777	0.01829	0.03217		U 065
0.02969	0.02445	0.02031	0.01636	0.01268		U 066
0.01043	0.00942	0.00788	0.00613	0.00454	0.00326	U 067
0.19065	0.18523	0.16133	0.15969	0.15434		U 068
0.13678	0.12119	0.11132	0.10259	0.09999		U 069
0.09464	0.08793	0.08059	0.07169	0.06305		U 070

TABLE B.6 CONTINUED

0.05476	0.04691	0.03965	0.08452	0.08280		U 071
0.02010	0.01834	0.01487	0.01195	0.00930		U 072
0.00705	0.00573	0.00513	0.00418	0.00311	0.00220	U 073
0.20351	0.19847	0.17330	0.17385	0.17044		U 074
0.15278	0.13630	0.12520	0.11587	0.11478		U 075
0.11075	0.10493	0.09816	0.08921	0.08025		U 076
0.07139	0.06273	0.05446	0.18760	0.18377		U 077
0.17994	0.01196	0.01077	0.00857	0.00664		U 078
0.00498	0.00369	0.00295	0.00262	0.00207	0.00146	U 079
0.20756	0.20312	0.17772	0.18046	0.17922		U 080
0.16232	0.14574	0.13386	0.12431	0.12514		U 081
0.12268	0.11829	0.11272	0.10444	0.09588		U 082
0.08716	0.07835	0.06968	0.29839	0.29230		U 083
0.28621	0.28012	0.00652	0.00578	0.00449		U 084
0.00334	0.00241	0.00174	0.00137	0.00120	0.00091	U 085
0.21014	0.20628	0.18079	0.18558	0.18647		U 086
0.17050	0.15398	0.14140	0.13168	0.13438		U 087
0.13373	0.13101	0.12691	0.11965	0.11188		U 088
0.10369	0.09515	0.08648	0.36142	0.35405		U 089
0.34667	0.33930	0.32454	0.00331	0.00288		U 090
0.00218	0.00155	0.00107	0.00075	0.00058	0.00050	U 091
0.20608	0.20286	0.17804	0.18456	0.18740		U 092
0.17284	0.15694	0.14410	0.13448	0.13895		U 093
0.14016	0.13928	0.13695	0.13115	0.12468		U 094
0.11758	0.10992	0.10188	0.36463	0.35719		U 095
0.34975	0.34231	0.32744	0.00000	0.00153		U 096
0.00130	0.00095	0.00064	0.00042	0.00029	0.00022	U 097
0.19809	0.19549	0.17176	0.17963	0.18413		U 098
0.17115	0.15619	0.14338	0.13404	0.14004		U 099
0.14297	0.14391	0.14340	0.13928	0.13438		U 100
0.12873	0.12237	0.11542	0.31890	0.31238		U 101
0.30588	0.29937	0.28635	0.00000	0.00390		U 102
0.00062	0.00051	0.00036	0.00023	0.00014	0.00010	U 103
0.18730	0.18526	0.16292	0.17173	0.17755		U 104
0.16620	0.15236	0.13984	0.13091	0.13812		U 105

TABLE B.6 CONTINUED

0.14256	0.14516	0.14639	0.14398	0.14077		U 106
0.13676	0.13196	0.12645	0.25215	0.24701		U 107
0.24186	0.23672	0.22642	0.00000	0.00000		U 108
0.01634	0.00023	0.00018	0.00012	0.00008	0.00004	U 109
0.17766	0.17610	0.15498	0.16453	0.17142		U 110
0.16151	0.14867	0.13643	0.12786	0.13612		U 111
0.14188	0.14597	0.14882	0.14805	0.14651		U 112
0.14415	0.14098	0.13703	0.18902	0.18516		U 113
0.18130	0.17745	0.16973	0.14678	0.00000		U 114
0.00000	0.02177	0.00008	0.00006	0.00004	0.00002	U 115
0.16186	0.16074	0.14155	0.15125	0.15869		U 116
0.15039	0.13897	0.12751	0.11959	0.12836		U 117
0.13499	0.14019	0.14432	0.14507	0.14512		U 118
0.14444	0.14300	0.14079	0.11361	0.11129		U 119
0.10897	0.10665	0.10201	0.33466	0.00000		U 120
0.00000	0.00034	0.00966	0.00002	0.00002	0.00001	U 121
0.14625	0.14548	0.12818	0.13775	0.14543		U 122
0.13856	0.12848	0.11787	0.11062	0.11958		U 123
0.12676	0.13275	0.13787	0.13987	0.14128		U 124
0.14206	0.14219	0.14161	0.08891	0.08710		U 125
0.08528	0.08347	0.07984	0.29356	0.00566		U 126
0.00000	0.00000	0.00534	0.00000	0.00001	0.00000	U 127
0.12028	0.11983	0.10562	0.11407	0.12108		U 128
0.11588	0.10778	0.09886	0.09283	0.10098		U 129
0.10777	0.11368	0.11896	0.12164	0.12390		U 130
0.12569	0.12699	0.12773	0.05520	0.05407		U 131
0.05295	0.05182	0.04957	0.00000	0.23800		U 132
0.00000	0.00000	0.00000	0.00000	0.00000	0.00000	U 133
0.27949	0.27908	0.24611	0.26782	0.28664	0.27626	U 134
0.25813	0.23674	0.22241	0.24424	0.26341	0.28094	U 135
0.29737	0.30778	0.31751	0.32647	0.33460	0.34168	U 136
0.07965	0.07802	0.07640	0.07477	0.07152	0.00000	U 137
0.43634	0.11478	0.00000	0.00000	0.00000	0.00000	U 138
0.00000	0.34868	0.27971	0.44000			U 139
0.25239	0.25283	0.22310	0.24539	0.26571	0.25864	U 140

TABLE B.6 CONTINUED

0.24329	0.22307	0.20967	0.23334	0.25538	0.27664	U 141
0.29760	0.31330	0.32907	0.34483	0.36063	0.37617	U 142
0.03402	0.03336	0.03267	0.03197	0.03058	0.14231	U 143
0.00000	0.41922	0.00000	0.00000	0.00000	0.00000	U 144
0.00000	0.00000	0.02235	0.23000			U 145
0.19670	0.19768	0.17451	0.19401	0.21254	0.20897	U 146
0.19792	0.18143	0.17055	0.19235	0.21363	0.23503	U 147
0.25697	0.27518	0.29426	0.31426	0.33536	0.35734	U 148
0.00369	0.00360	0.00352	0.00344	0.00330	0.07869	U 149
0.04196	0.00000	0.05757	0.03014	0.00000	0.00000	U 150
0.00000	0.00000	0.00000	0.00000			U 151
0.10536	0.10628	0.09385	0.10557	0.11715	0.11647	U 152
0.11116	0.10188	0.09574	0.10957	0.12368	0.13841	U 153
0.15404	0.16808	0.18332	0.19991	0.21813	0.23792	U 154
0.00000	0.00000	0.00000	0.00000	0.00000	0.00000	U 155
0.05304	0.00000	0.29143	0.10786	0.04500	0.00000	U 156
0.00000	0.00000	0.00000	0.00000			U 157
5.90000	5.60000	5.50000	5.55000	5.75000	6.00000	U 158
6.30000	6.65000	7.00000	7.40000	7.50000	7.55000	U 159
7.60000	7.55000	7.55000	7.45000	7.30000	7.35000	U 160
7.10000	7.00000	6.85000	6.80000	6.72000	6.76000	U 161
6.78000	6.80000	6.82000	7.00000	7.03000	7.40000	U 162
7.60000	7.90000	8.10000	8.30000			U 163
X.XXXX		URANIUM DENSITY CARD				
5.43600	4.36300	4.16100	4.02900	3.87600	3.73300	U--FC 1
3.56500	3.07800	2.15800	1.77100	1.69600	1.65800	U--FC 2
1.62000	1.59300	1.56100	1.53900	1.52900	1.52400	U--FC 3
1.48800	1.40400	1.25000	0.97300	0.60000	0.10900	U--FC 4
0.09000	0.04600	0.03000	0.01300	0.00300	0.00000	U--FC 5
0.00000	0.00000	0.00000	0.00000			U--FC 6
0.00000	0.00000	0.00000	0.00091	0.00198	0.00352	FSPCT 1
0.00552	0.00792	0.01024	0.01450	0.02014	0.02397	FSPCT 2
0.02940	0.03420	0.03740	0.04247	0.04536	0.04775	FSPCT 3
0.04774	0.04909	0.04823	0.04694	0.04558	0.04290	FSPCT 4
0.04080	0.03766	0.03502	0.03210	0.02909	0.02625	FSPCT 5
0.02394	0.02120	0.01877	0.01525	0.03510	0.03210	FSPCT 6
0.02720	0.01975					FSPCT 7

B.4 $LiF\text{-}BeF_2\text{-}UF_4$ Salts

The group effective resonance capture cross section of the fused salt (per U^{238} atom) is calculated as outlined in Appendix A. The resonance parameters of U^{238} are obtained from Hughes and Schwartz.[27]

TABLE B.7

URANIUM	U-238	LOW ENERGY NUCLIDE DECK					
8.10980	0.49650	0.06670	0.00000	0.002801	8.80000	U 164	
9.19240	0.39150	0.01610	0.00000	0.002801	9.75000	U 165	
10.49140	0.29860	0.00000	0.00000	0.002801	11.00000	U 166	
11.53100	0.45700	0.03200	0.00000	0.002801	12.30000	U 167	
12.64000	0.08615	0.00206	0.00179	0.002801	13.10000	U 168	
12.94500	0.05500	0.00000	0.00000	0.002801	13.51300	U 169	
11.71400	0.08600	0.00000	0.00000	0.002801	12.40500	U 170	
10.82000	0.08000	0.00000	0.00000	0.002801	11.50800	U 171	
10.62200	0.07800	0.00000	0.00000	0.002801	11.26700	U 172	
10.62200	0.07800	0.00000	0.00000	0.002801	11.21800	U 173	
10.62200	0.07800	0.00000	0.00000	0.002801	11.15500	U 174	
10.62200	0.07800	0.00000	0.00000	0.002801	11.10500	U 175	
10.62200	0.07800	0.00000	0.00000	0.002801	10.98600	U 176	
10.62200	0.07800	0.00000	0.00000	0.002801	10.91000	U 177	
10.62200	0.07800	0.00000	0.00000	0.002801	11.05300	U 178	
8.50000	0.00000	0.00000	0.00838	0.002801	11.35000	U 179	
0.00000	0.00000	0.00000	0.00000			U 180	
0.00000	0.00050	0.00150	0.00230			U--SR 1	
0.00350	0.00520	0.00740	0.01317			U--SR 2	
0.01128	0.01295	0.03991	0.03098			U--SR 3	
						U--SR 4	

TABLE B.8 U-238 (FUSED SALT) LOW ENERGY REACTION CROSS SECTIONS (BARNS)

LITHIUM, BERYLLIUM, URANIUM FLUORIDE -- (73-00-27)

GP	TOTAL	N,N	N,N'	CAPTURE	SURFACE
35	8.800	8.073	0.600	0.127	0.00000
36	9.750	9.100	0.500	0.150	0.00000
37	11.000	10.350	0.440	0.210	0.00000
38	12.300	11.620	0.400	0.280	0.00000
39	13.100	12.720	0.010	0.370	0.00000
40	13.503	13.000	0.000	0.503	0.00025
41	12.450	11.800	0.000	0.650	0.00065
42	11.703	10.900	0.000	0.803	0.00115
43	11.637	10.700	0.000	0.937	0.00185
44	11.757	10.700	0.000	1.057	0.00270
45	11.925	10.700	0.000	1.225	0.00400
46	11.922	10.700	0.000	1.222	0.00659
47	11.932	10.700	0.000	1.232	0.00636
48	11.879	10.700	0.000	1.179	0.00655
49	15.889	10.700	0.000	5.189	0.01710
50	11.250	8.500	0.000	2.750	0.01585

LITHIUM, BERYLLIUM, URANIUM FLUORIDE -- (71-09-20)

GP	TOTAL	N,N	N,N'	CAPTURE	SURFACE
35	8.800	8.073	0.600	0.127	0.00000
36	9.750	9.100	0.500	0.150	0.00000
37	11.000	10.350	0.440	0.210	0.00000
38	12.300	11.620	0.400	0.280	0.00000
39	13.100	12.720	0.010	0.370	0.00000
40	13.503	13.000	0.000	0.503	0.00025
41	12.450	11.800	0.000	0.650	0.00050
42	11.703	10.900	0.000	0.803	0.00095
43	11.637	10.700	0.000	0.937	0.00160
44	11.757	10.700	0.000	1.057	0.00250
45	11.925	10.700	0.000	1.225	0.00360
46	12.002	10.700	0.000	1.302	0.00562
47	12.104	10.700	0.000	1.404	0.00597
48	12.119	10.700	0.000	1.419	0.00620
49	17.416	10.700	0.000	6.716	0.01642
50	11.250	8.500	0.000	2.750	0.01493

TABLE B.8 CONTINUED

LITHIUM, BERYLLIUM, URANIUM FLUORIDE -- (67-16-17)

GP	TOTAL	N,N	N,N'	CAPTURE	SURFACE
35	8.800	8.073	0.600	0.127	0.00000
36	9.750	9.100	0.500	0.150	0.00000
37	11.000	10.350	0.440	0.210	0.00000
38	12.300	11.620	0.400	0.280	0.00000
39	13.100	12.720	0.010	0.370	0.00000
11	11.111	11.111	1.111	1.111	1.11111
40	13.503	13.000	0.000	0.503	0.00025
41	12.450	11.800	0.000	0.650	0.00050
42	11.703	10.900	0.000	0.803	0.00095
43	11.637	10.700	0.000	0.937	0.00150
44	11.757	10.700	0.000	1.057	0.00220
45	11.925	10.700	0.000	1.225	0.00315
46	12.057	10.700	0.000	1.357	0.00500
47	12.274	10.700	0.000	1.574	0.00567
48	12.544	10.700	0.000	1.844	0.00591
49	17.866	10.700	0.000	7.166	0.01585
50	11.250	8.500	0.000	2.750	0.01423

LITHIUM, BERYLLIUM, URANIUM FLUORIDE -- (71-16-13)

GP	TOTAL	N,N	N,N'	CAPTURE	SURFACE
35	8.800	8.073	0.600	0.127	0.00000
36	9.750	9.100	0.500	0.150	0.00000
37	11.000	10.350	0.440	0.210	0.00000
38	12.300	11.620	0.400	0.280	0.00000
39	13.100	12.720	0.010	0.370	0.00000
40	13.513	13.000	0.000	0.513	0.00015
41	12.470	11.800	0.000	0.670	0.00040
42	11.708	10.900	0.000	0.808	0.00075
43	11.647	10.700	0.000	0.947	0.00135
44	11.792	10.700	0.000	1.092	0.00205
45	11.965	10.700	0.000	1.265	0.00380
46	12.150	10.700	0.000	1.450	0.00424
47	12.491	10.700	0.000	1.791	0.00523
48	12.605	10.700	0.000	1.905	0.00575
49	19.333	10.700	0.000	8.633	0.01503
50	11.250	8.500	0.000	2.750	0.01344

TABLE B.8 CONTINUED

LITHIUM, BERYLLIUM, URANIUM FLUORIDE -- (74-16-10)

GP	TOTAL	N,N	N,N'	CAPTURE	SURFACE
35	8.800	8.073	0.600	0.127	0.00000
36	9.750	9.100	0.500	0.150	0.00000
37	11.000	10.350	0.440	0.210	0.00000
38	12.300	11.620	0.400	0.280	0.00000
39	13.100	12.720	0.010	0.370	0.00000
40	13.523	13.000	0.000	0.523	0.00015
41	12.470	11.800	0.000	0.670	0.00040
42	11.723	10.900	0.000	0.823	0.00075
43	11.687	10.700	0.000	0.987	0.00125
44	11.857	10.700	0.000	1.152	0.00185
45	12.090	10.700	0.000	1.390	0.00260
46	12.277	10.700	0.000	1.577	0.00370
47	12.604	10.700	0.000	1.904	0.00467
48	12.959	10.700	0.000	2.259	0.00517
49	21.116	10.700	0.000	10.416	0.01414
50	11.250	8.500	0.000	2.750	0.01278

LITHIUM, BERYLLIUM, URANIUM FLUORIDE -- (60-30-10)

GP	TOTAL	N,N	N,N'	CAPTURE	SURFACE
35	8.800	8.073	0.600	0.127	0.00000
36	9.750	9.100	0.500	0.150	0.00000
37	11.000	10.350	0.440	0.210	0.00000
38	12.300	11.620	0.400	0.280	0.00000
39	13.100	12.720	0.010	0.370	0.00000
40	13.523	13.000	0.000	0.523	0.00010
41	12.491	11.800	0.000	0.691	0.00025
42	11.733	10.900	0.000	0.833	0.00055
43	11.697	10.700	0.000	0.997	0.00100
44	11.892	10.700	0.000	1.192	0.00155
45	12.115	10.700	0.000	1.415	0.00230
46	12.332	10.700	0.000	1.632	0.00350
47	12.634	10.700	0.000	1.934	0.00445
48	13.119	10.700	0.000	2.419	0.00507
49	21.866	10.700	0.000	11.166	0.01380
50	11.250	8.500	0.000	2.750	0.01255

TABLE B.9 U-238 (FUSED SALT) LOW ENERGY NUCLIDE DECKS

URANIUM			LI,BE,U FLUORIDE (73-00-27)			U1 164
8.10980	0.49650	0.06670	0.00000	0.002801	8.80000	U1 165
9.19240	0.39150	0.01610	0.00000	0.002801	9.75000	U1 166
10.49140	0.29860	0.00000	0.00000	0.002801	11.00000	U1 167
11.53100	0.45700	0.03200	0.00000	0.002801	12.30000	U1 168
12.64000	0.08615	0.00206	0.00179	0.002801	13.10000	U1 169
12.94500	0.05500	0.00000	0.00000	0.002801	13.50345	U1 170
11.71400	0.08600	0.00000	0.00000	0.002801	12.45039	U1 171
10.82000	0.08000	0.00000	0.00000	0.002801	11.70292	U1 172
10.62200	0.07800	0.00000	0.00000	0.002801	11.63660	U1 173
10.62200	0.07800	0.00000	0.00000	0.002801	11.75750	U1 174
10.62200	0.07800	0.00000	0.00000	0.002801	11.92490	U1 175
10.62200	0.07800	0.00000	0.00000	0.002801	11.92240	U1 176
10.62200	0.07800	0.00000	0.00000	0.002801	11.93180	U1 177
10.62200	0.07800	0.00000	0.00000	0.002801	11.87880	U1 178
10.62200	0.07800	0.00000	0.00000	0.002801	15.88890	U1 179
8.50000	0.00000	0.00000	0.00838	0.002801	11.25000	U1 180
0.00000	0.00000	0.00000	0.00000			U1 SR 1
0.00000	0.00025	0.00065	0.00115			U1 SR 2
0.00185	0.00270	0.00400	0.00659			U1 SR 3
0.00636	0.00655	0.01710	0.01585			U1 SR 4

TABLE B.9 CONTINUED

URANIUM			LI,BE,U FLUORIDE (71-09-20)			U6 164
8.10980	0.49650	0.06670	0.00000	0.002801	8.00000	U6 165
9.19240	0.39150	0.01610	0.00000	0.002801	9.75000	U6 166
10.49140	0.29860	0.00000	0.00000	0.002801	11.00000	U6 167
11.53100	0.45700	0.03200	0.00000	0.002801	12.30000	U6 168
12.64000	0.08615	0.00206	0.00179	0.002801	13.10000	U6 169
12.94500	0.05500	0.00000	0.00000	0.002801	13.50345	U6 170
11.71400	0.08600	0.00000	0.00000	0.002801	12.45039	U6 171
10.82000	0.08000	0.00000	0.00000	0.002801	11.70292	U6 172
10.62200	0.07800	0.00000	0.00000	0.002801	11.63660	U6 173
10.62200	0.07800	0.00000	0.00000	0.002801	11.75750	U6 174
10.62200	0.07800	0.00000	0.00000	0.002801	11.92490	U6 175
10.62200	0.07800	0.00000	0.00000	0.002801	12.00170	U6 176
10.62200	0.07800	0.00000	0.00000	0.002801	12.10390	U6 177
10.62200	0.07800	0.00000	0.00000	0.002801	12.11920	U6 178
10.62200	0.07800	0.00000	0.00000	0.002801	17.41630	U6 179
8.50000	0.00000	0.00000	0.00838	0.002801	11.25000	U6 180
0.00000	0.00000	0.00000	0.00000			U6 SR 1
0.00000	0.00025	0.00050	0.00095			U6 SR 2
0.00160	0.00250	0.00360	0.00562			U6 SR 3
0.00597	0.00620	0.01642	0.01493			U6 SR 4

TABLE B.9 CONTINUED

URANIUM			LI,BE,U FLUORIDE (67-16-17)			U5 164
8.10980	0.49650	0.06670	0.00000	0.002801	8.80000	U5 165
9.19240	0.39150	0.01610	0.00000	0.002801	9.75000	U5 166
10.49140	0.29860	0.00000	0.00000	0.002801	11.00000	U5 167
11.53100	0.45700	0.03200	0.00000	0.002801	12.30000	U5 168
12.64000	0.08615	0.00206	0.00179	0.002801	13.10000	U5 169
12.94500	0.05500	0.00000	0.00000	0.002801	13.50345	U5 170
11.71400	0.08600	0.00000	0.00000	0.002801	12.45039	U5 171
10.82000	0.08000	0.00000	0.00000	0.002801	11.70292	U5 172
10.62200	0.07800	0.00000	0.00000	0.002801	11.63660	U5 173
10.62200	0.07800	0.00000	0.00000	0.002801	11.75750	U5 174
10.62200	0.07800	0.00000	0.00000	0.002801	11.92490	U5 175
10.62200	0.07800	0.00000	0.00000	0.002801	12.05670	U5 176
10.62200	0.07800	0.00000	0.00000	0.002801	12.27390	U5 177
10.62200	0.07800	0.00000	0.00000	0.002801	12.54420	U5 178
10.62200	0.07800	0.00000	0.00000	0.002801	17.86630	U5 179
8.50000	0.00000	0.00000	0.00838	0.002801	11.25000	U5 180
0.00000	0.00000	0.00000	0.00000			U5 SR 1
0.00000	0.00025	0.00050	0.00095			U5 SR 2
0.00150	0.00220	0.00315	0.00500			U5 SR 3
0.00567	0.00591	0.01585	0.01423			U5 SR 4

TABLE B.9 CONTINUED

URANIUM		LI,BE,U FLUORIDE (71-16-13)				U3 164
8.10980	0.49650	0.06670	0.00000	0.002801	8.80000	U3 165
9.19240	0.39150	0.01610	0.00000	0.002801	9.75000	U3 166
10.49140	0.29860	0.00000	0.00000	0.002801	11.00000	U3 167
11.53100	0.45700	0.03200	0.00000	0.002801	12.30000	U3 168
12.64000	0.08615	0.00206	0.00179	0.002801	13.10000	U3 169
12.94500	0.05500	0.00000	0.00000	0.002801	13.51345	U3 170
11.71400	0.08600	0.00000	0.00000	0.002801	12.47039	U3 171
10.82000	0.08000	0.00000	0.00000	0.002801	11.70792	U3 172
10.62200	0.07800	0.00000	0.00000	0.002801	11.64660	U3 173
10.62200	0.07800	0.00000	0.00000	0.002801	11.79250	U3 174
10.62200	0.07800	0.00000	0.00000	0.002801	11.96490	U3 175
10.62200	0.07800	0.00000	0.00000	0.002801	12.14950	U3 176
10.62200	0.07800	0.00000	0.00000	0.002801	12.49060	U3 177
10.62200	0.07800	0.00000	0.00000	0.002801	12.60510	U3 178
10.62200	0.07800	0.00000	0.00000	0.002801	19.33350	U3 179
8.50000	0.00000	0.00000	0.00838	0.002801	11.25000	U3 180
0.00000	0.00000	0.00000	0.00000			U3 SR 1
0.00000	0.00015	0.00040	0.00075			U3 SR 2
0.00135	0.00205	0.00380	0.00424			U3 SR 3
0.00523	0.00575	0.01503	0.01344			U3 SR 4
URANIUM		LI,BE,U FLUORIDE (74-16-10)				U4 164
8.10980	0.49650	0.06670	0.00000	0.002801	8.80000	U4 165
9.19240	0.39150	0.01610	0.00000	0.002801	9.75000	U4 166
10.49140	0.29860	0.00000	0.00000	0.002801	11.00000	U4 167
11.53100	0.45700	0.03200	0.00000	0.002801	12.30000	U4 168
12.64000	0.08615	0.00206	0.00179	0.002801	13.10000	U4 169
12.94500	0.05500	0.00000	0.00000	0.002801	13.52345	U4 170
11.71400	0.08600	0.00000	0.00000	0.002801	12.47039	U4 171
10.82000	0.08000	0.00000	0.00000	0.002801	11.72292	U4 172
10.62200	0.07800	0.00000	0.00000	0.002801	11.68660	U4 173
10.62200	0.07800	0.00000	0.00000	0.002801	11.85750	U4 174
10.62200	0.07800	0.00000	0.00000	0.002801	12.08990	U4 175
10.62200	0.07800	0.00000	0.00000	0.002801	12.27670	U4 176
10.62200	0.07800	0.00000	0.00000	0.002801	12.60390	U4 177
10.62200	0.07800	0.00000	0.00000	0.002801	12.95920	U4 178
10.62200	0.07800	0.00000	0.00000	0.002801	21.11630	U4 179
8.50000	0.00000	0.00000	0.00838	0.002801	11.25000	U4 180
0.00000	0.00000	0.00000	0.00000			U4 SR 1
0.00000	0.00015	0.00040	0.00075			U4 SR 2
0.00125	0.00185	0.00260	0.00370			U4 SR 3
0.00467	0.00517	0.01414	0.01278			U4 SR 4

TABLE B.9 CONTINUED

URANIUM		LI,BE,U FLUORIDE (60-30-10)				U2 164
8.10980	0.49650	0.06670	0.00000	0.002801	8.80000	U2 165
9.19240	0.39150	0.01610	0.00000	0.002801	9.75000	U2 166
10.49140	0.29860	0.00000	0.00000	0.002801	11.00000	U2 167
11.53100	0.45700	0.03200	0.00000	0.002801	12.30000	U2 168
12.64000	0.08615	0.00206	0.00179	0.002801	13.10000	U2 169
12.94500	0.05500	0.00000	0.00000	0.002801	13.52345	U2 170
11.71400	0.08600	0.00000	0.00000	0.002801	12.49039	U2 171
10.82000	0.08000	0.00000	0.00000	0.002801	11.73292	U2 172
10.62200	0.07800	0.00000	0.00000	0.002801	11.69660	U2 173
10.62200	0.07800	0.00000	0.00000	0.002801	11.89250	U2 174
10.62200	0.07800	0.00000	0.00000	0.002801	12.11490	U2 175
10.62200	0.07800	0.00000	0.00000	0.002801	12.33170	U2 176
10.62200	0.07800	0.00000	0.00000	0.002801	12.63390	U2 177
10.62200	0.07800	0.00000	0.00000	0.002801	12.44920	U2 178
10.62200	0.07800	0.00000	0.00000	0.002801	21.86630	U2 179
8.50000	0.00000	0.00000	0.00838	0.002801	11.25000	U2 180
0.00000	0.00000	0.00000	0.00000			U2 SR 1
0.00000	0.00010	0.00025	0.00055			U2 SR 2
0.00100	0.00155	0.00230	0.00350			U2 SR 3
0.00445	0.00507	0.01380	0.01255			U2 SR 4

APPENDIX C

Thermal Stress and Heat Transfer

The thermal-stress and heat-transfer calculations for the first wall and the first-wall coolant region of a blanket are best clarified by working a sample problem. Let us examine the blanket described in Table C.1; the properties of the first wall and the fused salt are given in Tables 3.1 and 3.3, respectively. The neutron energy flux incident on the blanket wall is assumed to be 5 Mw/m^2.

Table C.1. Description of blanket.

		First Wall	First-Wall Coolant
Material		Mo	71LiF-09BeF_2-20UF_4
Thickness	(cm)	1.0	6.25
Total heat generation	$\frac{watts}{cm^2}$	51.0	560.0
Surface-Heat Deposition	$\frac{watts}{cm^2}$	62.5	

C.1 THERMAL STRESS

Homeyer derived a formula for the maximum thermal stress in a metal plate which is subject to uniform-volume heat generation and a surface heat source on one side.

$$\sigma_{max})_T = \frac{\alpha E d_w}{6k_w(1-\nu)} (3q_s+2q_w d_w). \qquad (C.1)$$

(The notation is defined in a glossary at the end of this appendix.) The heating in the first wall is an exponential function with a sharp peak superimposed at the wall-coolant interface. The representation of this heating distribution by a constant function is a valid approximation, since the differences are only several per cent and the wall thickness is small. We define q_w as the average heat generation per centimeter in the wall.

From Eq. (C.1) we then find that the maximum thermal stress in the first wall at the wall-coolant interface is

$$\sigma_{max})_T = 11,870 \text{ psi}.$$

C.2 HEAT TRANSFER

The velocity of coolant flow is governed by the maximum allowed temperature rise in the fused salt. The average heat removed per unit volume of salt is given by

$$q_r = \frac{1}{d_c}(Q_c+Q_w+q_s). \tag{C.2}$$

For a maximum temperature rise of $\Delta T)_c$ in a coolant pass which is L_c cm long, the required coolant velocity is

$$v_c = \frac{q_r L_c}{\rho C_p \Delta T)_c}. \tag{C.3}$$

Turbulent flow is essential for adequate cooling of the first wall, and the coolant velocity must also satisfy this consideration. Flow turbulence is determined by the relationship

$$N_{Re} = \left(\frac{D_c v_c \rho}{\mu}\right) > 2000. \tag{C.4}$$

The film temperature drop at the wall is

$$\Delta T)_F = \frac{Q_w + q_s}{h_F}. \tag{C.5}$$

Here, the film coefficient, h_F, is evaluated from experimental relationships. McAdams[79] gives a formula that is adequate for our calculations:

$$h_F = 0.023\left(\frac{k_c}{D_c}\right)\left(\frac{D_c v_c \rho}{\mu}\right)^{0.8}\left(\frac{C_p \mu}{k_c}\right)^{0.4}, \tag{C.6}$$

in which the physical constants are evaluated at the coolant bulk temperature.

The effectiveness of the cooling system may be expressed in terms of the coolant pumping power expenditure to heat transfer ratio. For an annular coolant channel the pumping power is given by Homeyer as

$$W_f = \frac{1}{g_o} f v_c^2 \rho \left(1 + \frac{D_c}{4R_w}\right), \tag{C.7}$$

where f is evaluated from circular pipe data at N_{Re} given by (C.4). The ratio of friction loss to heat removal, r_f, is then

$$r_f = \frac{W_f}{Q_w + q_s}. \tag{C.8}$$

The temperature drop across the first wall is independent of the coolant characteristics. Homeyer gives

$$\Delta T)_w = \frac{d_w(3q_s+2q_w d_w)}{3k_w}, \qquad (C.9)$$

in which q_w is as defined in section C.1.

Let us assume that the coolant passage is 30 m long, and the inlet-outlet temperature difference of the fused salt is 70°C. For an average bulk temperature of 600°C, we find from Eqs. (C.2)-(C.6) that

$$v_c = 10.3 \text{ m/sec}$$

$$N_{Re} = 3.74 \times 10^5$$

$$h_F = 0.436 \text{ cal/cm}^2\text{sec°C}$$

$$\Delta T)_F = 62.4°C.$$

The friction factor, f, for smooth pipes is approximately 0.034 at the Reynold's number given above. Equations (C.7) and (C.8) then give

$$r_f = 0.0135.$$

From (C.9) we obtain

$$\Delta T)_w = 82.5°C.$$

GLOSSARY

Symbol	Definition	Units
C_p	Specific heat	cal/gm°C
d_c	Coolant thickness	cm
d_w	Wall thickness	cm
D_c	Equivalent diameter = $2d_c$	cm
E	Young's modulus	dyne/cm^2
f	Fanning friction factor	
g_c	Force-mass conversion factor = $32.2 \frac{lb^M_{ft}}{lb^F sec^2} = 1 \frac{gm\ cm}{dyne\ sec^2}$	
h_F	Heat-transfer film coefficient	cal/cm^2sec°C
k_c	Thermal conductivity (coolant)	cal/cm sec°C
k_w	Thermal conductivity (wall)	cal/cm sec°C
L_c	Length of coolant flow	cm
N_{Re}	Reynold's number	
q_r	Heat removed per unit volume of coolant	watts/cm^3
q_s	Surface heat generation	watts/cm^2
q_w	Average heating rate in wall	watts/cm^3
Q_c	Total heat generation in coolant	watts/cm^2
Q_w	Total heat generation in wall	watts/cm^2
q	Ratio of friction power loss to heat transfer	
R_w	Radius of first wall	cm
$\Delta T)_c$	Coolant inlet-outlet temperature difference	°C
$\Delta T)_F$	Film temperature drop	°C
$\Delta T)_w$	Wall temperature drop	°C

GLOSSARY (continued)

Symbol	Definition	Units
v_c	Coolant velocity	cm/sec
W_f	Friction power loss	watts/cm^2
α	Coefficient of linear expansion	(°C)$^{-1}$
μ	Fluid viscosity	centipoise
ν	Poisson's ratio	
ρ	Fluid density	gm/cm^3
$\sigma_{max})_T$	Thermal stress	dyne/cm^3

Acknowledgement

I wish to ackowledge the contributions to this study made by Professor David J. Rose and Professor Irving Kaplan of the Department of Nuclear Engineering, M. I. T., and by Dr. A. J. Impink, who is now at Westinghouse Electric Company, East Pittsburgh, Pennsylvania, and Dr. W. G. Homeyer, who is now at General Atomics, San Diego, California. The many discussions with Professor Rose, his helpful suggestions and constant encouragement are most appreciated. Professor Kaplan contributed significantly to this work and, with Professor Rose, supervised my thesis research.

Dr. Impink and Dr. Homeyer developed the theoretical basis and the computational methods used in this study, without which this work would not have been possible. I am indebted to them for many suggestions that they made concerning various aspects of the blanket problem; especially, for the large amount of time that they contributed to this study.

References

1. D. J. Rose and M. Clark, Jr., Plasmas and Controlled Fusion (The M. I. T. Press and John Wiley and Sons, Inc., New York, 1961).
2. A. J. Impink, Jr., Ph. D. Thesis, Department of Nuclear Engineering, M. I. T., 1963.
3. W. G. Homeyer, Sc. D. Thesis, Department of Nuclear Engineering, M. I. T., 1963.
4. P. S. Spangler, Sc. D. Thesis, Department of Nuclear Engineering, M. I. T., 1963.
5. L. M. Petrie, Sc. D. Thesis, Department of Nuclear Engineering, M. I. T., 1964.
6. Oak Ridge National Laboratory, Molten Salt Reactor Project Quarterly Progress Reports, USAEC Reports: ORNL-2431, 2474, 2551, 2626, 2634, 2684, 2723, 2799, 2840, 2890, 2973, 3014 (1958-1960).
7. D. J. Rose, W. G. Homeyer, A. J. Impink, Jr., and P. S. Spangler (unpublished work, 1962).
8. F. Powell, LWS 24920 (1953).
9. L. G. Barrett, KAPL-M-LGB-14 (1957).
10. C. R. Tipton, Jr. (ed.), Reactor Handbook, Vol. I (Materials, Second Edition, Interscience Publishers, New York, 1961).
11. R. F. Thoma (ed.), Phase Diagrams of Nuclear Reactor Materials, ORNL-2548 (1959).
12. "Molten Salt Reactor Project," Quarterly Progress Report, Oak Ridge National Laboratory, USAEC Report ORNL-2723 (1959).
13. A. N. Protopopov and B. M. Shiryaev, Zhur. Ensptl. Theoret. Fiz. 36, 954-955 (1959).
14. J. Kirkbride, NRDC-58 (1955).
15. E. P. Blizard (ed.), Reactor Handbook, Vol. 3, Part B (Interscience Publishers, New York, 2d edition, 1962).
16. P. J. Campion, J. W. Knowles, G. Manning, and G. A. Bartholomew, Canadian J. Phys. 37, 377-381 (1957).
17. L. V. Groshev, V. N. Lutsenko, A. M. Demidov, and V. I. Pelekhov, Atlas of Gamma Ray Spectra from Radiative Capture of Thermal Neutrons (Pergamon Press, New York, 1959).
18. W. H. Sullivan, Trilinear Chart of Nuclides, ORNL, USAEC, 1957.
19. Yu. S. Zamyatnin, I. N. Safina, E. K. Gutnikova, and N. I. Ivanova, J. Nucl. Energy 9, 194-199 (1959).
20. K. H. Hellwege (ed.), "Energy Levels of Nuclei A = 5 to A = 257" (Landolt-Bornstein Numerical Data and Functional Relationships in Science and Technology, New Series, Vol. 1, Springer-Verlag, 1961).
21. A. B. Smith, Phys Rev. 126, 718-725 (1962).
22. S. Yiftah, D. Okrent, and D. A. Moldauer, Fast Reactor Cross Sections, International Series of Monographs on Nuclear Energy (Pergamon Press, New York, 1960).
23. A. B. Smith, R. G. Nobles, and A. M. Friedman, ANL-6247 (1960).
24. P. C. Stevenson, H. G. Hicks, J. C. Armstrong, Jr., and S. R. Gunn, Phys. Rev. 117, 186-191 (1960).
25. E. Strom, E. Gilbert, and H. Israel, LA-2237 (1958).
26. E. P. Wigner, E. Creutz, H. Jupnik, and T. Snyder, J. Appl. Phys. 26, 260 (1955).
27. D. J. Hughes and R. B. Schwartz, BNL-325 (1958).

28. B. R. S. Buckingham, K. Parker, and E. D. Pendlebury, AWRE O-28/60 (1961).

29. M. Stovisskii and M. Tolstikov, Atomnaya Energiya 10, 508-510 (1961).

30. J. F. Barry, L. P. O'Connor, and T. L. Perkin, Proc. Phys. Soc. (London) 74, 685-689 (1959).

31. A. Lindner and M. Miskel, WASH-1018, p. 63 (1959).

32. R. C. Hanna and B. Rose, J. Nucl. Energy 8, 197-209 (1959).

33. J. L. Perkin, L. P. O'Connor, and R. F. Coleman, Proc. Phys. Soc. (London) 72, 505-513 (1958); AWRE O-59/57.

34. R. F. Coleman, B. E. Hawker, L. P. O'Connor, and J. L. Perkin, Proc. Phys. Soc. (London) 73, 215-220 (1959).

35. J. P. Butler and D. C. Santry, Can. J. Chem. 39, 689-696 (1961); see AECL-1180.

36. R. J. Prestwood and B. P. Bayhurst, Phys. Rev. 121, 1438-1441 (1961).

37. B. P. Bayhurst and R. J. Prestwood, LA-2493 (1960).

38. J. L. Perkin and R. F. Coleman, Reactor Science and Technology (J. N. E.) 14, 69 (1961).

39. A. Tewes, B. Caretto, C. Miller, and D. Methaway, WASH-1028 (1960), p. 66.

40. A. Cochran and B. Henkel, WASH-1006 (1958), p. 22.

41. A. Cochran and B. Henkel, WASH-1013 (1958), p. 34.

42. J. Halperin, H. W. Schmitt, and R. E. Druschel, WASH-1006 (1958), p. 25.

43. Yu. A. Zysin, A. A. Korrizkhykh, A. A. Lbov, and L. I. Sel'chenko, Atomnaya Energiya, Vol. 8, No. 4, p. 360, 1960.

44. M. M. Kalos and E. S. Troubetzkoy, NDA-2134-2 (1960).

45. R. J. Howerton, UCRL-5351 (1958).

46. A. N. Protopopov, Yu. A. Selitskii, and S. M. Solovev, Atomnaya Energiya 4, 190-191 (1958).

47. A. A. Berezin, G. A. Stol'arov, Yu. V. Nikol'skii, and I. E. Chelnokov, Atomnaya Energiya 5, 659-660 (1958).

48. A. M. Weinberg and E. P. Wigner, The Physical Theory of Neutron Chain Reactors (The University of Chicago Press, Chicago, 1958), p. 112.

49. H. Soodak (ed.), Reactor Handbook, Vol. 3, Part A (Interscience Publishers, New York, 1962), pp. 8-9.

50. E. P. Blizard (ed.), Reactor Handbook, op. cit., Vol. 3, Part B, pp. 24-25.

51. A. N. Protopopov and B. N. Shiryaev, Zhur. Eksptl. Theoret. Fiz. 36, 954-955 (1959).

52. B. D. Kuz'minov, AEC-TR-3944 (1959).

53. A. Bratenahl, J. M. Peterson, and L. P. Stoering, Phys. Rev. 110, 927 (1958).

54. L. A. Galloway, TID-11005 (1959-1960).

55. J. F. Vervier and A. Martegani, Phys. Rev. 109, 947 (1958).

56. P. H. Bowen, J. P. Scanlon, G. H. Stafford, J. J. Thresher, and P. E. Hodgson, Nucl. Phys. 22, 640-662 (1961).

57. A. B. Coon, L. M. Davis, R. E. Felthanser, and B. Nicodemus, Phys. Rev. 111, 250 (1958).

58. A. V. Cohen, Reactor Science and Technology (J. N. E.) 14, 180 (1961).

59. Yu. G. Degtyarev and V. G. Nadtochii, Atomnaya Energiya 11, 397 (1961).

60. L. Rosen and L. Stewart, LA-2111 (1957).

61. L. Cranburg and J. S. Levin, WASH-1018 (1959), p. 25.

62. J. H. Gibbons, R. L. Macklin, P. D. Miller, and J. H. Neiler, BNL-653 (1961), p. 4.

63. J. H. Gibbons, R. L. Macklin, and J. H. Neiler, WASH-1018 (1959), p. 36.

64. E. G. Bilpuch, Ann. Phys. 10, 455-476 (1960).

65. B. C. Diven, J. Terrell, and A. Hemmendinger, Phys. Rev. 120, 556-569 (1960).

66. B. C. Diven and J. Terrell, WASH-1021 (1959), p. 22.

67. P. Kafalas and R. R. Heinrich, ANL-5924 (1958), p. 115.

68. W. F. Henkel, WASH-1006 (1958), p. 21.

69. K. W. Allen, P. Bomyer, and J. L. Perkin, Reactor Science and Technology (J. N. E.) 14, 100 (1961).

70. W. E. Knight, P. F. Smith, and K. E. Warren, Phys. Rev. 112, 259 (1958).

71. J. L. Perkin and R. F. Coleman, Reactor Science and Technology (J. N. E.) 14, 69 (1961).

72. L. Dresner, Nucl. Sci. Eng. 10, 142 (1961).

73. L. Cranberg and J. S. Levin, Phys Rev. 109, 2063 (1958).

74. A. Hemmendinger, A/Conf. 15/P/663 (1958).

75. B. Adams, R. Batchelor, and T. S. Green, Reactor Science and Technology (J. N. E.)14, 85 (1961).

76. N. N. Flerov, A. A. Berezin, and I. E. Chelnikov, Atomnaya Energiya 5, 657 (1958); see also J. N. E. 11, 173 (1958).

77. P. Billand, C. Clair, and J. Ouvry, A/Conf. 151 P/1186 (1958).

78. J. W. Weale, H. Goodfellow, M. H. McTaggart, and M. L. Mullender, Reactor Science and Technology (J. N. E.) 14, 91 (1961).

79. W. H. McAdams, Heat Transmission (McGraw-Hill Book Company, New York, 1954), p. 219.

JOINT SERVICES DISTRIBUTION LIST

Department of Defense

Defense Documentation Center
Attn: TISIA
Cameron Station, Bldg. 5
Alexandria, Virginia 22314

Director, National Security Agency
Attn: C3/TDL
Fort George G. Meade, Maryland 20755

Mr. Charles Yost, Director
For Materials Sciences
Advanced Research Projects Agency, DOD
Washington, D.C. 20301

Director
Advanced Research Projects Agency
Department of Defense
Washington, D.C. 20301

Dr. James A. Ward
Office of Deputy Director (Research and Information Rm. 3D1037) DOD
The Pentagon
Washington, D.C. 20301

Dr. Edward M. Reilley
Asst. Director (Research)
Ofc of Defense Res. & Eng., DOD
Washington, D.C. 20301

Department of the Army

Librarian PTA130
United States Military Academy
West Point, New York 10996

Director
U.S. Army Electronics Laboratories
Fort Monmouth, New Jersey 07703
Attn: AMSEL-RD-ADT

DR	NR	SR
FU#1	PE	SS
GF	PF	X
NE	PR	XC
NO	SA	XE
		XS

Commanding General
U.S. Army Electronics Command
Attn: AMSEL-SC
Fort Monmouth, New Jersey 07703

C.O., Harry Diamond Laboratories
Attn: Mr. Berthold Altman
Connecticut Ave. & Van Ness St. N.W.
Washington, D.C. 20438

The Walter Reed Institute of Research
Walter Reed Army Medical Center
Washington, D.C. 20012

Director
U.S. Army Electronics Laboratories
Attn: Mr. Robert O. Parker, Executive Secretary, JSTAC (AMSEL-RD-X)
Fort Monmouth, New Jersey 07703

Director
U.S. Army Electronics Laboratories
Attn: Dr. S. Benedict Levin, Director Institute of Exploratory Research
Fort Monmouth, New Jersey 07703

Commanding Officer
U.S. Army Research Office (Durham)
Attn: CRD-AA-IP (Richard O. Ulsh)
P.O. Box CM, Duke Station
Durham, North Carolina 27706

Commanding Officer
U.S. Army Medical Research Laboratory
Fort Knox, Kentucky

Commanding Officer
U.S. Army Personnel Research Office
Washington, D.C.

Dr. H. Robl, Deputy Director
U.S. Army Research Office (Durham)
P.O. Box CM, Duke Station
Durham, North Carolina 27706

Commandant
U.S. Command and General Staff College
Attn: Secretary
Fort Leavenworth, Kansas 66207

Director
U.S. Army Eng. Geodesy, Intell. and Mapping
Research & Development Agcy.
Fort Belvoir, Virginia 22060

Commanding Officer
Human Engineering Laboratories
Aberdeen Proving Ground, Maryland 21005

Commanding Officer
U.S. Limited War Laboratory
Attn: Technical Director
Aberdeen Proving Ground, Maryland 21005

Commanding Officer
U.S. Army Security Agency
Arlington Hall, Arlington, Virginia 22212

C.O., Harry Diamond Laboratories
Attn: Dr. R. T. Young, Elec. Tubes Div.
Connecticut Ave. & Van Ness St., N.W.
Washington, D.C. 20438

U.S. Army Munitions Command
Attn: Technical Information Branch
Picatinney Arsenal
Dover, New Jersey 07801

Commanding General
Frankford Arsenal
Attn: SMUFA-1310 (Dr. Sidney Ross)
Philadelphia, Pennsylvania 19137

Commanding General
U.S. Army Missile Command
Attn: Technical Library
Redstone Arsenal, Alabama 35809

Commandant
U.S. Army Air Defense School
Attn: Missile Sciences Division, C&S Dept.
P.O. Box 9390
Fort Bliss, Texas 79916

Commanding Officer
U.S. Army Ballistics Research Lab.
Attn: V.W. Richards
Aberdeen Proving Ground
Aberdeen, Maryland 21005

Commanding Officer
U.S. Army Materials Research Agency
Watertown Arsenal
Watertown, Massachusetts 02172

Commanding General
U.S. Army Strategic Communications
Command
Washington, D.C. 20315

Commanding General
U.S. Army Materiel Command
Attn: AMCRD-RS-PE-E
Washington, D.C. 20315

Commanding Officer
Foreign Service & Technology Center
Arlington Hall
Arlington, Virginia

Research Plans Office
U.S. Army Research Office
3045 Columbia Pike
Arlington, Virginia 22204

Chief of Research and Development
Headquarters, Department of the Army
Attn: Physical Sciences Division P&E
Washington, D.C. 20310

Director
Human Resources Research Office
The George Washington University
300 N. Washington Street
Alexandria, Virginia 22314

Commanding Officer
U.S. Army Electronics R&D Activity
White Sands Missile Range
New Mexico 88002

Commanding Officer
U.S. Army Engineers R&D Laboratory
Attn: STINFO Branch
Fort Belvoir, Virginia 22060

Commanding Officer
U.S. Army Electronics R&D Activity
Fort Huachuca, Arizona 85163

Mr. Alvin D. Bedrosian
Room 26-131
Massachusetts Institute of Technology
Cambridge, Massachusetts 02139

Department of the Air Force

Battelle Memorial Inst.
Technical Library
505 King Avenue
Columbus, Ohio 43201

Goddard Space Flight Center
NASA
Greenbelt, Maryland 20771

Research and Tech. Div. (AFAPL)
Attn: APIE-2, Mr. Robert F. Cooper
Wright-Patterson AFB, Ohio 45433

Technical Library
White Sands Missile Range
New Mexico 88002

AFSC (Tech Library)
Andrews AFB
Washington, D.C. 20031

AUL-3T-9663
Maxwell AFB
Alabama 36112

JOINT SERVICES DISTRIBUTION LIST (continued)

DDR&E (Tech Library)
Rm. 3C 128
The Pentagon
Washington, D.C. 20301

Systems Engineering Group
Deputy for Systems Eng'g., SEPRR
Directorate of Tech. Pubs. & Specs.
Wright-Patterson AFB, Ohio 45433

APGC (PGBAP-1)
Eglin AFB
Florida 32542

RTD (Tech Library)
Bolling AFB
District of Columbia 20332

BSD (Tech Library)
Norton AFB
California 92409

ASD (Tech Library)
Wright-Patterson AFB
Ohio 45433

Industrial College of the Armed Forces
Attn: Library
Washington, D. C.

Southwest Research Institute
Library
8500 Culebra Road
San Antonio, Texas

Stanford Research Institute
Library
820 Mission St.
South Pasadena, Calif. 91030

Library
National Science Foundation
Washington 25, D.C.

Linda Hall Library
5109 Cherry St.
Kansas City, Mo.

Dr. H. Harrison
NASA (Code RRE)
Fourth and Independence Sts.
Washington, D.C. 20546

Mr. James Tippett
National Security Agency
Fort Meade, Maryland

Brig. Gen. J. T. Stewart
Director of Science & Technology
Deputy Chief of Staff (R&D)
USAF
Washington 25, D.C.

Dr. R. L. Sproull, Director
Advanced Research Projects Agency
Washington 25, D.C.

Lt. Col. Edwin M. Myers
Headquarters USAF (AFRDR)
Washington 25, D.C.

Dr. John M. Ide
Div. Director for Eng'g.
National Science Foundation
Washington 25, D.C.

Dr. Zohrab Kaprielian
University of Southern California
University Park
Los Angeles 7, California

Dr. Lowell M. Hollingsworth
AFCRL
L. G. Hanscom Field
Bedford, Massachusetts

Professor Nicholas George
California Institute of Technology
EE Department
Pasadena, California

Hon. Alexander H. Flax
Asst. Secretary of the Air Force
Office of the Secretary of the Air Force
(R&D)
Washington 25, D.C.

Prof. Arwin Dougal
University of Texas
EE Department
Austin, Texas

Mr. Roland Chase
National Aeronautics & Space Admin.
1512 H Street, N.W.
Washington 25, D.C.

AFAL (AVTE)
Wright-Patterson AFB
Ohio 45433

Systems Engineering Group (RTD)
Attn: SEPIR
Wright-Patterson AFB
Ohio 45433

JOINT SERVICES DISTRIBUTION LIST (Continued)

Commander
Space Systems Division (AFSC)
Office of the Scientific Director
Inglewood, California

Dr. G. E. Knausenberger
c/o Hq Co. Munich Post
APO 09407, New York, N.Y.

AVCO Research Lab, Library
2385 Revere Beach Parkway
Everett, Mass. 02149

California Institute of Technology
Aeronautics Library
1201 East California St.
Pasadena 4, Calif. 91102

Carnegie Institute of Technology
Science & Engineering Hunt Library
Schenley Park
Pittsburgh, Pa. 15213

Rand Corporation
1700 Main St.
Santa Monica, Calif. 90401

Aerospace Corp. (Tech Library)
P.O. Box 95085
Los Angeles, Calif. 90045

Lewis Research Center (NASA)
Technical Library
21000 Brookpark Road
Cleveland, Ohio

George C. Marshall Space Flight Center
(NASA)
Redstone Arsenal, Ala. 35808

High Speed Flight Center (NASA)
Technical Library
Edwards AFB, Calif. 93523

Ames Rsch. Center (NASA)
Technical Library
Moffett Field, Calif. 94035

CIA OCR/LY/IAS
IH 129 HQ
Washington, D.C. 20505

RADC (Tech Library)
Griffiss AFB, N.Y. 13442

AEDC (Tech Library)
Arnold AFS
Tennessee 37389

APGC (Tech Library)
Eglin AFB
Florida 32542

AFWL (WLIL, Technical Library)
Kirtland Air Force Base
New Mexico 87117

AFMDC (Tech Library)
Holloman AFB
New Mexico 88330

AFFTC (Tech Library)
Edwards AFB
California 93523

Space Systems Division
Los Angeles Air Force Station
Air Force Unit Post Office
Los Angeles, California 90045
Attn: SSSD

Churchill Research Range
Library
Fort Churchill
Manitoba, Canada

National Defense Library
Headquarters
Ottawa, Ontario, Canada

Director
National Aeronautical Establishment
Ottawa, Ontario, Canada

EDS (ESTI)
Laurence G. Hanscom Field
Bedford, Massachusetts 01731

Johns Hopkins University
Applied Physics Lab., Library
White Oak, Silver Spring, Maryland 20919

Los Alamos Scientific Lab
Attn: Technical Library
Los Alamos, New Mexico 87544

ARL (AROL)
Wright-Patterson AFB
Ohio 45433

Frank J. Seiler Rsch. Lab.
Library
USAF Academy, Colo. 80840

U.S. Atomic Energy Commission
Library
Gaithersburg, Maryland 20760

JOINT SERVICES DISTRIBUTION LIST (continued)

AFAPL (APIE-2, Lt. Barthelmey)
Wright-Patterson AFB, Ohio. 45433

Rome Air Dev. Center (RAWL, H. Webb)
Griffiss Air Force Base, New York 13442

S. H. Sternick
Aerospace Com - Attn: ESNC
Waltham Federal Center
424 Trapelo Road
Waltham, Massachusetts 02154

AFCRL (CRFE-Dr. Nicholas Yannoni)
L. G. Hanscom Field
Bedford, Massachusetts

Mr. Rocco H. Urbano, Chief
AFCRL, Appl Math. Branch
Data Sciences Laboratory
Laurence G. Hanscom Field
Bedford, Massachusetts

AFCRL
Office of Aerospace Res., USAF
Bedford, Mass.
Attn: CRDA

Dr. Louis C. Block
AFCRL (CROO)
Laurence G. Hanscom Field
Bedford, Massachusetts 01731

Commander, AFCRL
Attn: C. P. Smith (CRBS)
L. G. Hanscom Field
Bedford, Massachusetts

AFETR (Tech Library MU-135)
Patrick AFB, Florida 32925

Mr. C. N. Hasert
Scientific Advisory Board
Hq. USAF
Washington 25, D. C.

Dr. Harvey E. Savely, SRL
Air Force Office of Sci. Res.
Office Aerospace Research, USAF
Washington 25, D. C.

Department of the Air Force
Headquarters, United States Air Force
Washington 25, D. C.
Attn: AFTAC/TD-1

John Crerar Library
35 West 33rd St.
Chicago, Ill.

LOOAR (Library)
AF Unit Post Office
Los Angeles, Calif. 90045

Office of Research Analyses
Library
Holloman AFB, New Mexico 88330

Office of Research Analyses
Attn: Col. K. W. Gallup
Holloman AFB, New Mexico 88330

ARL (ARD/Col. R. E. Fontana)
Wright-Patterson AFB
Ohio 45433

Brig. Gen. B. G. Holzman, USAF (Ret.)
National Aeronautics and Space Admin.
Code RS
Washington, D. C. 20546

AFRST (SC/EN)
Lt. Col. L. Stone
Room 4C 341
The Pentagon
Washington, D. C. 20301

Commander
Rome Air Development Center
AFSC
Office of the Scientific Director
Griffiss AFB, Rome, New York

Commander
Research & Technology Division (AFSC)
Office of the Scientific Director
Bolling AFB 25, D. C.

Commander
Air Force Systems Command
Office of the Chief Scientist
Andrews AFB, Maryland

Commander
Air Force Cambridge Research Lab.
Office of the Scientific Director
L. G. Hanscom Field
Bedford, Massachusetts

Commander
Aerospace Research Laboratories (OAR)
Office of the Scientific Director
Wright-Patterson AFB, Ohio

Commander, Aerospace Systems Division
AFSC
Office of the Scientific Director
Wright-Patterson AFB, Ohio

JOINT SERVICES DISTRIBUTION LIST (continued)

AFAL
AVR(L)
Wright-Patterson AFB
Ohio 45433

Air Force Cambridge Res. Lab.
L.G. Hanscom Field
Bedford, Massachusetts 01731
Attn: CRDM, Mr. Herskovitz

Commander
Air Force Office of Scientific Research
Washington 25, D.C.
Attn: SREE

Director
Air University Library
Maxwell A.F. Base, Alabama

NASA/AFSS/1 FOB6
Tech Library, Rm. 60084
Washington, D.C. 20546

USAFA (DLIB)
U.S. Air Force Academy
Colorado

ARPA
Tech Info Office
The Pentagon
Washington, D.C. 20301

AFCRL(CRXL)
L.G. Hanscom Field
Bedford, Mass. 01731

U.S. Regional Sci. Office (LAOAR)
U.S. Embassy
APO 676, New York, N.Y.

AEC
Div. of Tech Info. Ext.
P.O. Box 62
Oak Ridge, Tennessee

Dr. Hermann H. Kurzweg
Director of Research - OART
NASA
Washington, D.C. 20546

AFIT (MCLI)
Tech Library
Wright-Patterson AFB, Ohio 45433

Prof. W. H. Radford
Lincoln Laboratory, A-183
244 Wood Street
Lexington, Massachusetts

Department of the Navy

Chief of Naval Operations
Pentagon OP 07T
Washington, D.C.

Commanding Officer
Office of Naval Research Branch Office
Navy 100, Fleet P.O. Box 39
New York, New York

Library
U.S. Navy Electronics Lab.
San Diego, California 92152

Commander
U.S. Naval Air Development Center
Johnsville, Pennsylvania
Attn: NADC Library

Commanding Officer
Office of Naval Research Branch Office
495 Summer Street
Boston, Massachusetts 02110

Commanding Officer
U.S. Navy Underwater Sound Laboratory
Ft. Trumbull, New London, Connecticut

U.S. Navy Post Graduate School
Monterey, California
Attn: Electrical Engineering Department

Commander, Naval Ordnance Laboratory
White Oak, Maryland
Attn: Technical Library

Chief, Bureau of Ships, Attn: Code 680
Department of the Navy
Washington, D.C. 20360

Chief, Bureau of Weapons
Department of the Navy
Washington, D.C. 20360

Dr. Arnold Shostak, Code 427
Head, Electronics Branch
Physical Sciences Division
Office of Naval Research
Washington, D.C. 20360

Chief of Naval Research, Code 427
Department of the Navy
Washington, D.C. 20360

Director
Naval Research Laboratory
Washington, D.C. 20390